Variable Stiffness of Metamaterial Composite Structure

A thesis

submitted in partial fulfilment

of the requirements for the degree

of

Master of Engineering

at

The University of Waikato

by

FAN YANG

THE UNIVERSITY OF
WAIKATO
Te Whare Wānanga o Waikato

2022

Acknowledgement

This paper is the culmination of a long and arduous journey that began in 2019 and ended in 2022 after numerous setbacks and difficulties, and was only possible because of the support of many people.

I am very grateful to my Supervisor Mr. Ilanko Sinniah. He has given me invaluable guidance throughout my research. During the COVID-19, he did not give up on my study even though I was in another country. When he learned that I could not get back to New Zealand, he always helped me find a way to do my research remotely. During this period, I experienced being forced to change my research content and had to search for a suitable laboratory in China. When the situation in China began to become serious, I was forced to change the subject matter again and had to use computer simulation experiments during the whole process. Because I have a background in material science and didn't know how to use software at all, Mr. Ilanko actively helped me contact the software team in Australia for remote online teaching. I would also like to thank Leap Australia for their help during the whole process of learning ANSYS. Many thanks to the University of Waikato for providing a remote system for students to use. I am also very grateful to Sun Xutao for his help. Finally, I would like to thank all the people who directly and indirectly helped me complete the paper. I sincerely wish that everything goes well for you and happiness follows. Covid-19 still exists in 2022, but no winter lasts forever; a spring is sure to follow. May everything we work for have a positive outcome.

Contents

A.1Methods

A.2 Results

B.

Stiffness of Bars Used in ANSYS Modelling

1 Abstract

In recent years, numerous researchers have studied metamaterials because of their extraordinary mechanical properties that other materials do not possess. The concept of metamaterials has been widely introduced into the field of earthquake engineering. [1]

This thesis presents the results of research aimed at finding a metamaterial structure with adaptive stiffness that could be used in the design of isolators and protective barriers. Such a material would reduce impact force transmission experienced by a vehicle in the event of an accident, and could also protect people in buildings during an earthquake. The goal is to develop the concept of a metamaterial that would have non-linear stiffness, and offer higher resistance against small displacements (high stiffness) but lower resistance (low stiffness) in the event of sudden impacts experienced during large dynamic excitations, While deformation in the plastic zone also results in non-linearity, the metamaterial will have the advantage of being fully elastic, and it can be used repeatedly which is environmentally friendly and reduces maintenance costs. The reversible non-linearity is obtained by using stiffness changes associated with change in geometry. Theoretical analysis and numerical results show that it may be possible to develop such a metamaterial from cells which contain adaptive mechanisms embedded in a flexible matrix. Metamaterial can provide variable stiffness and enable significant reductions in the transmission of dynamic forces.

1 Introduction

At the beginning of this project, the overall purpose was to find an adaptive structure that would protect buildings from earthquake damage. To this end, the goal was to develop a material that under normal loadings would have high stiffness around the equilibrium state but when subjected to large forces the material would become flexible and minimize transmission of forces. It then transpired that such a material may also be useful in automobile industry to make shells that would behave in the same way under accident impact loadings. Most of the anti-collision mechanisms on the market are disposable, so they face the problem of being more expensive because they are single-use. and are not environmentally friendly. Therefore, this project aims to find a Material that can be reused, which can reduce the number of injuries, save lives and reduce property losses.

In order to minimize the losses due to earthquake damage, numerous countries have been conducting various observations and studies. At present, the earthquake early warning system has achieved some results in reducing earthquake disaster losses, but it is difficult to design a structure that can withstand earthquake forces only through accurate calculations of static stress and displacement. Seismic resistance not only depends on the required bearing capacity but also depends on the ability of the structure to absorb energy. Due to the randomness of earthquakes and accidents, the differences between various structures, and the complexity of the structure itself, maximizing seismic resistance is a challenging task. In a major earthquake, damage will be unavoidable, but structures must absorb energy and must not collapse. Therefore, in addition to careful calculations to ensure that the static design standards are met, structural analysis should also fully consider the ductility and energy absorption capacity of a building.

1.1 Background

Earthquakes are one of the most threatening natural disasters to mankind. They are sudden and unpredictable and often cause a large number of casualties. My country (China) is a country with a high incidence of earthquake disasters. At the beginning of the 20th century, my country has accounted for about 35% of earthquakes of magnitude 7 or higher in the world. From 1949 to 1991, the number of deaths due to earthquakes in China accounted for 54% of the total number of deaths from various natural disasters. The two largest earthquakes, the Tangshan Earthquake and the Wenchuan Earthquake, killed 242,000 and 69,000, respectively, and injured 164,000 and 374,000 [2].

Li Shengcai et al [3] recorded various domestic production safety accidents in 2021, including traffic accidents, mining accidents, chemical accidents, construction accidents, municipal accidents (Various safety accidents occurred in housing construction and municipal construction projects) and other accidents. From January to December traffic-related accidents accounted for 30.19 to 48.28% of all accidents over this period. Thus, it can be seen that traffic-related accidents routinely accounts for the highest proportion of deaths from accidents.

In order to better avoid disasters caused by earthquakes and accidents, the aim of this thesis was to find a special structure that can change its overall stiffness and adaptively reduce the transmission of external forces. For this purpose, a variable stiffness structure made of metamaterials was considered, which only becomes flexible when a large force is occasionally transmitted. These destructive forces are those that may be created and transmitted by large movements (earthquakes) or impacts (vehicle accidents).

1.2 Literature Review

Earthquakes are among the top disasters; for example, the Tangshan Earthquake and the Wenchuan Earthquake in 2008 seriously impacted the country's economic and social development, and people's lives and property. Moreover, compared with other natural disasters, earthquakes have the characteristics of unpredictability, low probability and high risk.

Figure 1 is a statistical chart of the death toll from major earthquakes in the world over the past 100 years. There are many deaths due to earthquakes every year [4].

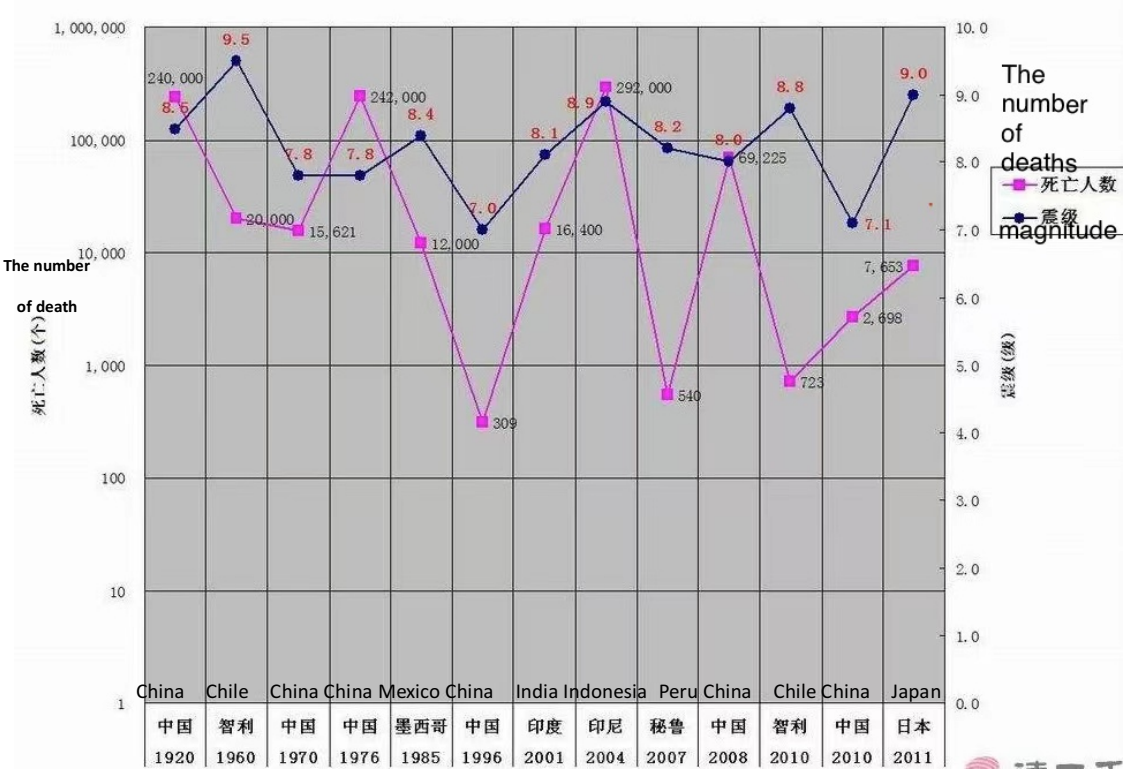

Figure 1: Statistics of death toll from major earthquakes in the world over the past 100 years [4]

On December 27, 2008, the Sixth Meeting of the Standing Committee of the Eleventh National People's Congress of China revised the "Law of the People's Republic of China on Earthquake Prevention and Disaster Mitigation", which aims to vigorously promote the modernization of earthquake preparedness and disaster reduction in the new era. The purpose of the country's vigorous implementation of the anti-seismic policy is to reduce the economic losses of earthquakes, reduce economic losses, and protect people's lives. With the continuous development of

the construction industry, people's living standards are constantly improving, and people have higher requirements and standards for the living in and using various buildings. At present, the structural material of most of the high-rise buildings is concrete. This is because a concrete structure has strong seismic resistance that can maximize the safety of the building. Based on this, the performance of high-rise concrete anti-seismic structures is one aspect currently being researched. In [5], the main principles of high-rise concrete building anti-seismic structural design are described, and an optimization method of building these structures is proposed.

One of the most critical aspects of the optimization method described in [5] is the need to effectively determine building layout. Generally speaking, under the action of horizontal seismic waves, each floor of a building will be significantly displaced, and be subject to full deformation, global translation, global torsion, and shear deformation. Therefore, different structures need to apply different control methods, and only in this way can the deformation be effectively controlled. The control methods include, among others, reducing column distance, reducing beam distance, setting steel arms, applying double anti-side systems, and setting vertical support. Designers need to adopt a staggered design method to increase the span of the building, thereby effectively improving the seismic capacity of the overall structure of the building, so that will not cause tensile effects on the weaker floors of the building, and will not cause large displacement and deformation.

While the above design methods can improve the ability of a structure to withstand earthquakes when ground movement induces internal forces in structures, there are methods which can reduce the force that can be transmitted to a structure such as isolation. As a popular passive seismic mitigation strategy, seismic isolation technology has been widely used in urban construction all over the world. Usually, foundation isolation means to introduce a flexible vibration isolation system (such as rubber bearings) between the structure and the foundation to reduce the seismic input energy of the structure. Since its inception, seismic isolation technology has been extensively studied, and novel devices have continued to emerge in order to adapt the seismic isolation system to different types of external impacts.

A semi-active damper was added to a seismic isolation layer, and the seismic isolation performance of the semi-active seismic isolation system was studied [6][7]. A distributed composite artificial foundation isolation system of rubber-soil mixture has also been used to block horizontal and vertical vibration input [8][9]. A seismic isolation column was also proposed to replace the traditional structural column so as to protect the structure from near-fault earthquakes [10]. However, seismic isolation systems still have shortcomings that cannot be ignored, such as the risk of over-displacement and overturning of these systems. Although the addition of dampers reduces the displacement of the seismic isolation layer, it may also significantly reduce the fitness effect of the upper structure [11].

The direct-down urban earthquake has a direct effect on those of us living in China. Urban direct-down earthquakes, a term proposed by Japanese scholars, where the city is in the epicenter or within the epicenter area of potential earthquakes. An earthquake that occurs vertically below a city is called a direct-down urban earthquake. This type of earthquake poses a direct threat to large cities, and the casualties, social function damage, and economic losses caused by it will greatly exceed non-urban "direct-type earthquakes". Urban direct earthquakes, especially large earthquakes, have caused serious damage to urban buildings, structures and related facilities, and the disasters caused are extremely tragic, and they are one of the biggest threats to urban safety [12]. Figure 2 shows the earthquake damage in the city of Wenchuan.

Figure 2: The direct-down urban earthquake brought disaster to Wenchuan, China on May 12, 2008 [12].

In order to ensure that when an earthquake disaster occurs, the impact of the disaster on the building is minimized, it is necessary to prioritize the seismic design of the building structure. A steel structure is a common feature of modern buildings, so research on the seismic design of steel structures will have a positive impact on research into the seismic design of building structures. Guan et al [13] introduced the basic situation surrounding building steel structures, expounded the factors affecting the stability of a steel structure, and analyzed the seismic design of the structure and its application on the basis of these factors.

Earthquake loss analysis is of great significance to disaster prevention and mitigation, and earthquake loss analysis based on actual damage is a relatively

direct and effective method. However, due to the lack of detailed seismic damage data, current earthquake loss analysis based on actual earthquake damage mostly relies on the analysis of building groups or the overall analysis of certain types of buildings. The seismic damage and loss of each component, especially the damage to non-structural components can be analyzed in detail at the component level of the building. Based on more than 3 million detailed earthquake damage records from16 New Zealand earthquakes, Liu Yuan et al [14] first analyzed the loss of buildings in the earthquake from the two aspects of structural damage and non-structural damage, and then analyzed the buildings in detail at component level damage to the main components. The research results show that in earthquake disasters, more than 80% of the building losses come from non-structural damage, of which wall decoration damage is the main component of non-structural damage loss, followed by the loss of wall covering and ceiling. Plate foundations and piles are the main components in the damage to structural members. The results of this study indicate that special attention should be paid to the seismic damage of non-structural components in the future seismic design and construction of buildings. These are also situations which show the limitation on relying of strengthening a structure alone. Isolation devices can protect not only the structure but also non-structural components.

With the development of the economy, more and more super high-rise buildings have appeared in China. The number of super high-rise buildings distributed in high-intensity areas has also increased. Therefore, the seismic design of super high-rise buildings has become particularly important. Commonly used methods for structural seismic design include traditional seismic methods, seismic damping or isolation methods, and damping-seismic hybrid application methods. The seismic isolation design and energy dissipation design of structures have been greatly developed, and the hybrid application technology of seismic and seismic isolation is still under development. Yu Meng et al. [15] combined the shock absorption and isolation design with the structural design of the proposed super high-rise building, and discussed the possibility of using the shock absorption-isolation hybrid seismic

technology in practical engineering. In this study, YJK software (YJK software is a fully-professional design software that can provide simulations of buildings, structures such as bridges, electromechanical systems, etc.) was used to establish structural analysis models for three schemes: Scheme one is a traditional seismic structure model; Scheme two is a base isolation structure model; and Scheme three is a hybrid application structure model of vibration reduction and isolation. The modal analysis of the structure of the three schemes was carried out, and the dynamic characteristics of the structure of the three schemes were analyzed.

The conclusions from this paper are as follows: (1) When a small earthquake act, compared with Scheme 1, the shock absorption effect of Scheme 2 and Scheme 3 is basically the same, and the inter-story displacement is reduced by 10% to 30%. During the moderate earthquake, the shock absorption effect of the third scheme is more obvious, and the inter-story displacement is reduced by 45% to 75%. When there is a large earthquake, for the 1st to 10th floors of the structure, the third plan has better shock absorption effect. Due to the different layout of the isolation bearings, the second plan has a better shock absorption effect for the structure above the seismic isolation layer, but the third plan still has a better shock absorption effect. The mixed application of shock absorption and isolation can effectively improve the seismic performance of the structure. (2) The results of the elastic time history analysis of large earthquakes show that the hybrid application technology of shock absorption and isolation provides two safety lines of defense for the structure and increases the safety of the structure. (3) By adopting shock absorption and isolation hybrid application technology, the amount of concrete and steel bars in the superstructure can been significantly reduced, which improves the economics of the structure. Therefore, it has been suggested that it is feasible to apply the hybrid application technology of vibration reduction and isolation in practical engineering. However, this author is not aware of any actual implementation of this technology.

In addition to the disasters caused by the earthquake, car accidents also claim the

lives of many people. With the continuous development of the market economy, the number of motor vehicles is also increasing, which has generated widespread attention to road traffic and people's needs for road traffic safety. There are many ways to protect lives ranging from prevention of a car accident to the emergency measures after a car accident.

The low-speed crash performance of a car is an important indicator when considering car safety and economy of maintenance [16]. The front and rear bumpers of the car are the main protective parts of the car body structure. When a low-speed collision occurs, the bumpers can absorb the energy of the collision, alleviate the impact of the collision on the car body, and reduce the damage to the car body structure. Therefore, optimizing the design of the automobile bumper structure has always been a research focus of automobile manufacturing. Under the general trend of lightweight automobiles, while optimizing the design of the bumper structure and installation, the use of lightweight manufacturing materials can not only improve the safety of the car in a low-speed collision, but it can also improve the fuel economy of the vehicle. At this time, plastic car bumpers are gradually replacing traditional metal car bumpers. With the development of technology, plastics are being more widely used as automobile manufacturing materials due to their advantages such as convenient material acquisition, excellent performance and low price. However, plastics are made of PE products from petroleum refining, and petroleum resources are becoming limited. In addition, most plastics only degrade very slowly in the natural environment, so they have become a significant ecological pollutant. Although plastics can be recycled, the main obstacle when recycling waste plastics is sorting. Mixing different types of plastics cannot be effectively used, which is time-consuming and labor-intensive. And in the event of a car accident, it is possible for a fire to start after a car accident, and plastic burns easily and produces toxic gases when burned. It also has the disadvantages of poor heat resistance and easy aging [17]. The same study analyzed the current situation regarding the use of plastic products and the mechanism of how waste plastics harm the environment, and has summarized the serious

pollution caused by waste plastics landfill and incineration.

According to The New Zealand Injury Prevention Outcomes Report – June 2012, [18] it can be seen that the degree of motorization in New Zealand is high (that is, the proportion of vehicles per capita is high). It can be seen from Figure 3 that from 2004 to 2005, the increase in the number of hospitalizations peaked, and the number of accidents peaked in 2005-7. This is due to increased injuries in motorcycle accidents [19]. Being two-wheeled, a motorcycle is not as stable as a four-wheeled vehicle, and the rider's body is exposed. It cannot be protected by the vehicle itself. There are also some motorcyclists who ride at speed and like to shuffle through traffic.

According to a data provided by the traffic management department, the traffic accident death rate of motorcycles is 450 per 100,000, while the traffic accident death rate of cars is only 0.19 per 100,000. Following the death of William Snell, a famous baseball player, during a motorcycle race in 1956, relevant scientific research institutions in the United States listed the design of safety helmets as a key research project. After repeated experiments, the experts proved that the head was hit hard during the accident, and a helmet could have effectively protected the it [20]. Helmets (not only for motorcyclists, but also in a number of sports) could be another use for metamaterials. So, any new metamaterial could also be beneficial in improving the design of helmets.

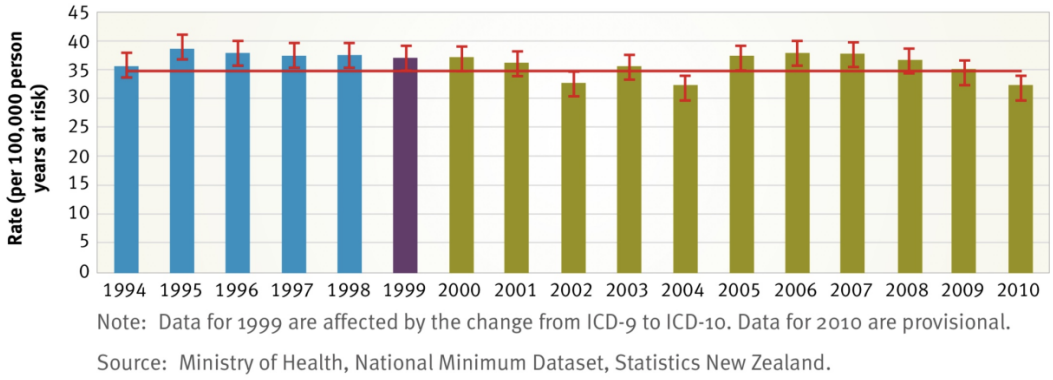

Figure 3: road crash serious injuries, age-standardized rate per 100,000 population, 1994–2010[18]

In recent years, with the rapid economic growth, the number of cars in the world

has increased year by year, and the number of traffic accidents has also increased year by year. The safety of vehicle occupants during automobile collisions has attracted more and more attention from researchers. As one of the main load-bearing and energy-absorbing components of a car in a frontal collision, the bumper not only protects vulnerable parts of the car from damage and thus reduces maintenance costs but it also reduces the severity of a collision between vehicles and pedestrians. Therefore, it must have a strong comprehensive crash resistance performance. The rear bumper of a passenger car needs to have a protective effect on the car body in case of accidents, such as a rear-end collision, so its rigidity and strength characteristics are very important [21].

Considering the materials used in shock-absorbing and isolating structures, polypropylene (PP) has low density, low cost, large output, and excellent physical properties. It has become one of the most used plastics in automobiles, but its shortcomings such as low temperature brittleness has limited its application in bumpers. Furthermore, polypropylene car bumpers will age due to weather factors such as light, temperature, and humidity during service. For instance, to study the aging mechanism of polypropylene automobile bumper materials, [21] selected artificially accelerated aging methods to age the bumpers, and analyzed the weather resistance of the materials by comparing the changes in the appearance and mechanical properties of the materials before and after aging. The results show that the toughness of polypropylene car bumpers deteriorates after aging.

Zhang Haiyang et al [21] also discussed two commonly used fiber-reinforced composite materials for body structure—long glass fiber reinforced polypropylene composite material (LGFT) and continuous carbon fiber reinforced epoxy resin matrix composite material (CFRP) on the bumper anti-collision beams of automobiles' lightweight applications. The preparation of LGFT and CFRP materials and related mechanical performance tests were carried out, and the relevant parameters of finite element simulation analysis were obtained based on experiments and reverse analysis. Taking an aluminum bumper anti-collision beam of a certain car model as a prototype, LGFT and CFRP composite materials with

equal stiffness were designed. Comprehensive analysis was conducted on crashworthiness and lightweight performance of the composite bumper anti-collision beams relative to the aluminum anti-collision beam. The results show that LGFT and CFRP anti-collision beams have a significant lightweight effect when meeting the requirements of crashworthiness. Compared with the original aluminum bumper anti-collision beams, the mass is reduced by 11.2% and 46.1% for LGFT and CFRP, respectively. Therefore, under the condition of equal stiffness requirements, fiber-reinforced composite materials can better realize the lightweight requirements of automobile bumper anti-collision beams. However, the failure mode of carbon fiber reinforced composites is more complex, and the load-bearing performance is not stable [21].

As can be seen from the above, while there are many solutions to reducing injuries to people in accidents, all the materials used have some unavoidable drawbacks, whether they be metal, plastic, fiber-reinforced or concrete. Most notably, in the event of an accident these would probably fail and need to be replaced, which could be very expensive and not environmentally friendly. Therefore, reusable metamaterials would be desirable for this purpose.

As can be seen from the above discussion, both earthquake disasters and vehicle impact events can take people's lives and damage or destroy property very suddenly, and search for a metamaterial for the purpose of isolation is potentially very useful. The linear theory of vibration isolation is detailed in [22]- [25]. References [26]- [28] describe a linear vibration isolator, called dynamic anti resonance vibration isolator, which will activate when the inertial force generated by the lever mass offsets the spring force. The inertial force generated by the lever mass leads to an increase in the effective mass of the system, so the resonant frequency decreases, and the isolator is able to work in a lower frequency range. This type of isolator has been used for helicopter rotor isolation and floor machine isolation [29]- [34]. Linear isolators only work when their natural frequency is well below the excitation frequency. Therefore, they are limited to moderate environmental disturbances. Under severe environmental disturbances such as shock, shock loading or ground

motion, their frequency spectrum will certainly also contain dangerous low frequency components. Under these conditions, the isolator can exhibit excessive deflection, which can cause excessive stress on, or even damage to, the system. Therefore, efficient nonlinear isolators must be considered as these can serve a variety of applications such as isolation equipment installed on ships in which may encounter heavy seas and extreme waves. Protect buildings, bridges, liquid storage tanks, oil pipelines, and nuclear reactor plants from the destructive effects of earthquakes. Non-linear isolators can protect insulated electronics, cooling systems at the front of equipment that should be protected from shaking, and passengers from uneven surfaces [35]. Due to the urgent need to protect structural devices, nuclear reactors, mechanical components, and sensitive instruments from seismic ground motion, shock, and shock loads, nonlinear vibration isolation theory has seen significant development. [35] demonstrates the latest development of nonlinear vibration isolators without active control, which do not involve other linear or nonlinear damping means. Firstly, the basic concept, characteristics and inherent phenomena associated with nonlinear of nonlinear isolator are introduced, and then the specific types of nonlinear isolators, including an extremely low frequency isolator, are discussed.

Ref [36] proposed a new type of high-performance ship equipment impact protection device composed of multi-layer negative stiffness cosine curved beam connections. The impact resistance mechanism is based on the nonlinear mechanical properties of the cosine-shaped curved beam rigidly fixed at both ends under transverse load. The results show that the proposed impact isolation device has excellent performance, and as the number of layers of negative stiffness beams is increased, the impact resistance is enhanced.

Structures that can change stiffness, and are environmentally friendly and reusable are the first choice for shock-absorbing structures.

Quasi-zero stiffness isolation is such a nonlinear system that has to be mentioned in terms of shock absorption. Inspired by the negative stiffness characteristics of origami metamaterials, Shiwei Liu et al [37] provides the idea of a special QZS

isolation system. According to the geometric relationship of folding angles, the influence of the structural parameters on the stiffness was studied, and the negative stiffness mechanism of the origami mechanism was revealed. The simulation results show the effectiveness and advantages of the proposed origami vibration isolator. The proposed vibration isolation system has great design flexibility and shows great potential in the field of low frequency vibration isolation.

Due to the particularity of its own structure, the quasi-zero stiffness vibration isolation system is more widely used in low-frequency vibration isolation than the traditional linear vibration isolation system when the system parameters are ideally designed. But because it belongs to a nonlinear system, a change of system parameters may change the vibration isolation equipment from small amplitude to large amplitude, which is not conducive to the normal operation of the equipment [38].

Ref [39] designed a new passive quasi-zero stiffness vibration isolator (QZS-VI) and analyzed its static and dynamic mechanical properties. After designing a novel V-shaped lever, leaf spring and cross-shaped structure combination (VL-PS-CS) vibration isolation platform, the researchers constructed a nonlinear QZS-VI by paralleling VL-PS-CS and coil springs. QZS-VI achieved excellent high static and low dynamic stiffness and nonlinear friction performance.

Vibration isolation systems with quasi-zero stiffness properties have been widely studied because of their high static stiffness and low dynamic stiffness. However, the effective displacement range of QZS is usually small, which greatly limits its application in practical engineering. It is difficult for sensitive equipment in engineering applications to be free from the interference of vibration or shock, so isolators need to be installed to improve the anti-interference capability of the equipment. Due to their limited vibration isolation and impact resistance capacity, it has become more and more difficult for passive isolators to meet the higher requirements of vibration isolation and impact resistance in complex environment. However, the practical application of active control isolators is limited because of their high energy consumption and high cost. Between the two, semi-active control

isolators need less external energy to provide excellent vibration control, and is more stable than active control; Moreover, when working in a wide frequency range, a semi-active control isolator's performance is more flexible than passive control [40]. The necessary innovation is to try to expand the effective displacement range of the QZS system through a semi-active control strategy. Guilin et al [40] designed and analyzed a QZS system with a slanted spring structure. The dynamic stiffness of the system is directly related to the initial inclination of the spring, and a semi-active control method with a displacement feedback control strategy is proposed. Compared with the linear system, the proposed new system has better vibration isolation, especially in the low frequency band.

Systems subjected to impact and impact loads will exhibit severe vibration, and they need special isolation devices. Impact loads are encountered in many mechanical applications, and in order to protect a given object from these disturbances, a vibration protection system is placed between the vibration source and the object. Alabuzhev et al. [41] introduced some quasi zero stiffness vibration isolation systems; this type of vibration isolator has been used for vibration isolation of vehicles [42], shock-action hand-held machines [43]- [45], railway vehicle suspensions and operator seats [46] [47].

while the available isolators are good for machinery and for isolation from horizontal earthquakes, for vertical earthquakes there is a problem. The structure needs to be able resist gravity force due to self-weight and movement of people and furniture without moving much, in an earthquake it needs to be able to let the ground move and minimize force from passing to the building. This means the isolator must have non-linear force-displacement relationship and the QSZ isolators offer a possible solution in such cases. There have been a number of papers in this area in recent years and even after commencement of this thesis work there have been new papers [47] - [50], but as far this author is aware they are all on single isolator mechanism and do not include a metamaterial with a series of such mechanisms embedded in a matrix.

Mehran Shahraeeni et al [47] focuses on the effect of damping nonlinearity on its dynamics and performance. Quasi zero stiffness (QZS) isolators are usually studied using linear damping elements because they take advantage of stiffness nonlinearity. Mehran Shahraeeni et al [47] simulated a horizontal spring-type quasi-zero stiffness isolator with geometrically nonlinear damping, which provided basic insights for the design of a QZS isolator with geometric nonlinear damping. The results show that the vertical damper provides pure linear damping, the horizontal damper provides the necessary nonlinear damping.

This is why recent papers have a focus on non-linear isolators. This thesis contains the results of an investigation into how a metamaterial can be developed for this purpose and the mechanism used in a single cell of the metamaterial is similar to the ones used in recent references but with the addition of a matrix and without damping. The scope of this research is limited to studying the non-linear force displacement relationship only and before its implementation further work is needed to consider the effect of mass and damping in a full vibration analysis.

1.3 Goals of the project

In order to reduce the transmission of forces during an accident or earthquake, a flexible material is needed. However, during normal operations, a building or a car door need to be stiff as otherwise unwanted displacements (building wobbling when people walk, or car door buckling when opened) can take place. In equilibrium, the material should be stiff, but when subject to large forces it needs to become flexible. So, a metamaterial with an adaptive stiffness is thus suitable.

Therefore, the overall goal of the project is to design a metamaterial with this adaptive stiffness characteristic, taking into account the various structural arrangements composed of different materials.

While the ultimate aim would be to use renewable resources (for example natural fibers), in order to demonstrate the concept of this method, the scope of the project is limited to using a combination of different materials to develop a metamaterial that will minimize transmission of forces when it is subject to deformations away from the equilibrium position.

The metamaterial consists of a repeating arrangement of cells, with each cell containing flexible elements such as springs and a matrix made up of low elastic modulus and rigid elements (reinforcements) that carry most of the load. The concept will be developed with a mathematical model. The performance of the model was evaluated where possible analytically or by using a Finite Element Software package called ANSYS.

At the beginning of the project, experimental work was planned but due to COVID-19 restrictions and the author having to take a year off (not being able to travel back to New Zealand) and then resuming work remotely, it was not possible to conduct any functional experiments. Some preliminary experimental work carried out to investigate the suitability of different materials is reported in Appendix A, but it has not been possible to progress further along this line.

2 Concept and theory of an adaptive stiffness metamaterial cell

2.1 Description of the cell

A metamaterial for this purpose includes a matrix of very high flexibility, and a number of structures (frames that behave like mechanisms) of identical shape. These structures have the potential to be highly flexible as well, but only when large dynamic displacements are caused away from the static equilibrium position. The individual structural units are referred to as cells.

The matrix retains the cell arrangement but is not intended to carry much load, which is taken by the cells. The ultimate purpose of the cell is to reduce cell stiffness with displacement. As the force increases, the compressive stress in the frame in the direction perpendicular to the loading increases, and this reduces the stiffness of the overall structure, similar to the effect of compressive force reducing the lateral stiffness of beams. This is called geometric stiffness or geometrical stiffness [51] because it depends on geometry and compression rather than material properties.

As the angle of rigid components in the mechanism measured from an axis perpendicular to the loading decreases, the ability of the components to axially restrain vertical forces decreases. Thus, these mechanics provides the stiffness that decreases with load, which is required for this metamaterial.

A single unit of the mechanism is shown in Figure 4. This will be called a metamaterial cell. The angle referred to in the previous paragraph is labeled θ In this figure. Later, some of these units of cells are embedded in the matrix to form metamaterials as shown in Figure 33.

There are two factors that affect the performance of the cell, one is the initial angle θ and the other is the ratio of K_v and K_h. The following section gives the relevant derivations.

2.2 Analysis of a single cell

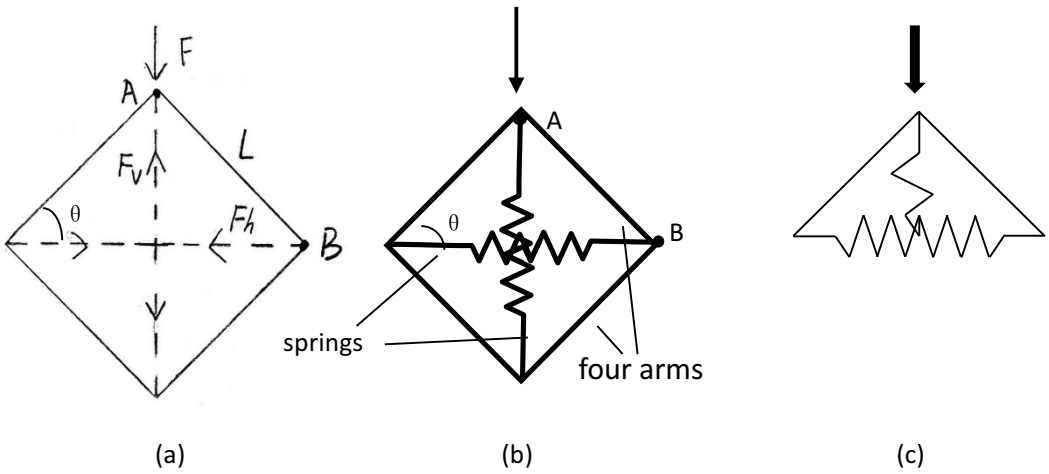

Figure 4：Single structure

The analysis of this single cell mechanism is similar to the ones available in the literature for such non-linear isolators, but the author derived these from first principles, to understand it better. Both the force and displacement are given in terms of the angle of inclination of the arms. A force analysis was performed on this structure. In Figure 4 (a), the black solid lines represent the fibers which are embedded in a matrix such as resin (which is not shown). The broken lines indicate the equivalent lateral and longitudinal forces (from the resin). Figure 4(c) is a schematic of the upper half of the structure, which is used in the subsequent MATLAB analysis.

For lateral force is F_h, and $K_h$represents the stiffness. Similarly, for the longitudinal force F_v, K_v represents the stiffness. The subscripts v and h were initially chosen to indicate the directions of gravity force (vertical) and the one perpendicular to it but in general v refers to the direction of the external force and h is the direction of the induced compression that helps to reduce the stiffness, and these may be considered as lateral and longitudinal.

Consider the equilibrium of Point A in Figure 4 by using the free body diagram in Figure

5.

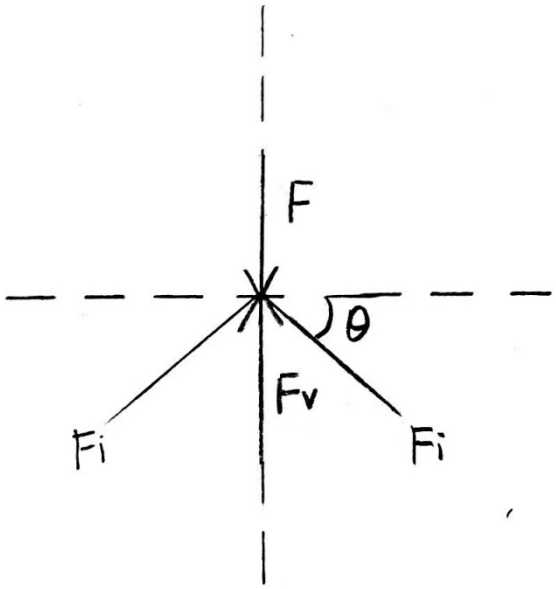

Figure 5：Free-body diagram of the point A

For equilibrium,

$F = F_v + 2F_i \sin\theta$ (1)

Consider the equilibrium of Point B in Figure 4 by using the free body diagram in Figure 6.

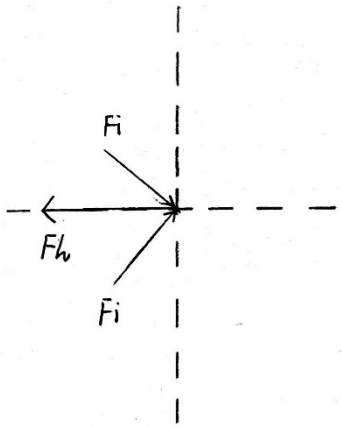

Figure 6：Free-body diagram of the point B

$F_h = 2F_i \cos\theta$ (2)

Put (2) into (1)

$$F - F_v - F_h \tan\theta = 0$$

$$F = F_v + F_h \tan\theta \quad (3)$$

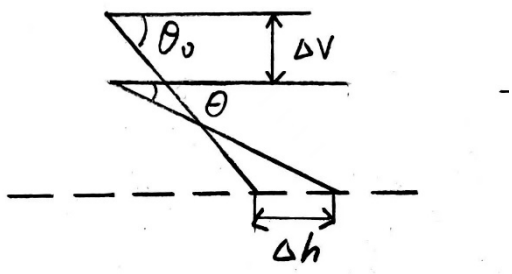

Figure 7: Analytical displacement

$$\Delta_v = L\sin\theta_0 - L\sin\theta \quad (4)$$

$$F_v = K_v\Delta_v = K_vL(\sin\theta_0 - \sin\theta) \quad (5)$$

$$F = K_vL(\sin\theta_0 - \sin\theta) + F_h\tan\theta \quad (6)$$

$$F_h = K_h\Delta_h = K_hL(\cos\theta - \cos\theta_0) \quad (7)$$

$$F = K_vL(\sin\theta_0 - \sin\theta) + K_hL(\cos\theta - \cos\theta_0)\tan\theta \quad (8)$$

Equations (4) and (8) are used to obtain the force displacement curves using a MATLAB code with different points chosen by varying the parameter θ.

These are valid for a mechanism shown in Figure 4 only. If only the top half is considered then the term K_h should be multiplied by 2.

3 MATLAB Results

The system in Figure 4(c), half of the structure, is the one used in the process of MATLAB analysis.

In the MATLAB results section, the influence of several different factors on the force-displacement curves is discussed, such as initial angle of rigid components, horizontal stiffness and vertical stiffness.

In order to get a stiffness that is initially large and decreases as the force increases, the curve of force-displacement has to rise initially and then its slope should decrease as the force increases. Therefore, the ultimate goal of this part of the discussion is to find the curves of force-displacement that can achieve the ideal state with the best coordination of initial angle, and horizontal and vertical stiffness. It is also important to make sure that the total stiffness does not become negative as this would make the system unstable.

In order to scientifically analyze the experimental results, control variables are used. First of all, the horizontal and vertical stiffness remains consistent, and different initial angles are changed to compare the curves of force-displacement in order to understand how the behavior changes with angle and, if possible, to find the most appropriate angle.

Then the initial angle and horizontal stiffness are controlled (remain unchanged) and the value of vertical stiffness is varied. This is used to compare the results of graphs of forces-displacements due to different vertical stiffness. Similarly, the comparison diagram of horizontal stiffness is obtained by controlling the initial angle and vertical stiffness.

3.1 Curve of force and deformation of the full structure

We assume that the values of K_v and K_h are both 5000. According to formula (7), it is assumed that L = 100 centimeters.

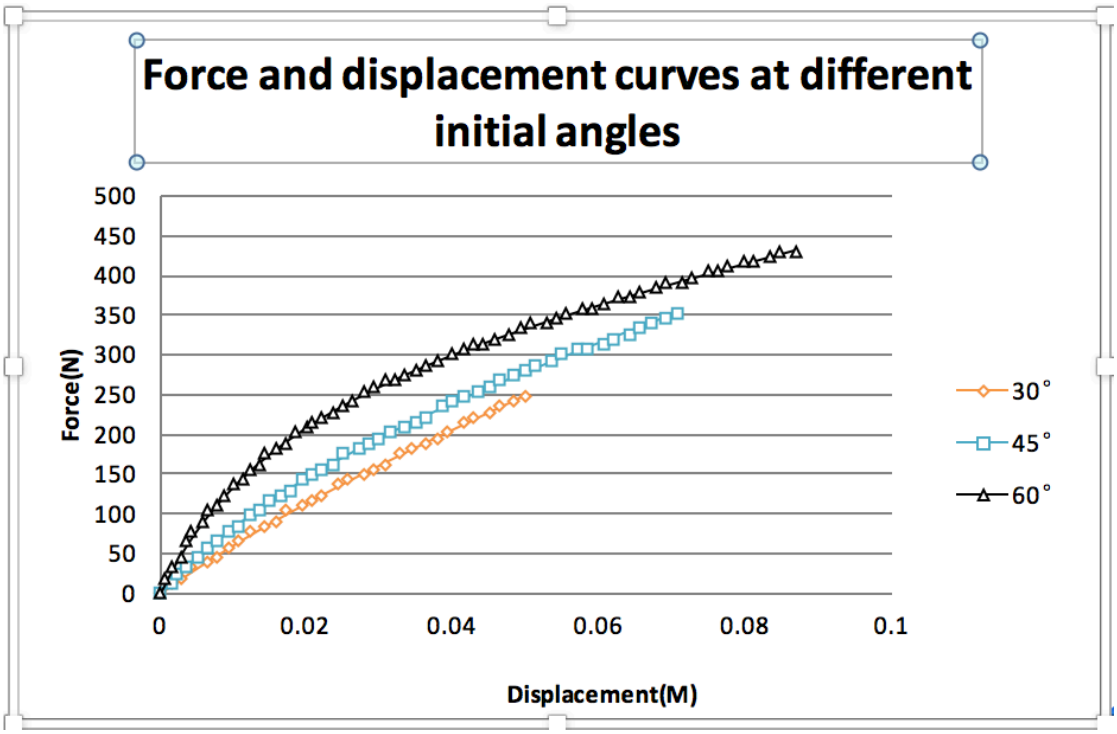

Figure 8: Force-displacement curves at different initial angles for K_v=5000 and K_h=5000

Figure 8 is the curve of force-displacement at different angles when both K_h and K_v are 5000.

From the comparison of the three force-displacement figures, it can be seen that the trends for initial angles of 30 degrees and 45 degrees are similar, almost straight, which means that the slope (stiffness) is almost constant. But this is not a desired result. The goal of the experiment is to change the stiffness during structural deformation. However, when the initial angle is 60 degrees, the situation changes. In the force-displacement diagram, the curve gradually becomes flat, which indicates that the stiffness changes. This is a very interesting situation because it means that the overall stiffness of the structure has changed significantly. From Figure 8, it can be judged that a larger initial angle makes the test material functions have the characteristics of a metamaterial.

Subsequently, in order to observe which of K_h and K_v can affect the experimental results more, different values of K_h and K_v were assigned, while keeping one or the other and the initial angle constant.

Figures 9 to 11 are the results obtained by changing the value of K_v when the constant K_h value is 5000 at initial angles of 30, 45, and 60 degrees, respectively.

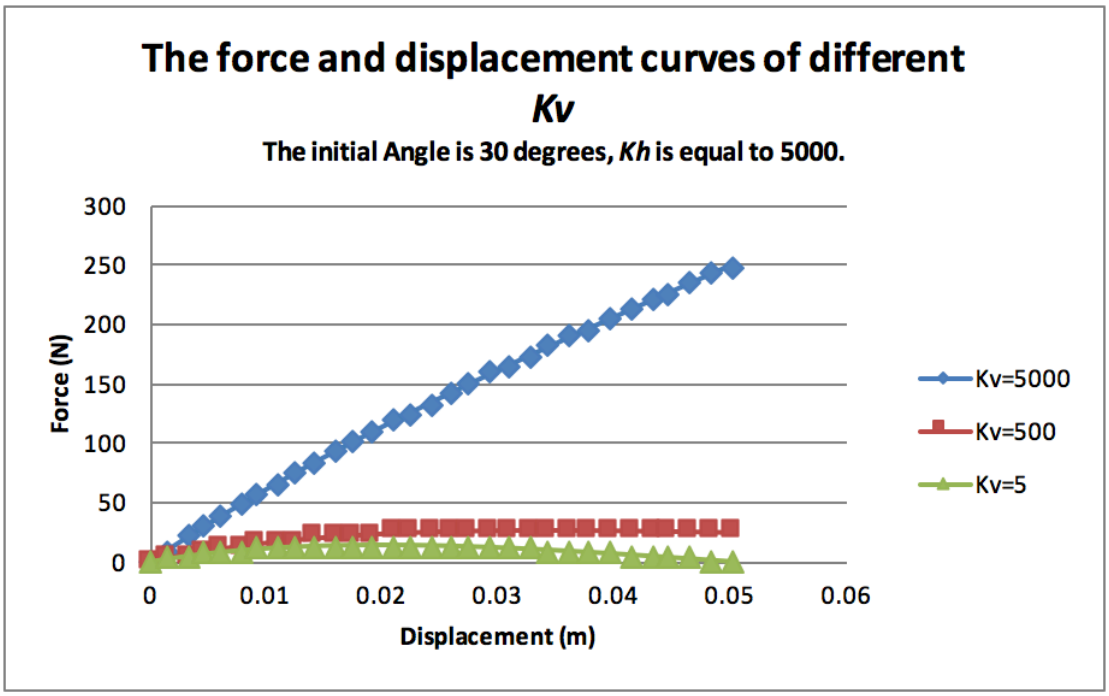

Figure 9: Force-displacement curves at different K_v at K_h=5000 and 30 degrees.

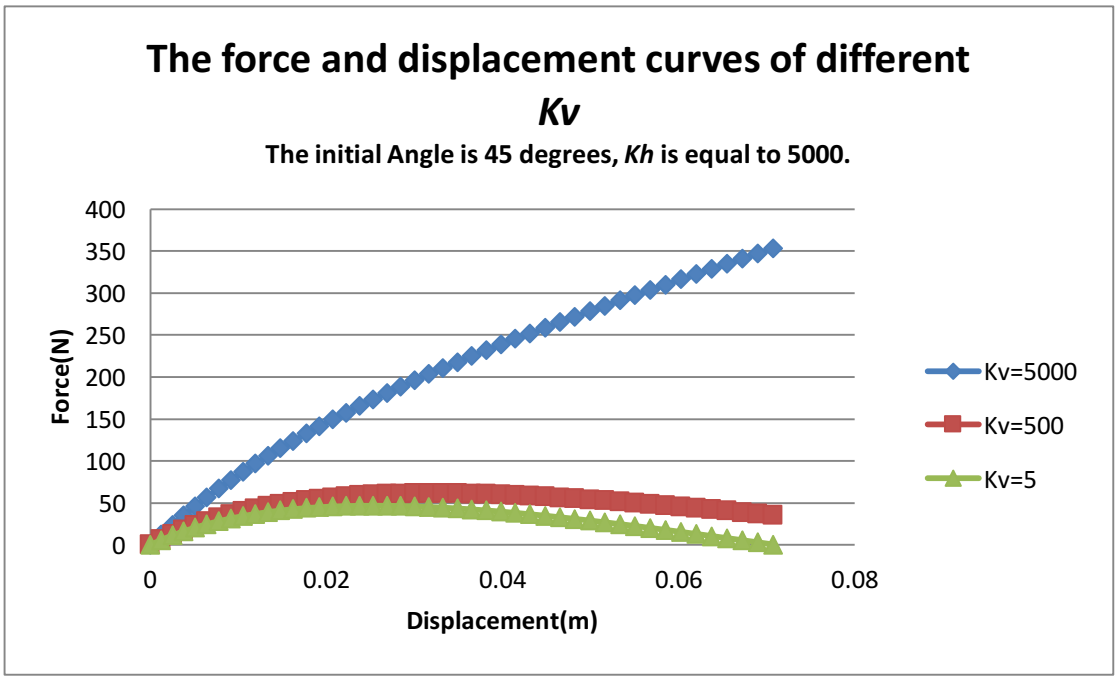

Figure 10: Force-displacement curves at different K_v at K_h=5 000 and 45degrees.

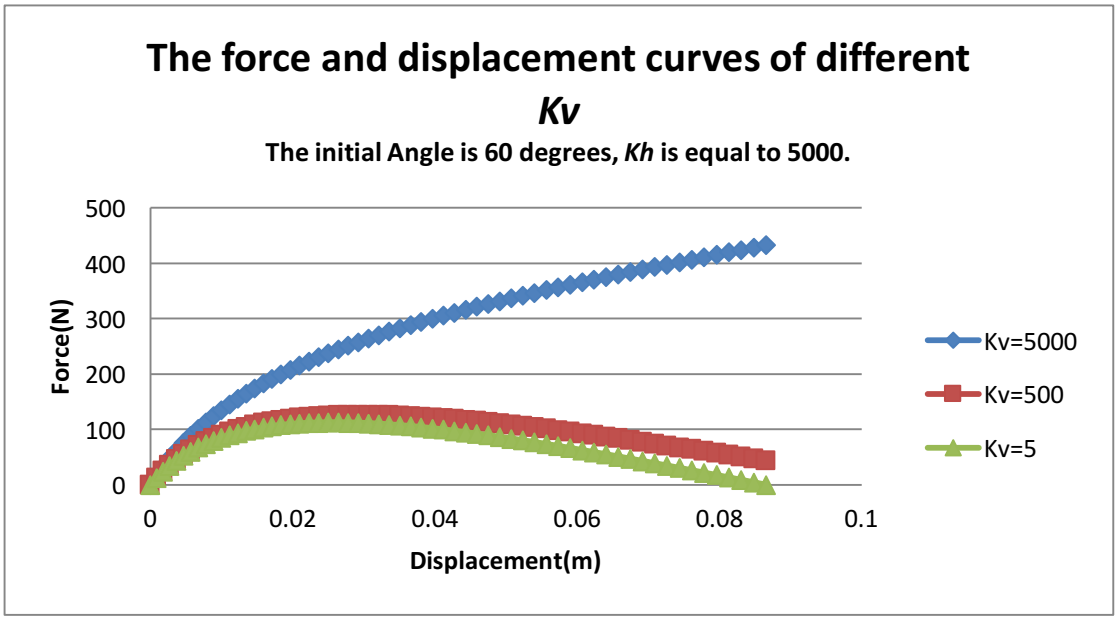

Figure 11: Force-displacement curves at different K_v at K_h=5000 and 60 degrees.

It can be clearly seen from these three graphs that no matter what the initial angle, when K_v is less than K_h, the more obvious is the change in the straightness of the graph, which indicates a change in stiffness. When the slope of the graph becomes negative, the stiffness is negative, which implies the structure has become unstable. The change in stiffness is the desired result, and the best state is that the stiffness is very high at the beginning and then reduces to 0.

However, stiffness should not be allowed to become negative because the structure will then change from a stable state to an unstable state. This means that although the overall structural stiffness has changed greatly when the K_v is smaller, the structure may reach an unstable state in the later stages, which should be avoided.

It would be desirable if the structure could be used repeatedly (a subsidiary aim of this study). With this aim in mind, stiffness should become lower to reduce force transmission, but it should not be close to zero as this would lead to result in very large displacement and could lead to instability.

Figures 12 to 14 are the results obtained by changing the value of K_h when K_v has a constant value of 5000 at initial angles of 30, 45, and 60 degrees, respectively.

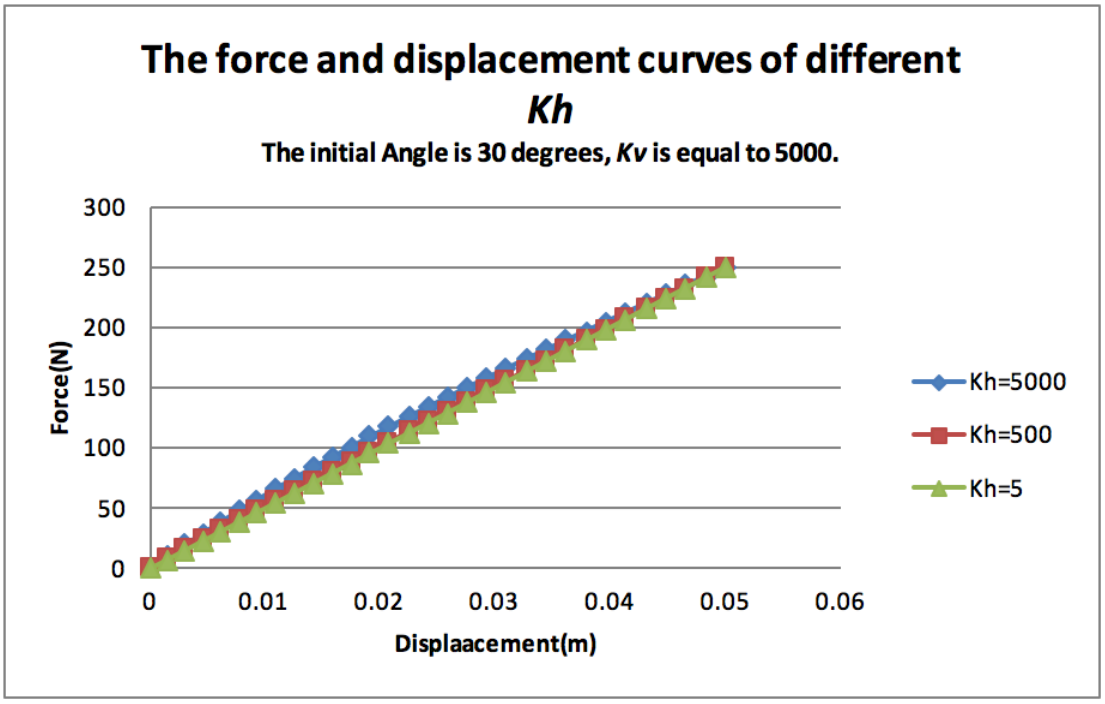

Figure 12: Force-displacement curves at different K_h at K_v=5000 and 30 degrees.

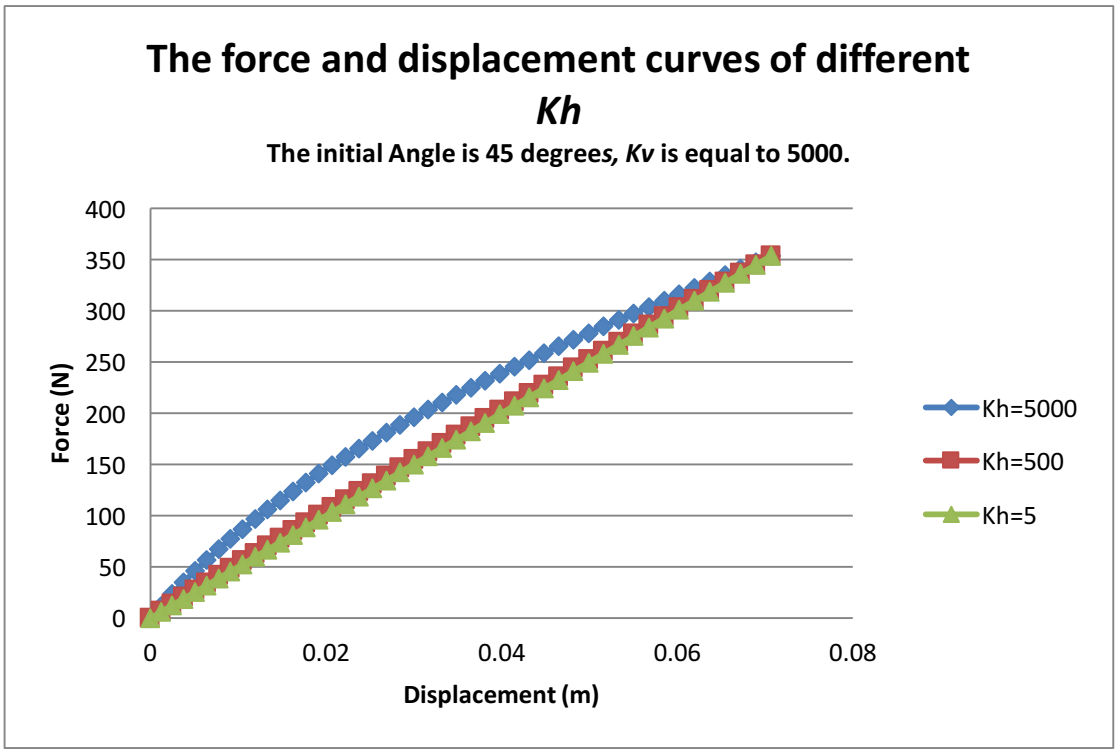

Figure 13: Force-displacement curves at different K_h at K_v=5000 and 45 degrees.

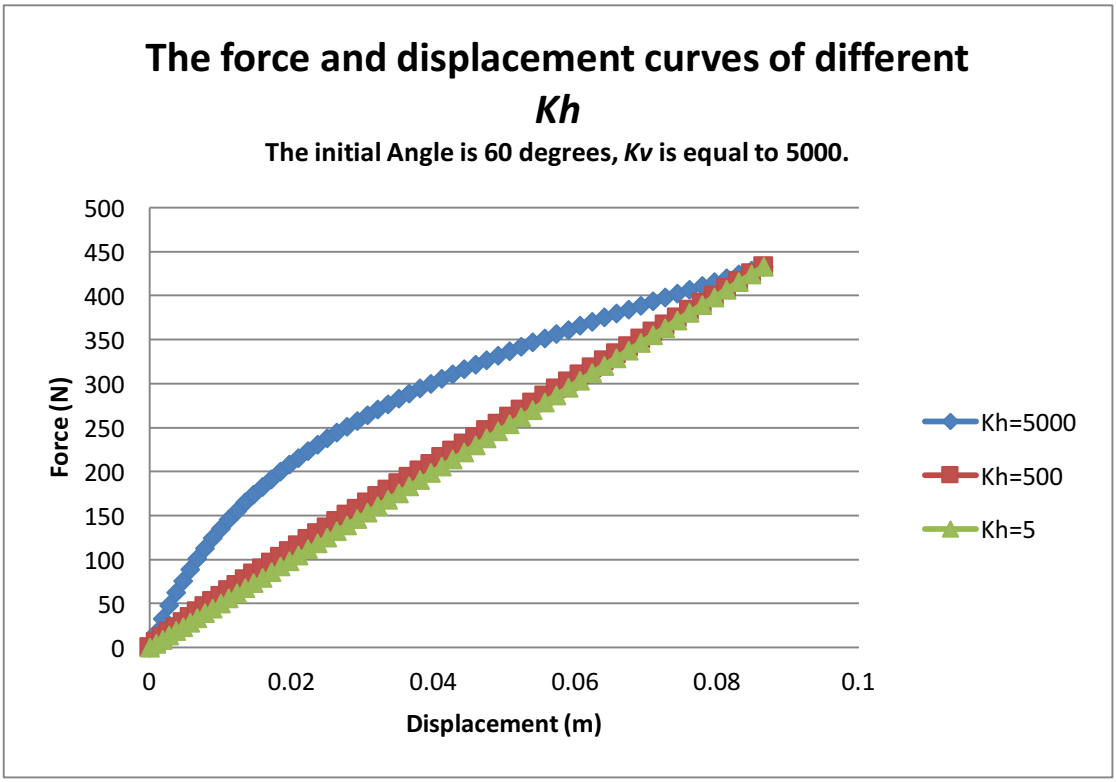

Figure 14: Force-displacement curves at different K_h at K_v=5000 and 60 degrees.

It can be concluded from these three graphs that regardless of the angle, the larger the K_h of the structure, the more it meets the requirements that stiffness decreases with displacement, which also confirms the relationship between K_h and K_v: When K_v is small or K_h is large, the state of the structure is more in line with the results expected for variable stiffness.

3.2 Curve of force and deformation of half structure

It was recognized that the results could be obtained by only considering half of the structure using symmetry. Figure 15 shows the MATLAB analysis of a half structure, and the same method for controlling variables.

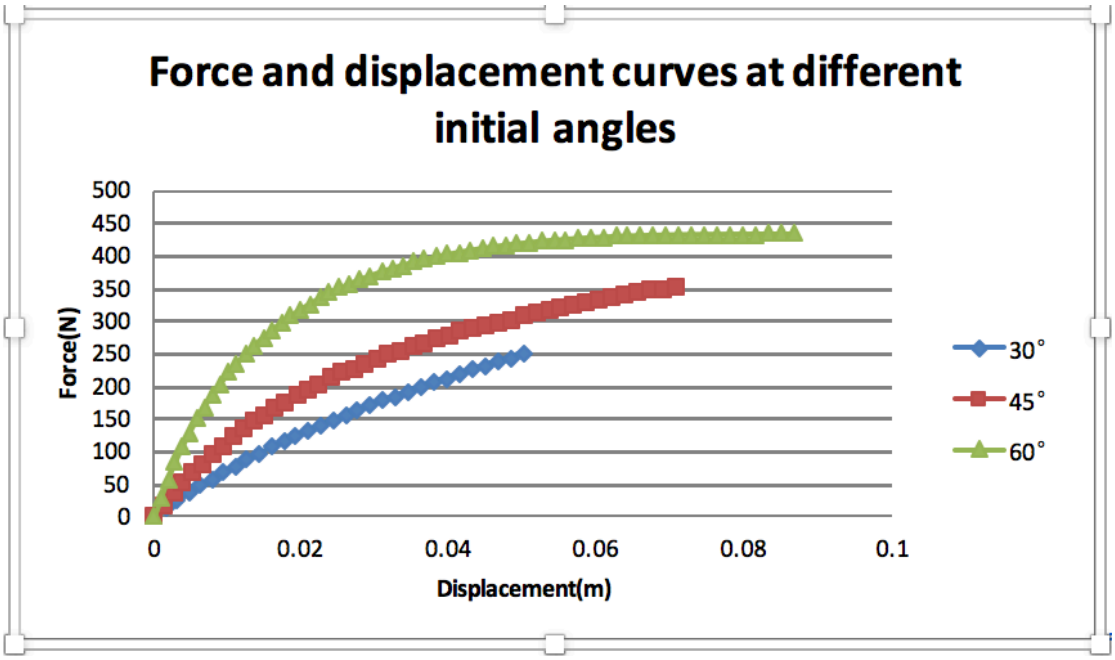

Figure 15: Force-displacement curves at different initial angles K_v=5000 and K_h=5000.

Figure 15 is the curve of force-displacement at different angles when both K_h and K_v are 5000.

As with the analysis result of the entire structure, the larger the angle, the more obvious the change in structural stiffness.

What can be seen from this figure is that the results for half the structure and the whole structure are consistent as expected.

Subsequently, the control variables of K_h or K_v were analyzed. The same parameters were set, and the results obtained for the half structure were consistent with those obtained for the full structure. Consequently, the graphs and discussion are similar, so they do not need to be repeated.

As with initial angle variable and *K* values constant, the force and displacement curves of half the structure are consistent with those of the whole structure. As can be seen

from these comparison graphs, the result is the same when K_v is much smaller than K_h no matter what the angle is. It is not difficult to find from the process that the premise of data change is to control some variables, so the ratio of the two stiffness can simplify the existence of a variable. Either $\frac{K_v}{K_h}$ or $\frac{K_h}{K_v}$ can be considered, one of them is selected here for demonstration. It was then decided to consider the force-displacement relationship for different values of the ratio of $\frac{K_v}{K_h}$, and under the premise of controlling variables (keeping another stiffness value constant), it is found that a difference in the actual value of stiffness does affect the shape of the curve, so this means that the most critical factor is actually the ratio.

The ratio of K_V and K_h

Figure 16 and Figure 17 show the force-displacement curves at the same ratio of $\frac{K_v}{K_h}$

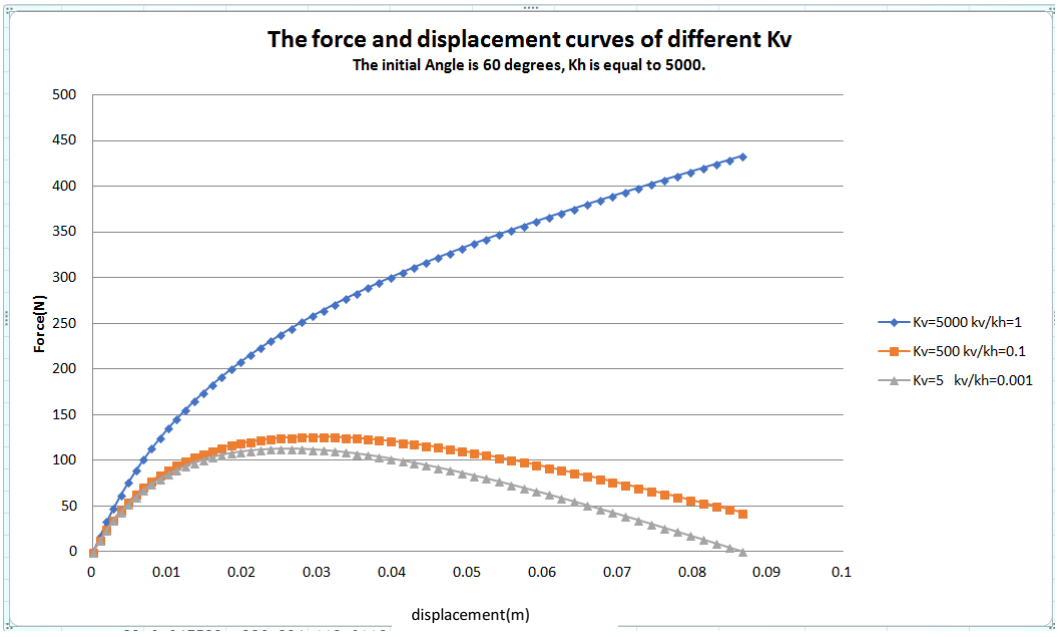

Figure 16: Force-displacement curves at different $\frac{K_v}{K_h}$.

K_h in Figure 16 is 5000, and K_v of the three curves is 5000, 500 and 5 respectively. This means that $\frac{K_v}{K_h}$ values are 1, 0.1 and 0.001, respectively.

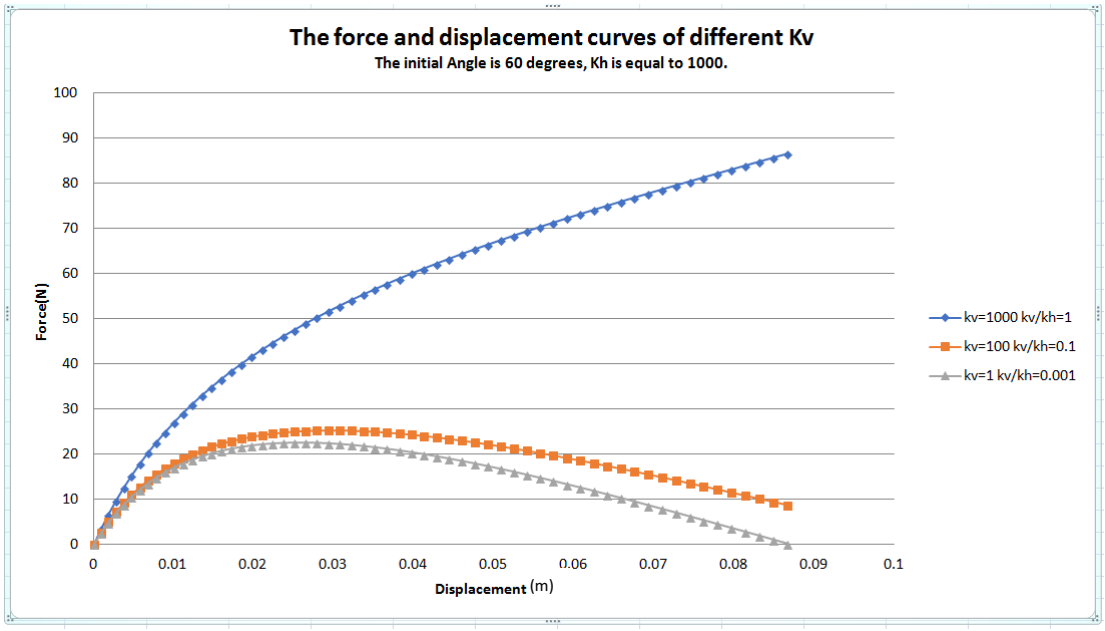

Figure 17: Force-displacement curves at different $\frac{K_v}{K_h}$.

K_h in Figure 17 is 1000, and K_v of the three curves is 1000, 100 and 1, respectively.

This means that $\frac{K_v}{K_h}$ values are 1, 0.1 and 0.001, respectively.

By comparing Figures 16 and 17, it can be seen that the two figures have different values of K_V and K_h, but the changing trend of the figures is consistent.

There may be different values for K_V and K_h, but the ratio of $\frac{K_v}{K_h}$ is the same, which proves that the most critical factor is the ratio rather than a single value of either *K*. The shape of the curves of force-displacement for any given initial angle is affected only by the ratio of K_V and K_h, and the best result for non-linear variation occurs when this ratio is as low as possible.

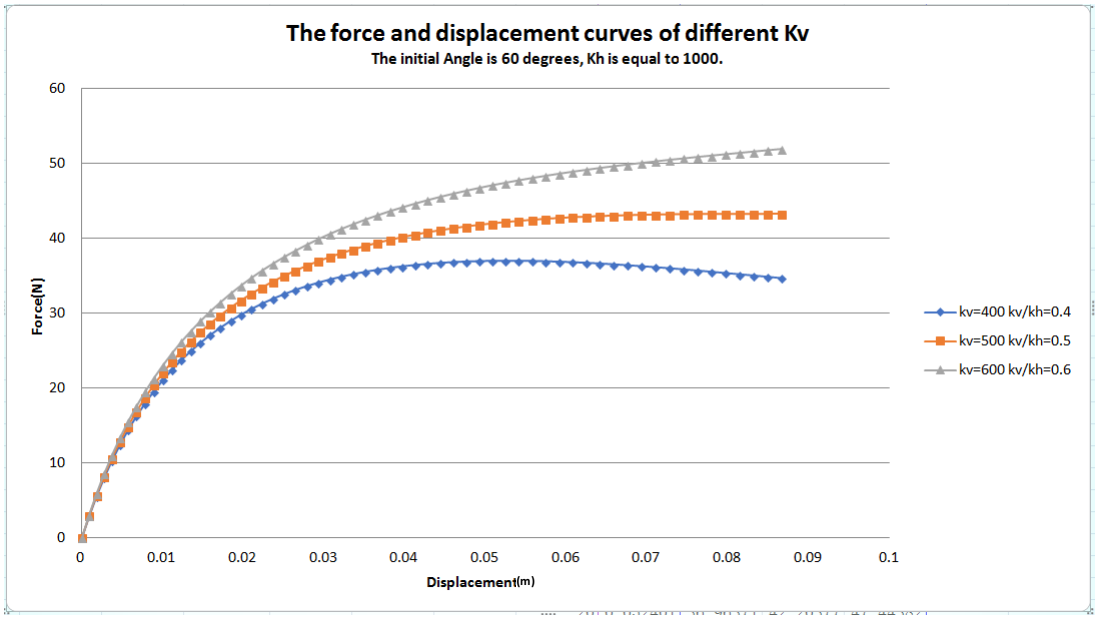

Figure 18: Force-displacement curves at different $\frac{K_v}{K_h}$

Figure 18 explores what ratio can achieve better results. It can be seen from Figures 17 and 16 that no matter what the specific values of K_v and K_h are, a ratio between 1 and 0.1 will have better stiffness changes. Therefore, after further exploration, a target ratio was set between 0.4 and 0.6. The results obtained are shown in Figure 18. When the ratio is 0.5, the slope (stiffness) of the latter part of the curve is close to 0. If the ratio is higher than 0.5 the system becomes unstable. A lower ratio means less nonlinearity, so 0.5 is the best value for nonlinearity.

Initial Angle

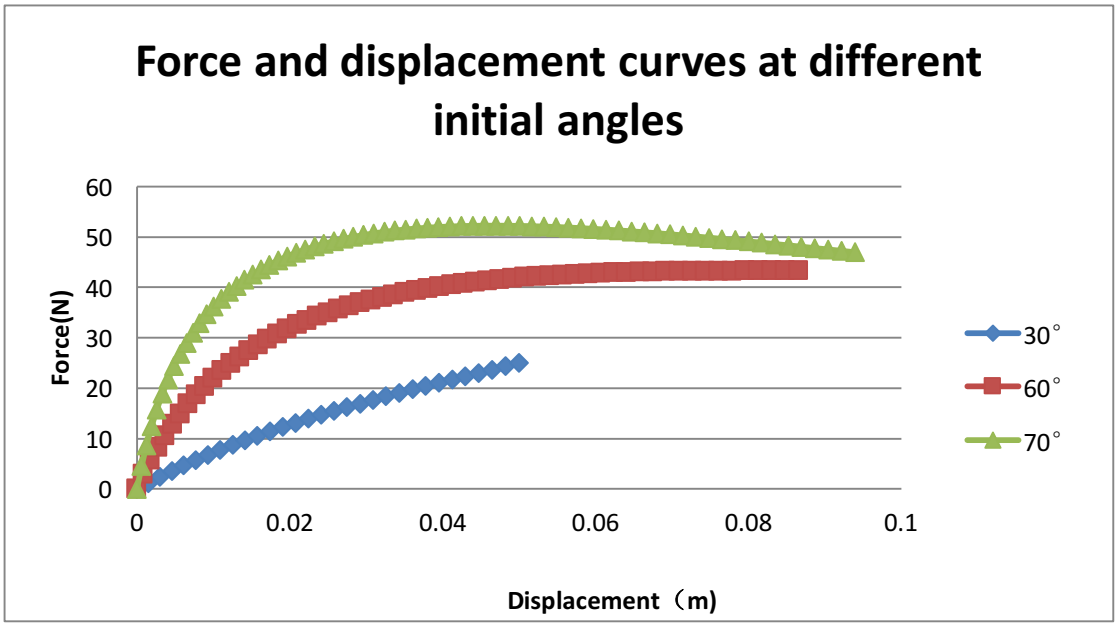

Figure 19: Force-displacement curves at different initial angles

This is a graph identifying which initial angle is the best angle when the ratio of $\frac{K_v}{K_h}$ is constant at 0.5. It can be seen from the figure that if the angle is too small, the nonlinear stage cannot be reached, while if the angle is too large, the system will eventually become unstable. So, 60 degrees is chosen as a suitable angle when $\frac{K_v}{K_h}$ is 0.5.

This can also be proven using the following theoretical derivations, which the author carried out only after getting the numerical results presented above, but it explains how the best ratio of the stiffnesses can be calculated. As the displacement and force are both expressed in terms of θ chain rule is used to find the stiffness.

Let $\Delta v = y = Lsin\theta_0 - Lsin\theta$

$$F = K_v L(sin\theta_0 - sin\theta) + K_h L(\cos\theta - cos\theta_0)tan\theta$$

$$\frac{dF}{d\theta} = -K_v L\cos\theta + K_h L\left(\cos\theta - \frac{cos\theta_0}{cos^2\theta}\right)$$

$$\frac{dy}{d\theta} = -L\cos\theta$$

$$\frac{dF}{dy} = \frac{dF}{d\theta} \times \frac{d\theta}{dy} = \frac{= -K_v L\cos\theta + K_h L\left(\cos\theta - \frac{cos\theta_0}{cos^2\theta}\right)}{-L\cos\theta} = K_v - K_h(1 - \frac{cos\theta_0}{cos^3\theta})$$

The best answer for the force-displacement curve is when $\frac{dF}{dy} = 0$

$K_v = K_h(1 - \frac{\cos\theta_0}{\cos\theta^3})$

If static equilibrium is at $\theta = 0$, $K_v = K_h(1 - \cos\theta_0)$

When $\boldsymbol{\theta_0} = 60°, K_v = \frac{K_h}{2}$

3.3 Discussion

This part belongs to the analysis of MATLAB. MATLAB is used because it can simulate the results of nonlinear equations under the premise of given partial conditions through formulas and is convenient when doing a parametric study. Through the force analysis of a single cell, the formulas relating the force, angle and stiffness were obtained. Therefore, the results in three different situations were analyzed, and the method of controlling variables was used. First, with the horizontal and vertical stiffness remaining the same, it was possible to find out what initial angle would be more suitable to obtain the results, which turned out to be 60 degrees. Then the best results for variable stiffness with an initial angle of 60 degrees was searched for. It was decided to limit the angle to 60 degrees as a further increase could make the system become unstable sooner, and in practice this reduced the distance between the two arms limiting the length of the horizontal spring. Then keeping the initial angle and horizontal stiffness constant, varying the vertical stiffness showed the effect of vertical stiffness on the force-displacement relationship. Then keeping the initial angle and vertical stiffness constant, the horizontal stiffness was varied to study its effect on the overall stiffness.

MATLAB image analysis showed that the greater the initial angle, the non-linearity increased. It was also found that the smaller the K_v, for a given K_h, the higher the range of non-linearity, and the opposite trend was observed when changing K_h, for a given K_v, the larger the K_h, the higher the non-linearity.

An improved analysis method was used to examine the relationship between K_v and K_h. A plot of the force and displacement using different ratios of $\frac{K_v}{K_h}$ showed that when the ratio is 0.5, the result is the best result for nonlinearity for the chosen angle of 60 degrees. The analysis presented later explains why this is the best ratio but in general the following equation gives the best ratio for any chosen angle

$K_v/K_h = (1 - \cos\theta_0)$

3.4 Summary

Whether the whole structure or half of the structure is considered, the force-displacement relationship for the metamaterial cell is consistent. Among the three angles with the same horizontal stiffness and vertical stiffness, 60° is thought to be the best angle. Generally, one can see that the higher the initial angle, higher the change in geometry, and therefore the best angle would the highest possible. However, practical implementation is likely to create limitations on this, and in this study the highest angle is chosen as 60°. When the horizontal stiffness and the initial angle are constant, a smaller vertical stiffness produces a more obvious the stiffness change. Similarly, when the initial angle and vertical stiffness remain unchanged, a greater horizontal stiffness produces a more obvious the stiffness change. Further analysis shows that the determining factor that controls the shape of the curve for any given initial angle is the $\frac{K_v}{K_h}$ ratio.

Thus, the analyses show that the lower the $\frac{K_v}{K_h}$, the closer the result is to the desired nonlinear behavior, and the larger the initial angle, the closer the result is to the desired nonlinear behavior. However, the ratio is limited to 0.5 to avoid instability.

4 Analysis discussion and results

A cell problem has been solved with MATLAB. But solving it with MATLAB would be very difficult if it was put into matrix to form a composite material, so ANSYS was used for further simulations.

In order to test the effectiveness of ANSYS, the results of analyzing a single cell were first compared with MATLAB to check whether the results are consistent and the ANSYS modelling is correct.

The completed comparison between MATLAB and ANSYS shows that both results agree fully. The subsequent simulation involving multiple cells and the addition of a matrix will be carried out using ANSYS.

In the subsequent ANSYS modeling, most of the settings are held the same; for example, the spring is the spring element; arms of all frame parts are truss elements; arms in frame structure are all structural steel; and all the matrix is Neoprene rubber. The variables are the different boundary conditions of each model, which are listed in the following sections of each model.

4.1 Comparison of the ANSYS and MATLAB results for a single cell

The horizontal and vertical stiffness of a given spring is used for comparison

The process is as follows: the stiffness value of the spring is given in ANSYS and analyzed in MATLAB. The MATLAB code enables easy calculation of the force for a given displacement as there is an explicit expression for this, but computing the displacement for a given force would involve finding the roots of a non-linear equation, so it was avoided. However, when using ANSYS the displacement can be computed for any given force quite easily. So, the force obtained from the MATLAB code for any given displacement is brought back to ANSYS and the corresponding displacement computed. The result agreed with the displacement input used in the MATLAB code. The force-displacement curves obtained using both methods were compared and analyzed. Figure 20 shows the ANSYS model of 1-Cell without matrix.

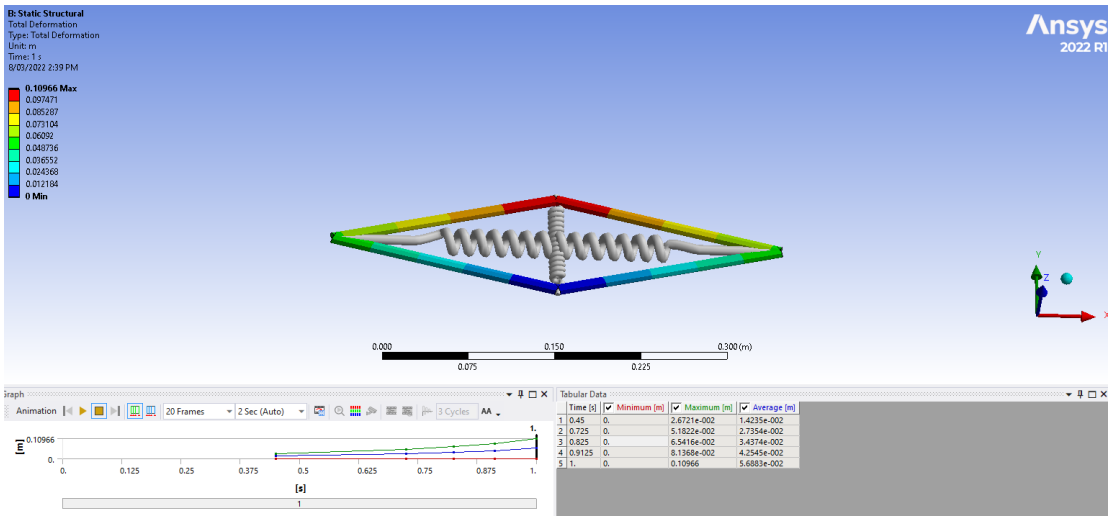

Figure 20: A cell with an initial Angle of 30 degrees

The colors in the graph are the way ANSYS represents the results of the modeling problem, and do not specifically represent the magnitude of the displacement in each segment. In fact, the arm should be a rigid body, and the force and displacement bearing force of each position should be consistent.

The boundary conditions are: the bottom point is the fixed point, the force is applied to the vertex, and the top point can only move up and down.

In a 30-degree (initial angle) structure, the inclined bar has a length of about 200 mm and a cross section of 10mm. The stiffness of the horizontal spring is 5000 N/m, and the stiffness of the vertical spring is 500 N/m.

The stiffness is entered into MATLAB to get the curve of force-displacement.

```
clear all

close all

Kv =1000;

Kh = 10000 ;

L = 0.2;

X = pi/6;

i = 1;

for i=1:30

    Y =i*pi/180;

F(i) = Kv*L*(sin(X)-sin(Y))+Kh*L*(cos(Y)-cos(X))*tan(Y);

y(i) = 2*L*(sin(X)-sin(Y));

end

plot(y,F)
```

Figure 21: MATLAB Running Process

L is length of arms;

k_v is Stiffness in the vertical direction;

k_h is Stiffness in the horizontal direction;

X in the figure is the initial Angle;

i is a parameter for the program to run;

Y is the Angle of change which means from the initial angle to 0;

y(i) is displacement from the initial angle to 0;

F(i) is force;

Because the upper and lower parts of cells are analyzed separately in MATLAB software, the stiffness that ANSYS produces needs to be multiplied by 2 in MATLAB. In addition, in order to facilitate the comparison with ANSYS results, the displacement of MATLAB needs to be doubled.

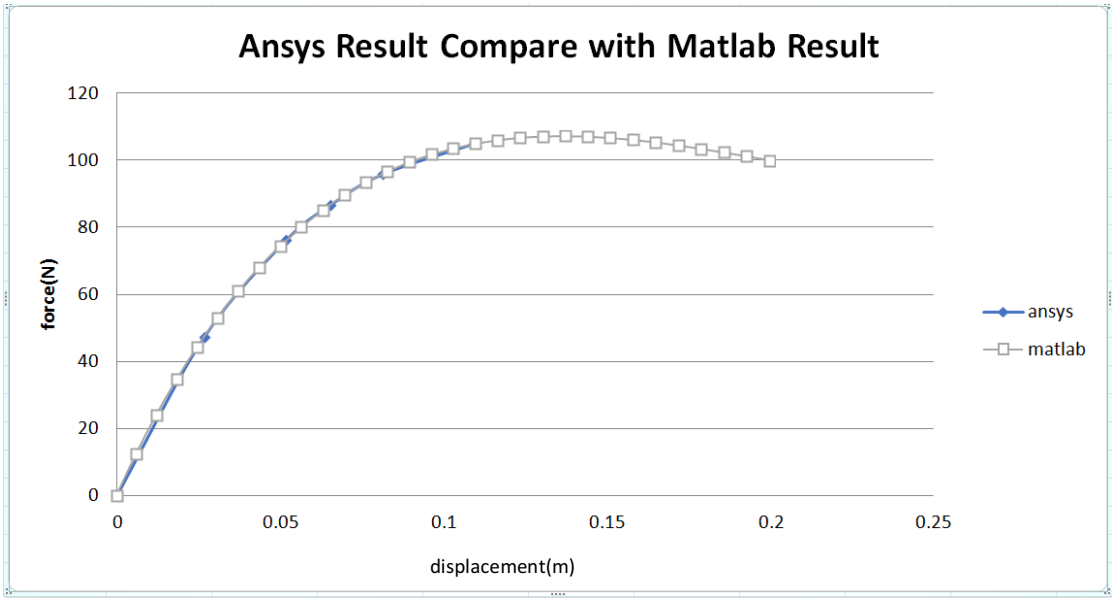

Figure 22: Force-displacement curves

In the figure, the blue line represents ANSYS results and the gray line is the result from MATLAB, and they are hard to distinguish because they are very consistent. The steel truss element appears to have acted as anticipated (as a rigid element). This means that ANSYS programs can take over the work of MATLAB, and it is easier to add multiple cells and matrix. It should be noted that ANSYS results are limited to about 0.11 m displacement (after which there are no ANSYS results) as the system becomes unstable beyond this point and ANSYS does not execute a solution.

4.2 Cells with springs

Initial modelling was done using bars of very small cross section because the author was unsure of how to incorporate springs into the model, but this caused numerical problems. However, once the problem was solved, horizontal and vertical springs were used in the model.

Figure 23 to 25 shows the simulation process and results of a single cell

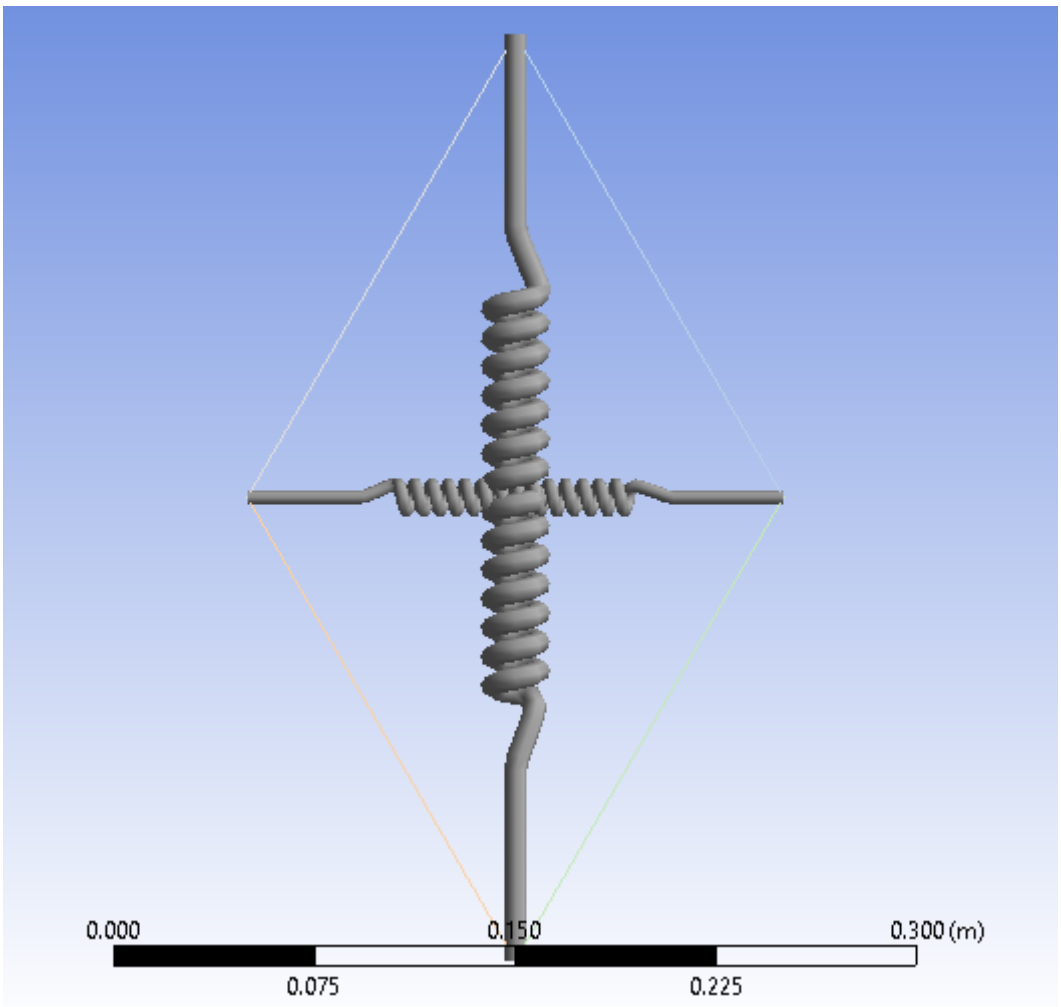

Figure 23: A single cell with springs

Figure 23 is the initial state of a single cell with springs. In this model, the initial boundary conditions are: the bottom point is the fixed point, the force is applied to the vertex, and the top point can only move up and down.

Angle of 60 degrees was chosen, with k_v= 500 k_h=1000, because the results obtained using MATLAB showed that these are best for obtaining the stiffness changes. As already mentioned, k_v brings better results if it is smaller than k_h. The

inclined bars still maintain the diameter of 10 mm, L=200 mm.

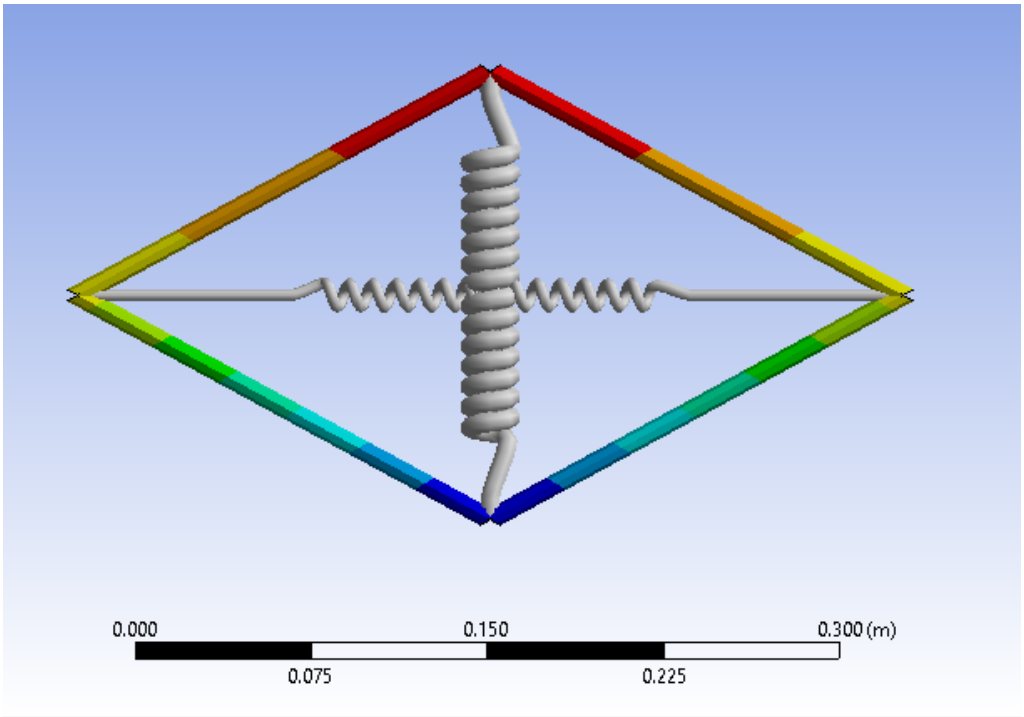

Figure 24: The final shape of the displacement on a single cell

Figure 24 is based on Figure 23 and the final shape is obtained by applying 160N pressure to the top. The horizontal spring is stretched and the vertical spring is compressed.

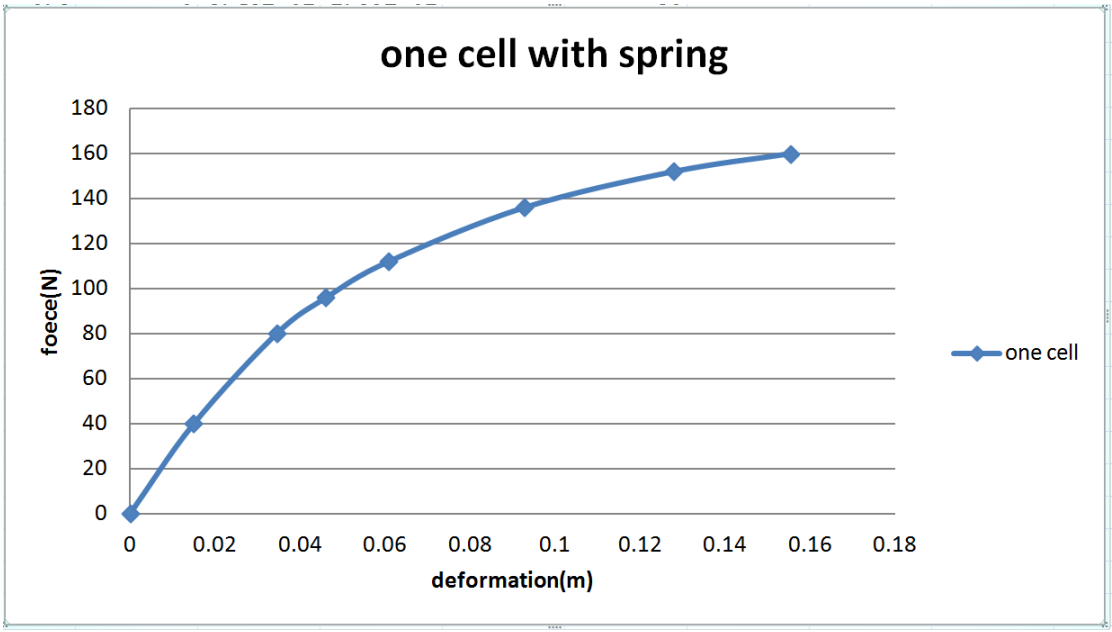

Figure 25: Curves of force-displacement of a single cell

Finally, the force-displacement curve of a single cell model is obtained. In the figure,

the stiffness increases at the beginning, but gradually decreases with the application of force.

Figures 26 to 28 shows the simulation process and results of two cells

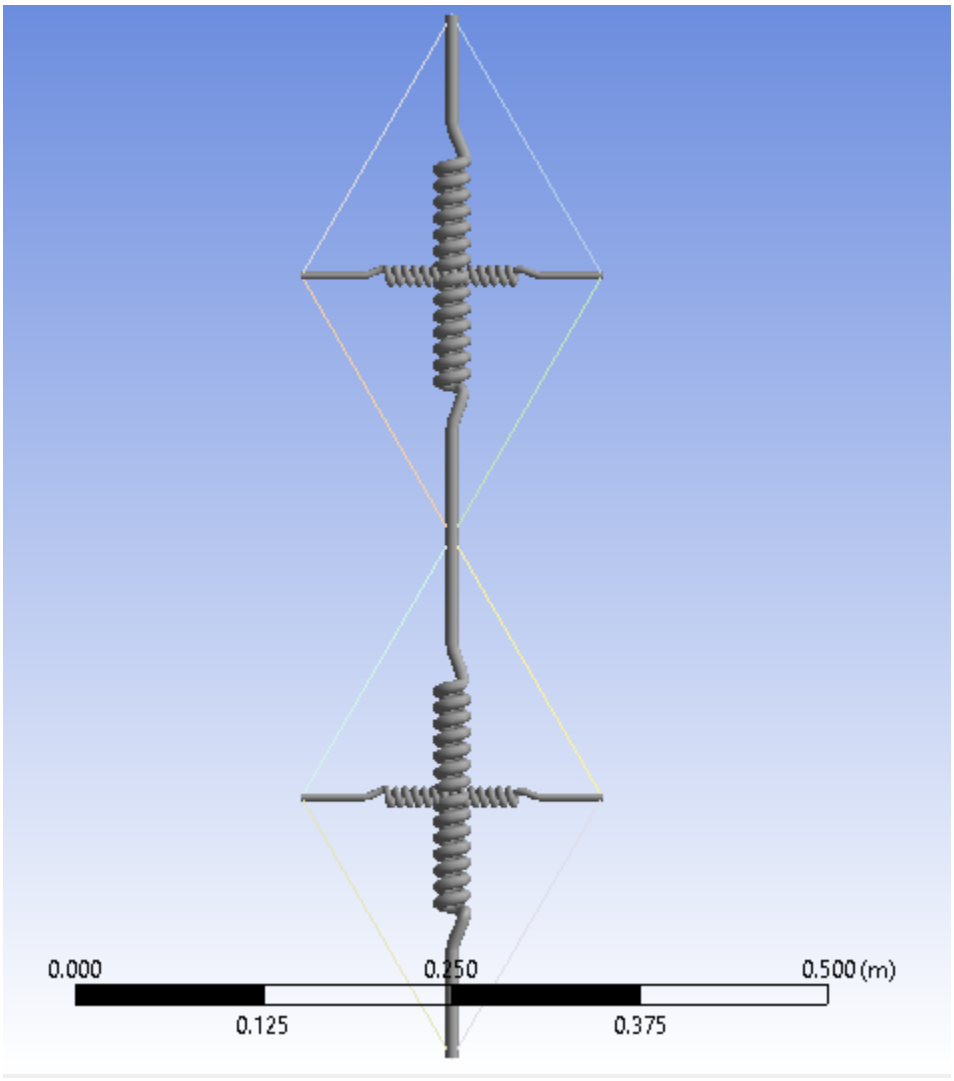

Figure 26: two cells with springs

The boundary conditions are: the bottom point is the fixed point, the force is applied to the vertex, and the top point and the middle connecting point can only move up and down.

The modeling process in Figure 26 is similar to that in Figure 23 above. The same length and diameter are selected for the inclined bar, and the initial angle and stiffness of spring are also kept the same.

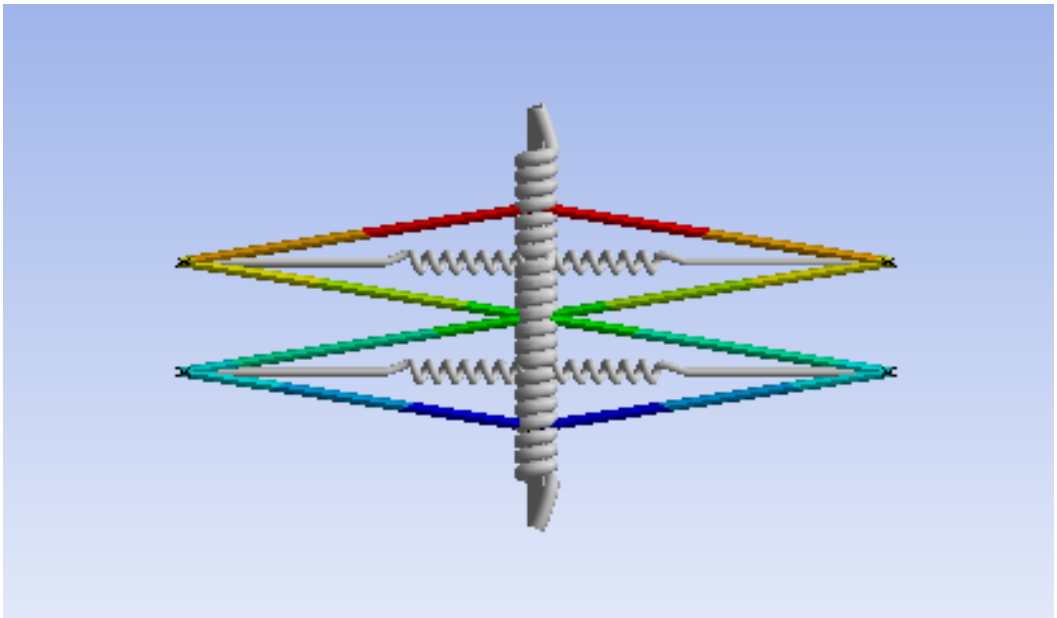

Figure 27: The final shape of the displacement on two cells

Figure 27 is the final shape of Figure 26 with a force of 300N at the top

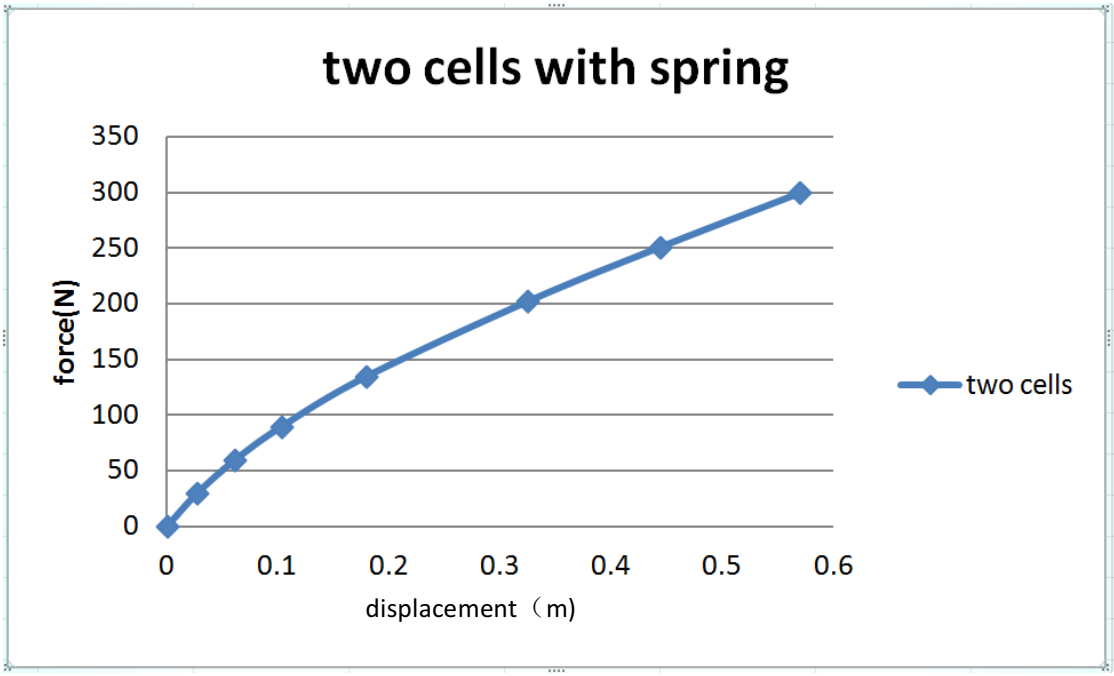

Figure 28: Curves of force-displacement of two cells

Figure 28 also conforms to the expected change.

Figure 29 to 31 shows the simulation process and results of four cells

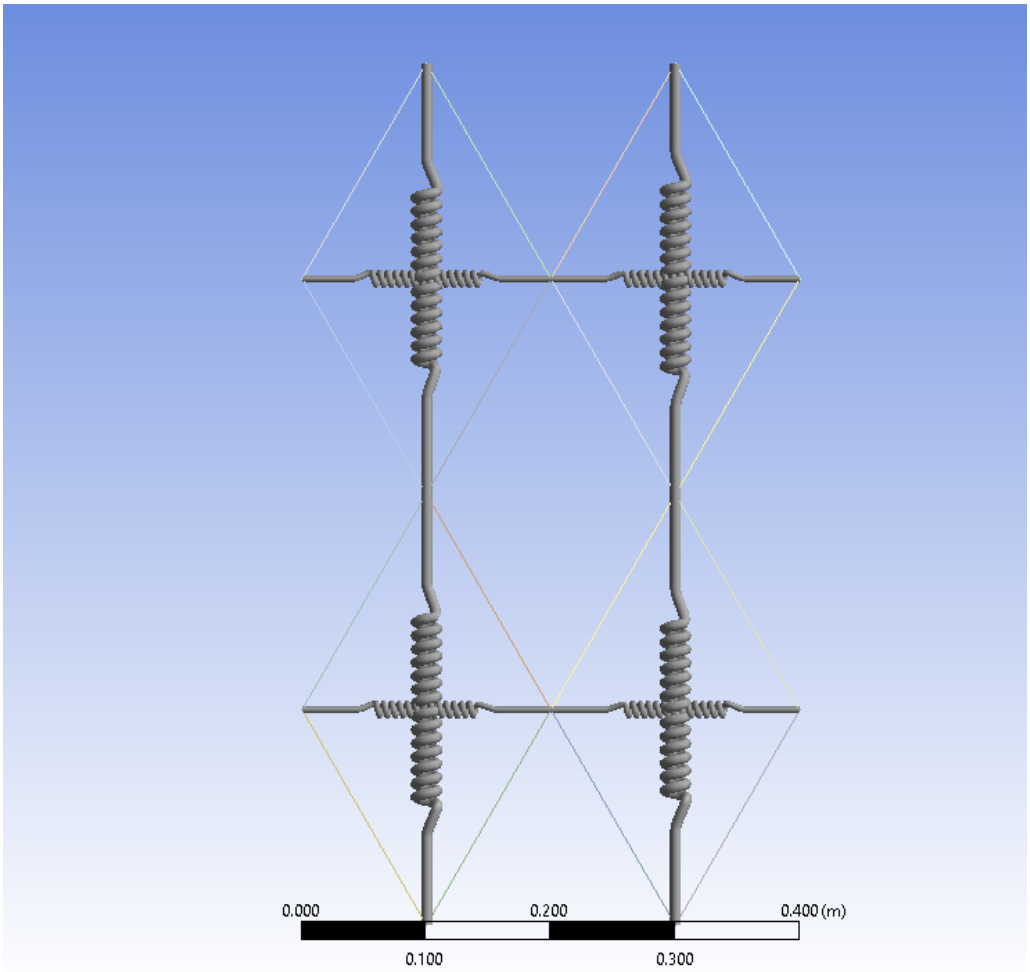

Figure 29: four cells with spring

Figure 29 shows a model of four cells where the data for individual cells remains the same as before

The boundary conditions are as follows: the right point at the bottom is a fixed point, the force is applied to two vertices, and the bottom left point can only move in the horizontal direction; The vertex on the right, and the point connecting the middle on the right, can only move up and down.

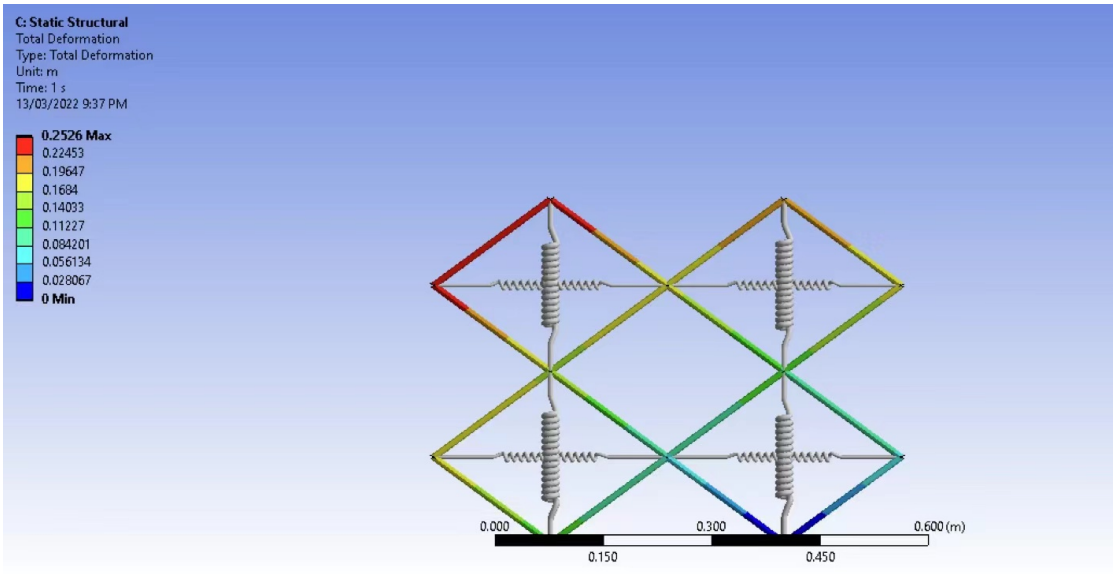

Figure 30: The final shape of the displacement on four cells

Figure 30 is the final shape of Figure 28 with a force of 290N at the top

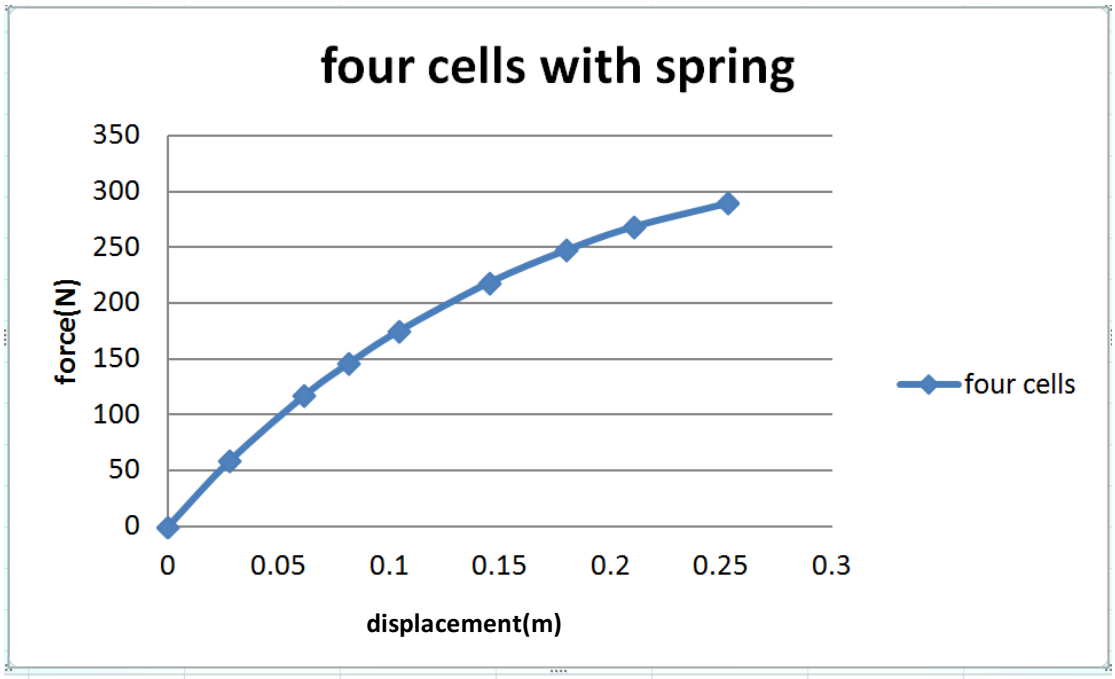

Figure 31: Curves of force-displacement of four cells

The trend of force-displacement curve given by the model of four cells shown in Figure31 is also very consistent with expectations.

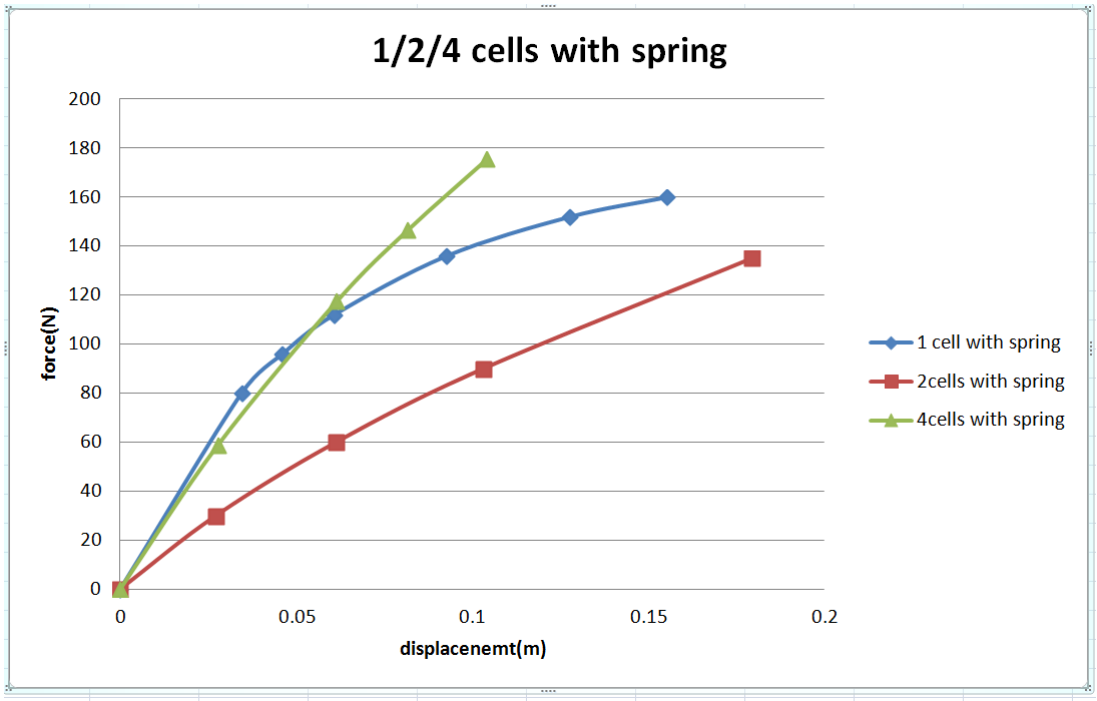

Figure 32: Curves of force-displacement of cells

Figure 32 shows a partial composite of the data from the 1,2 and 4 cell diagrams.

4.3 cell with matrix

4.3.1 30 degrees four cells with the matrix

The following is a matrix addition to the cell.

Placing both horizontal and vertical springs in the frame may cause unnecessary contact and thus affect the performance of the model. Therefore, the horizontal spring was removed from the frame structure and placed externally to better connect the matrix.

The model in Figure 33 was anatomically analyzed using half of the cross-section of the entire model. This state of the model is more conducive to modeling operations and collection of results.

Since the thickness of the substrate is generally halved, it is easier to build a model and observe the changes in the internal structure. Therefore, it is important to note that not only the base thickness is reduced, but also the rebar diameter, force and spring stiffness need to be halved compared to the entire model..

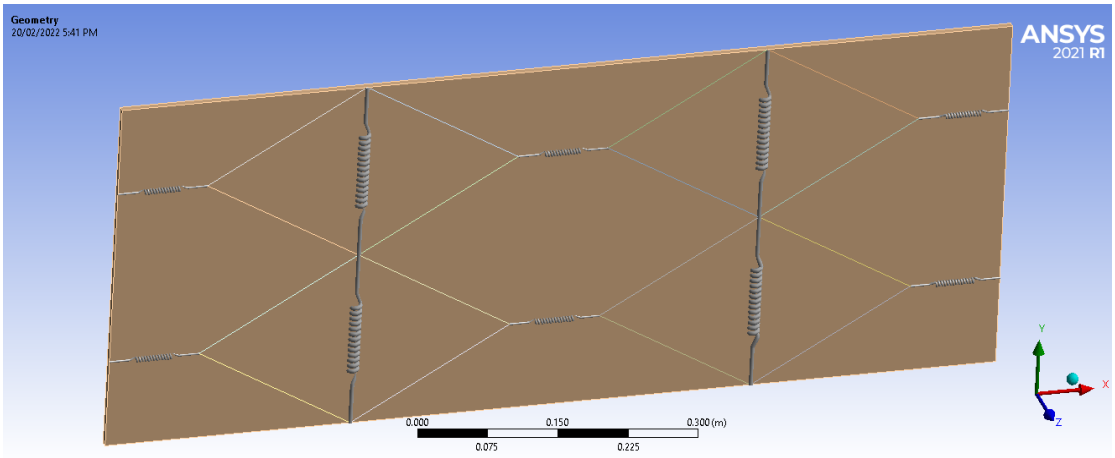

Figure 33: Four spring cells with matrix, 30 degrees

The boundary conditions are as follows: the bottom surface is a fixed surface; the force is applied to the top surface.

Figure 34 and Figure 35 are the analysis diagrams of the part without matrix and the part with matrix respectively. Both of them show the ANSYS model of 4-Cell

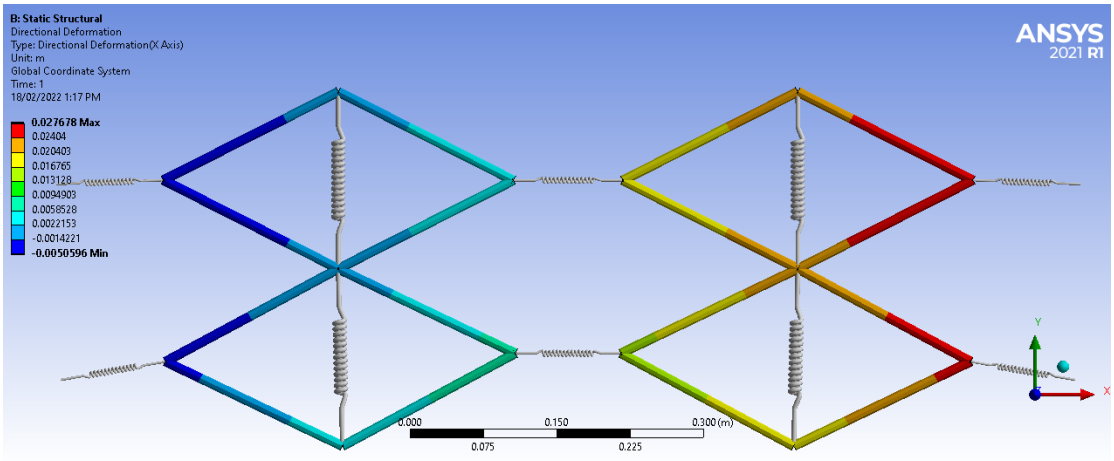

Figure 34: The displacement of the frame after applying force

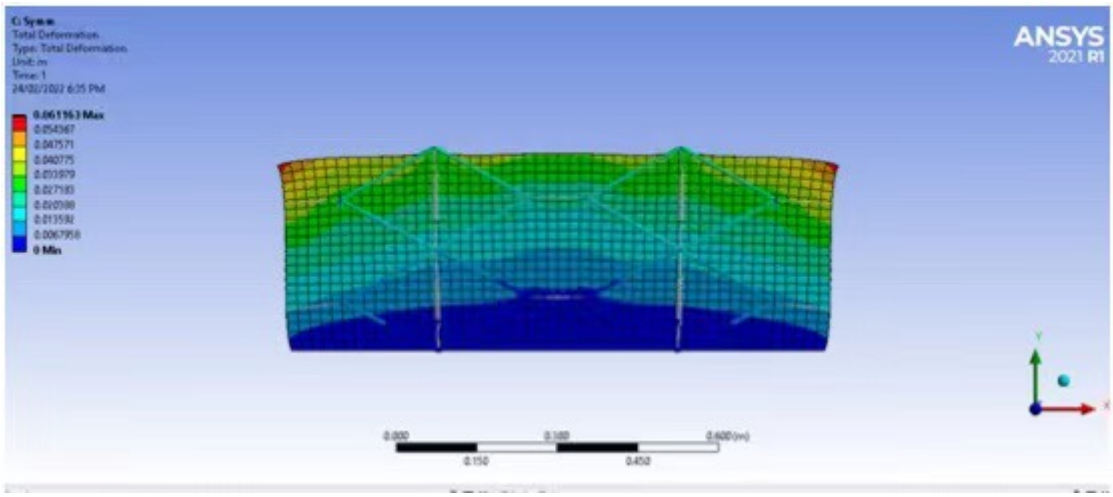

Figure 35: Deformation diagram of the structure with 4 cells spring on the outside with matrix under 100N force

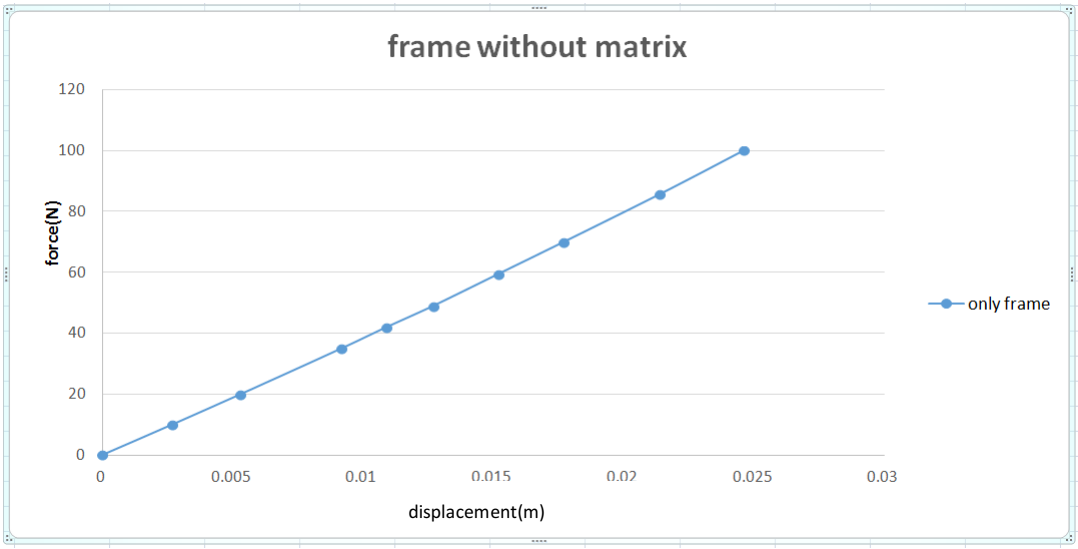

Figure 36: The force-displacement curve with 100N applied

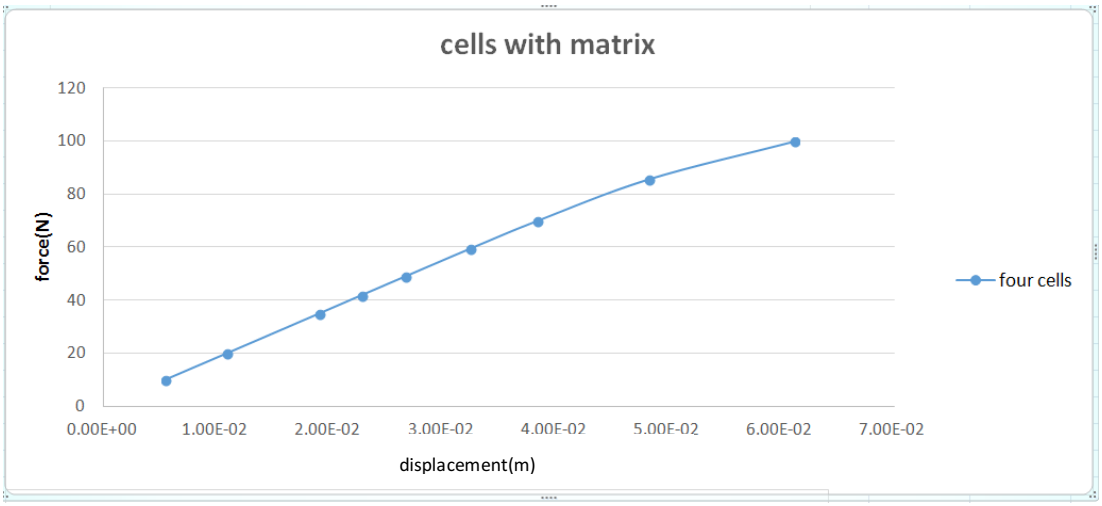

Figure 37: The force-displacement curve with 100N applied

When analyzing the results, it was found that when the force applied was to 100N, neither the frame without matrix nor the 4 cells reached a good nonlinear state. (Figure 36) nor the curves of force-displacement (Figure 37) reached a good nonlinear state. The loss of non-linearity when the horizontal springs are placed externally to the cell is likely to be due to the lack of lateral support at the boundaries to provide sufficient compression force, whereas for the cases with internal springs the spring force would have been induced due to the tension in the spring.

According to the empirical analysis, there should be a problem of too a small force, so increasing the force by either decreasing horizontal stiffness or decreasing vertical stiffness can make the model more nonlinear.

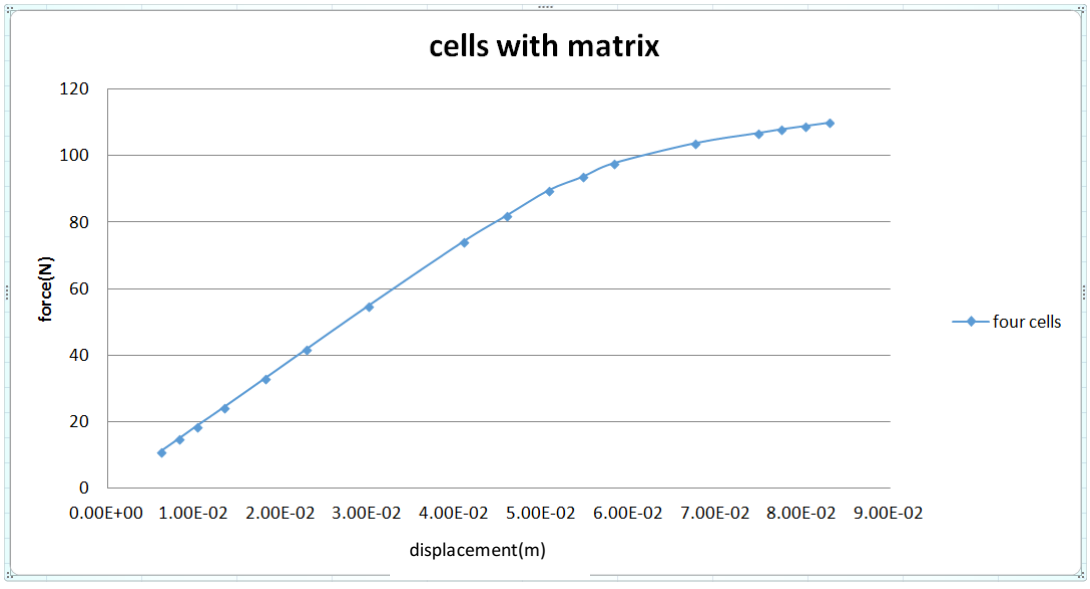

Figure 38: The force-displacement curve with 110N applied

Thus, Figure 38 is obtained. When the force applied is increased to 110N, a longer nonlinear section is obtained.

Another trial to adjust the lateral stiffness of the model was made. The longitudinal stiffness of the six springs in the horizontal direction were reduced (previously 1000 N/m).

In both the horizontal and vertical directions). The spring stiffness was changed to 800 N/m and 500 N/m, but the result was the same. The maximum force that the model can handle successfully remains at 110N.

When the spring stiffness was further adjusted to 100 N/m, a change occurred and the maximum allowable force increased to 120N.

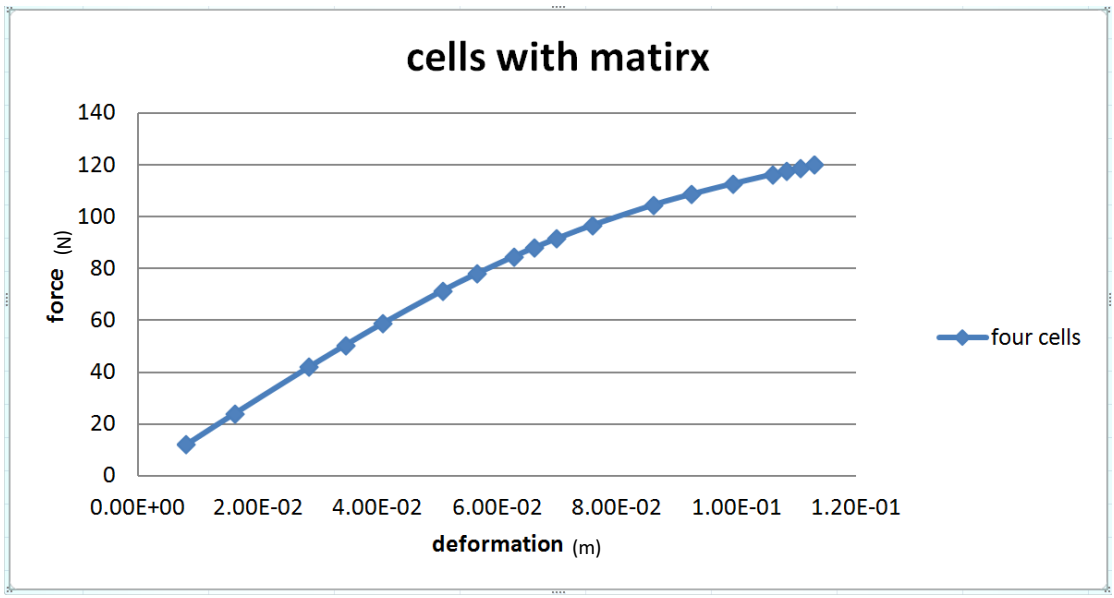

Figure 39: The force-displacement curve with 120N applied

4.3.2 60 degrees four cells with the matrix

4.3.2.1 The spring is outside the frame

In the 60-degree model, the diameter of bars is 5mm,

k_v =250 N/M k_h =500 N/M and the thickness of rubber is 7.5mm.

110N pressure is applied on the top plane.

Figure 40 shows the 4-cell ANSYS model with an initial Angle of 60 degrees. Figure 41 shows the final change state of Figure 40.

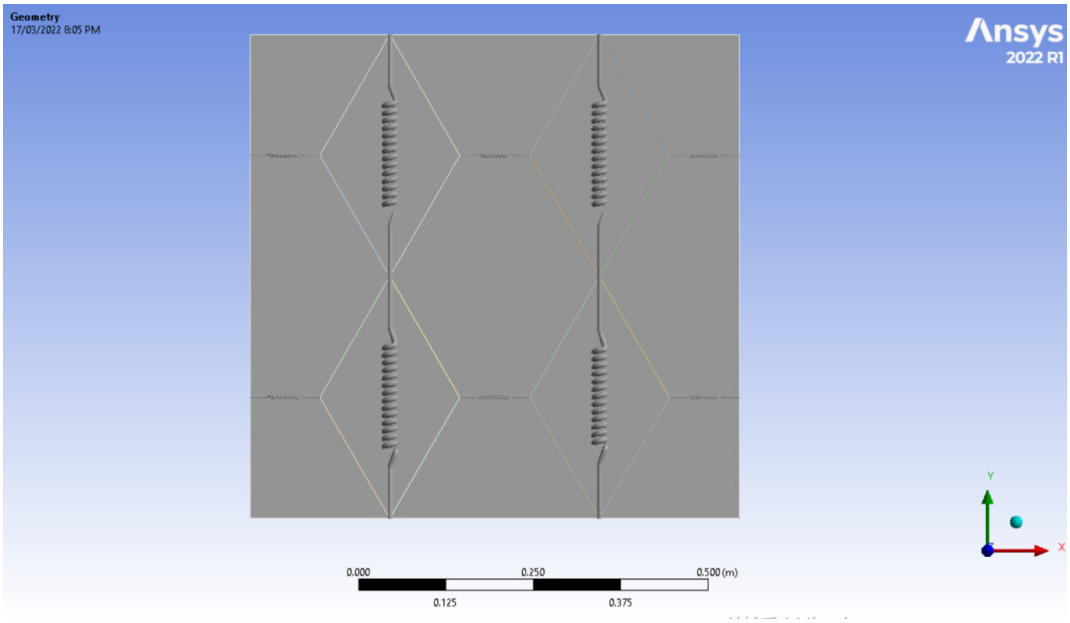

Figure 40: four spring cells with matrix 60degree

The boundary conditions are as follows: the bottom surface is a fixed surface; the force is applied to the top surface.

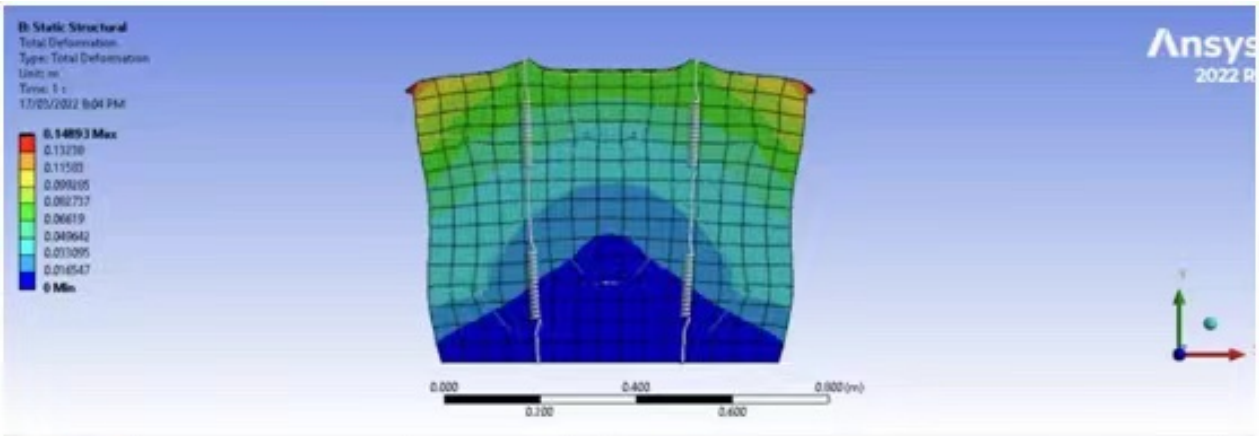

Figure 41: Deformation diagram of the structure of 4cells spring on the outside with matrix under 110N force

Figures 42 and 43 show the force and displacement curves with and without matrix, respectively.

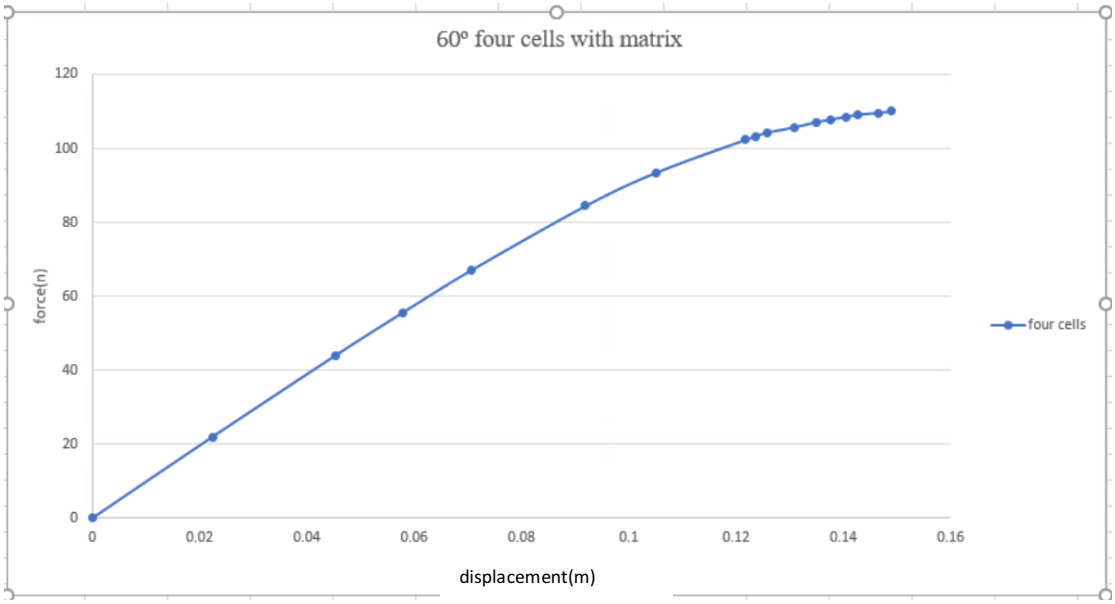

Figure 42: The force-displacement curve with 110N applied

The curves of force-displacement in Figure 42 are obtained.

It can be seen from the graph that the curve trend gradually flattens out and the structure gradually appears to reach a critical stage where the stiffness approaches zero.

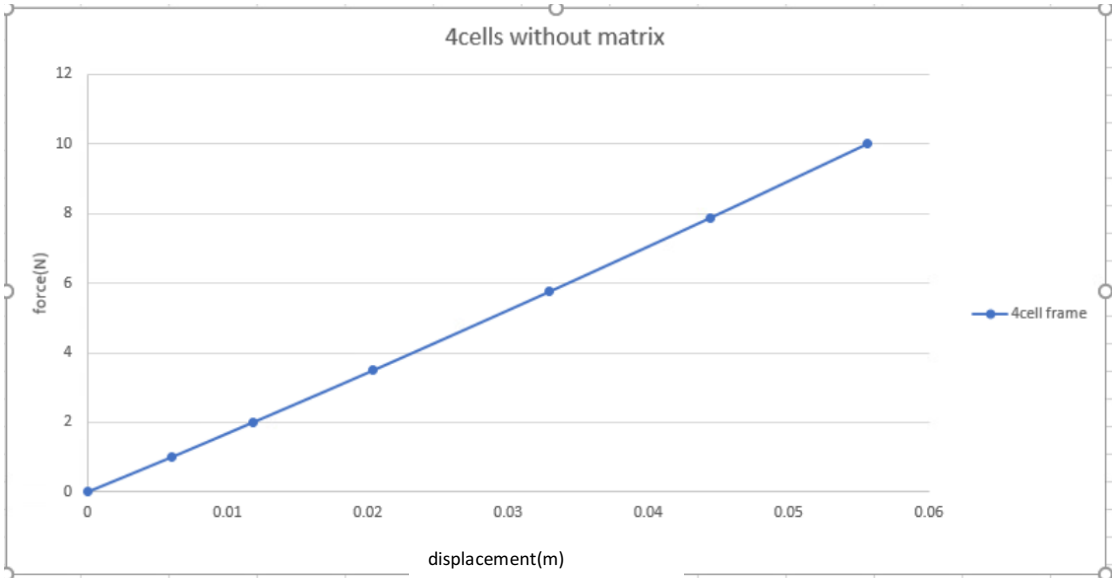

Figure 43: The force-displacement curve with 10N applied

k_v =250 N/M k_h =500 N/M and the thickness of rubber is 7.5mm.

At the same time, 159N pressure is applied on the top plane.

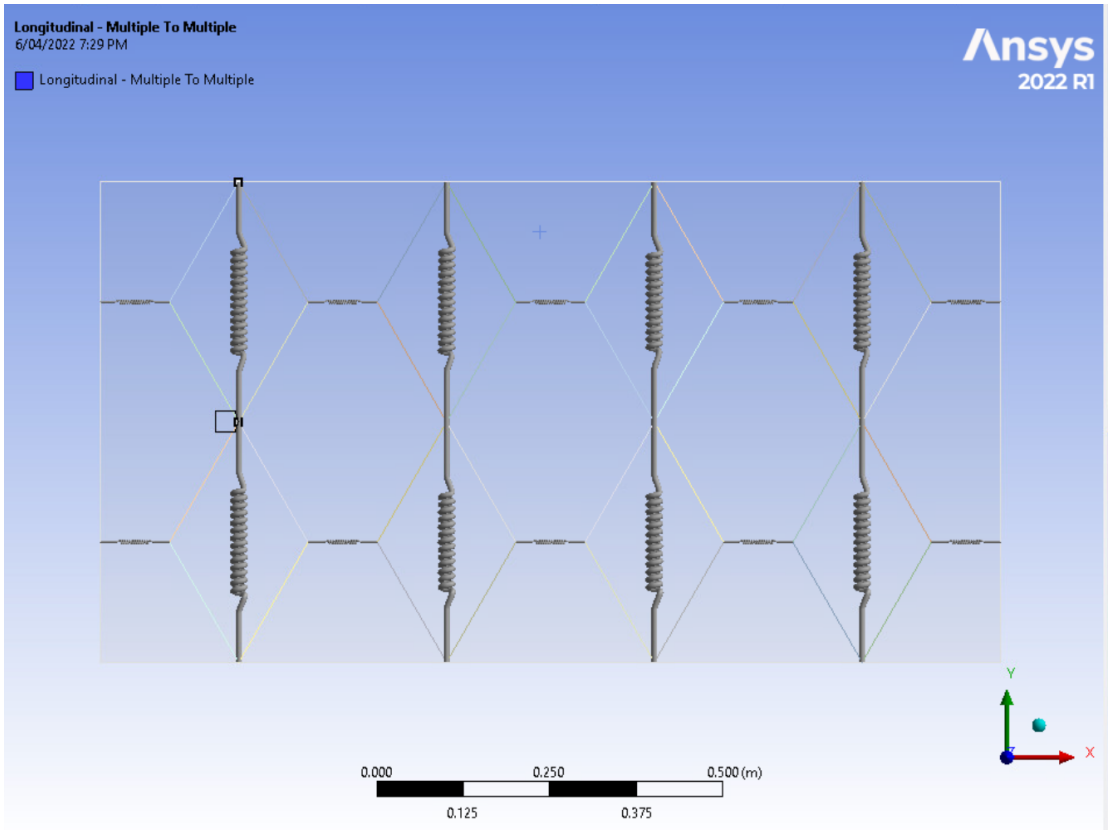

Figure 44: 8 cells with matrix at 60degree

Figure 44 shows the 8-cell ANSYS model with an initial Angle of 60 degrees. Figure 45 shows the final change state of Figure 44.

The boundary conditions are as follows: the bottom surface is a fixed surface; The force is applied to the top surface.

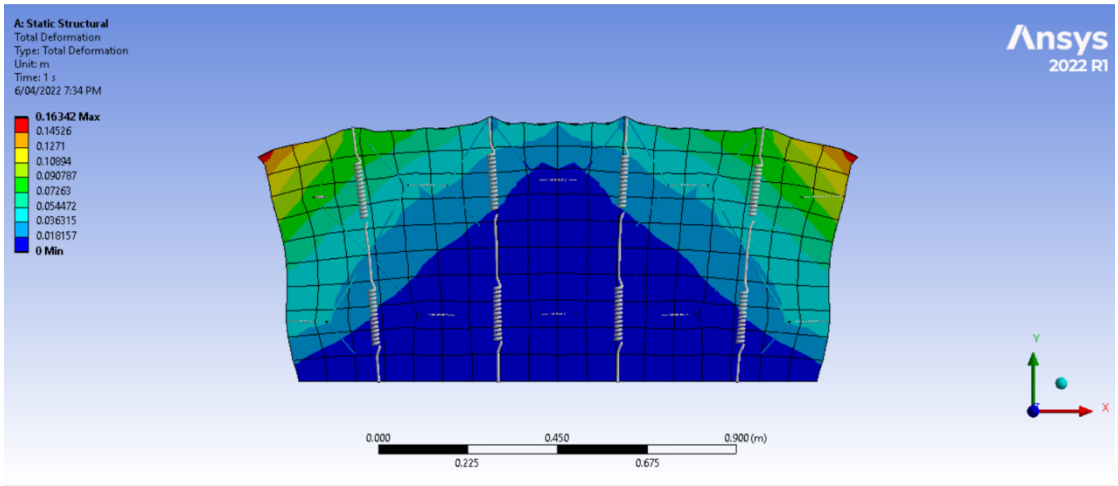

Figure 45: Deformation diagram of the structure of 8cells spring on the outside with matrix under 159N force

Figures 46 and 47 show the force and displacement curves with and without matrix, respectively.

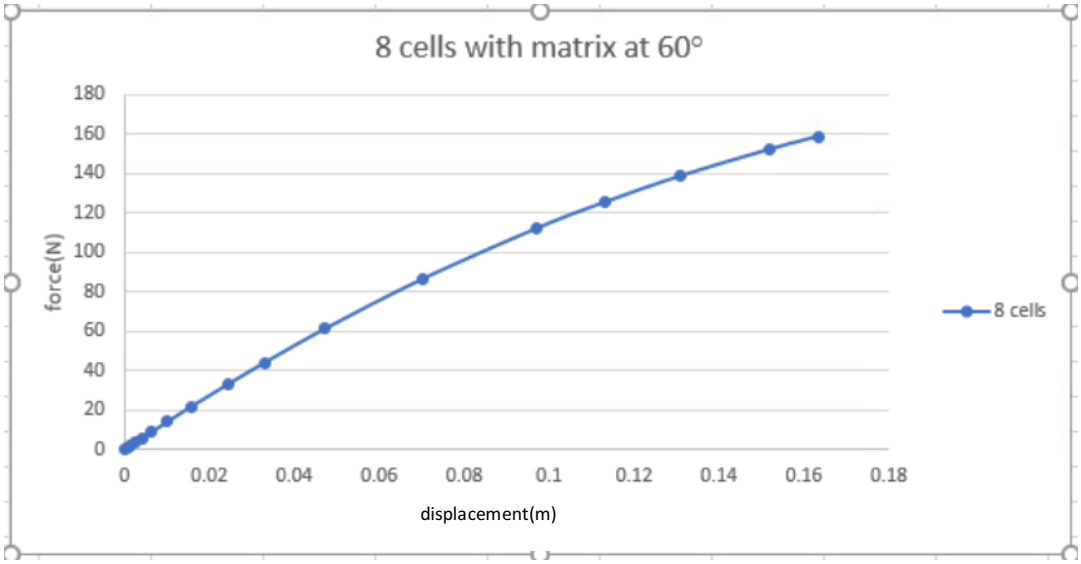

Figure 46: The force-displacement curve with 159N applied

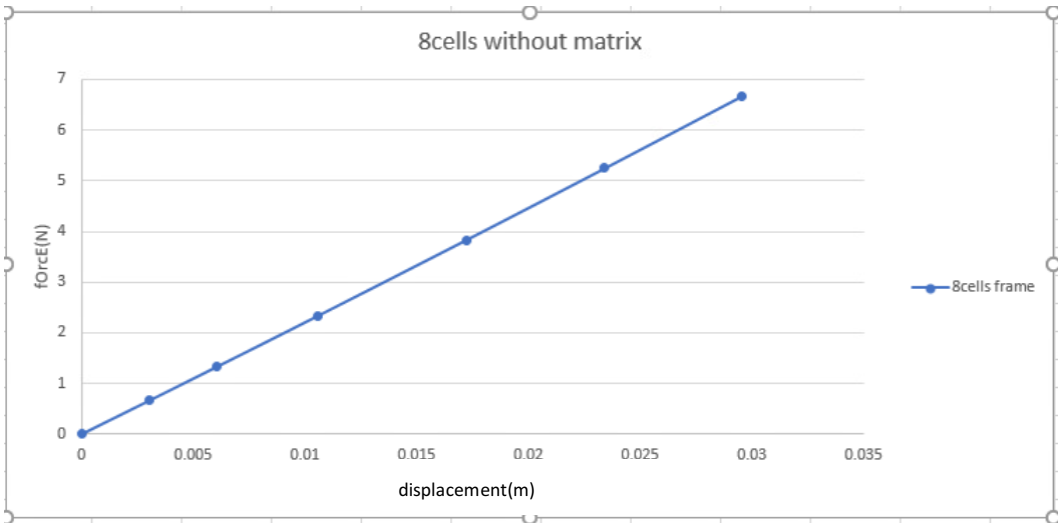

Figure 47: The force-displacement curve with 6.66N applied

4.3.2.2 The spring is inside the frame

In the above analysis process, it was found that if only the frame structure is analyzed, in order to easily facilitate the stability of the structure, it is necessary to control the number of horizontal cells. These to be singular or of odd number to ensure the symmetry of the model with the center having a node at the base, so that it is convenient to set the middle point at the bottom as the fixed point.

Figure 48 shows the model simulation of three groups of cells. In order to ensure the consistency of boundary conditions with or without a matrix, the bottom surface can only be moved laterally when there is a matrix. When there is no matrix, center point is set as a fixed point, and the rest of the bottom endpoints can only perform lateral movement.

Figure 48-52 shows the 6-cell model in which cells are directly connected.

Figure 48 shows the ANSYS model of 6-cell with matrix, and Figure 49 shows the force-displacement curves of 6-cell with matrix.

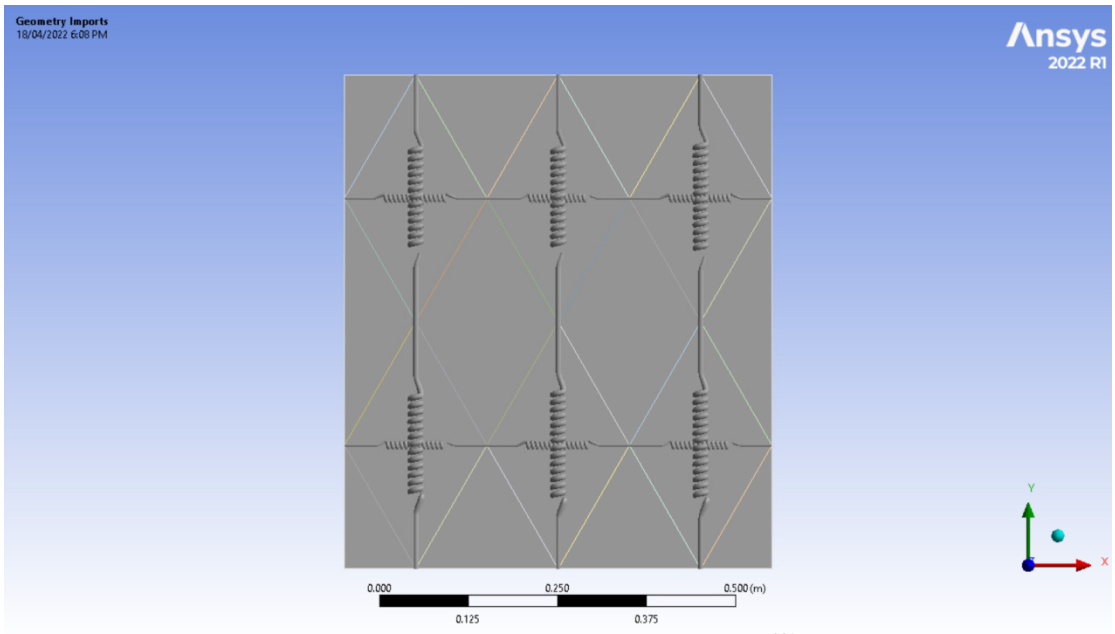

Figure 48: 6 cells with matrix at 60 degrees

The boundary conditions are as follows: the bottom surface is a fixed surface; the force is applied to the top surface.

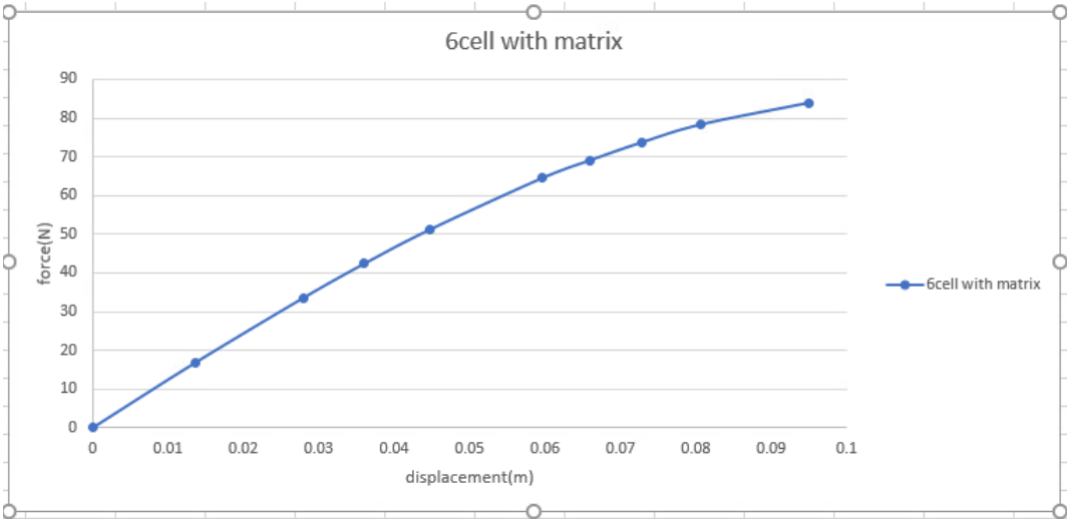

Figure 49: The force-displacement curve

Figure 50 shows the ANSYS model of 6-cell without matrix, and Figure 52 shows the force-displacement curves of 6-cell without matrix.

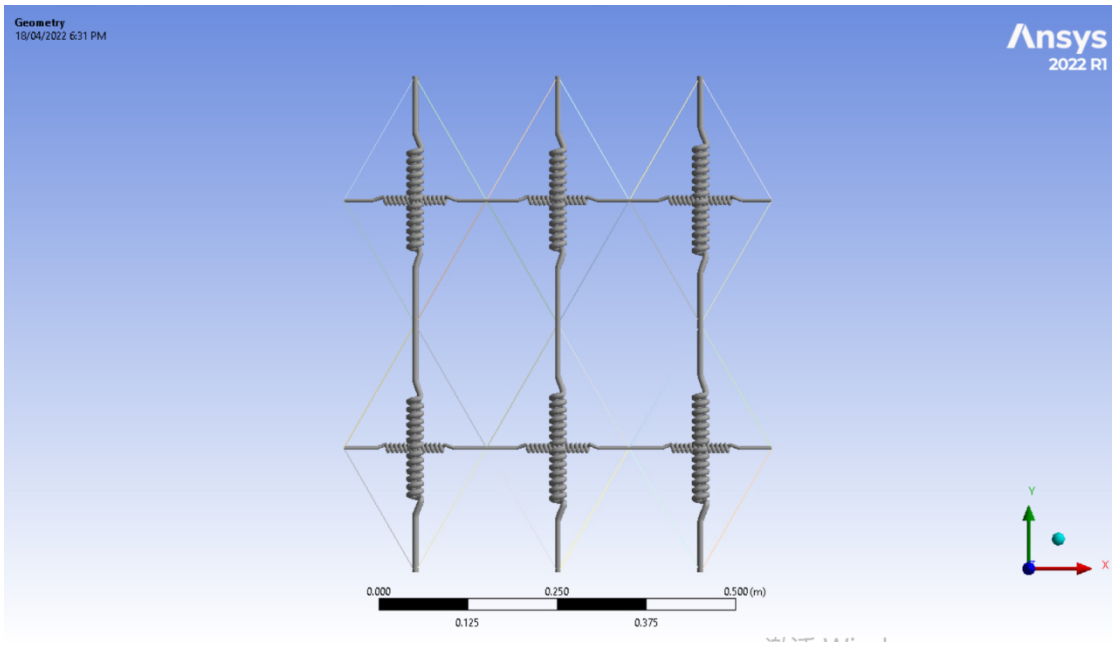

Figure 50: 6 cells without matrix at 60degree

The boundary conditions are: the point in the middle of the bottom is the fixed point; The force is applied at all points on the top; The points on the left and right of the bottom can only move horizontally; And the middle vertex can only move vertically with its middle connection point.

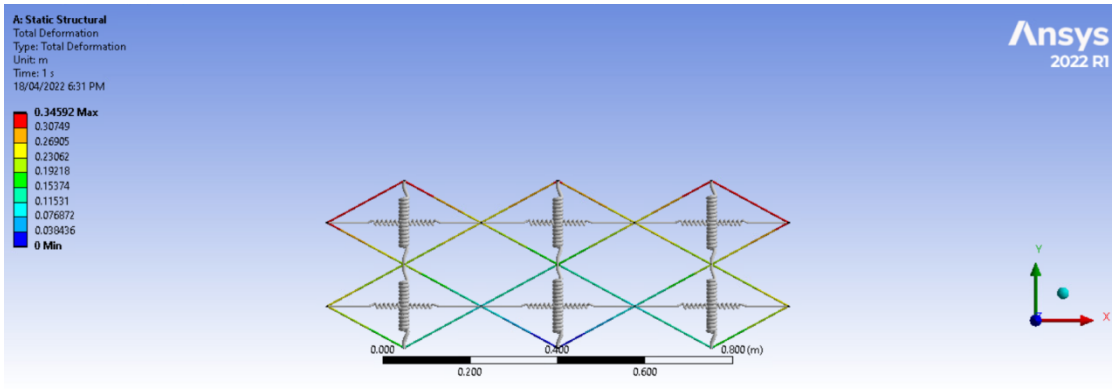

Figure 51: Deformation diagram of the structure of 6 cells spring on the inside with matrix under 245N force

Figure 51 shows the final compressed state diagram of 6-cell without matrix

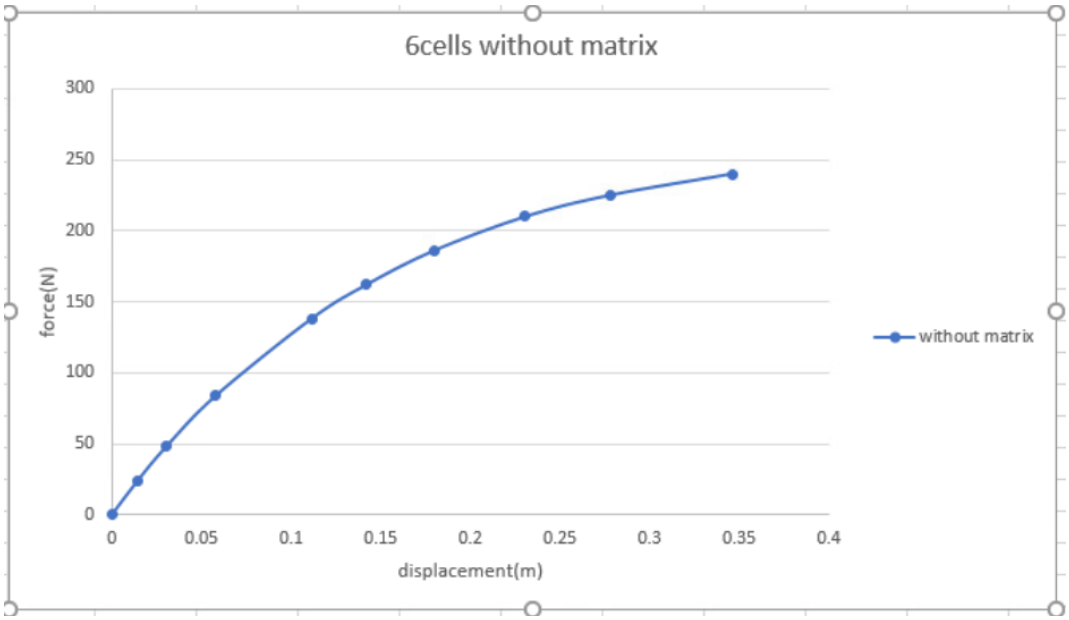

Figure 52: The force-displacement curve

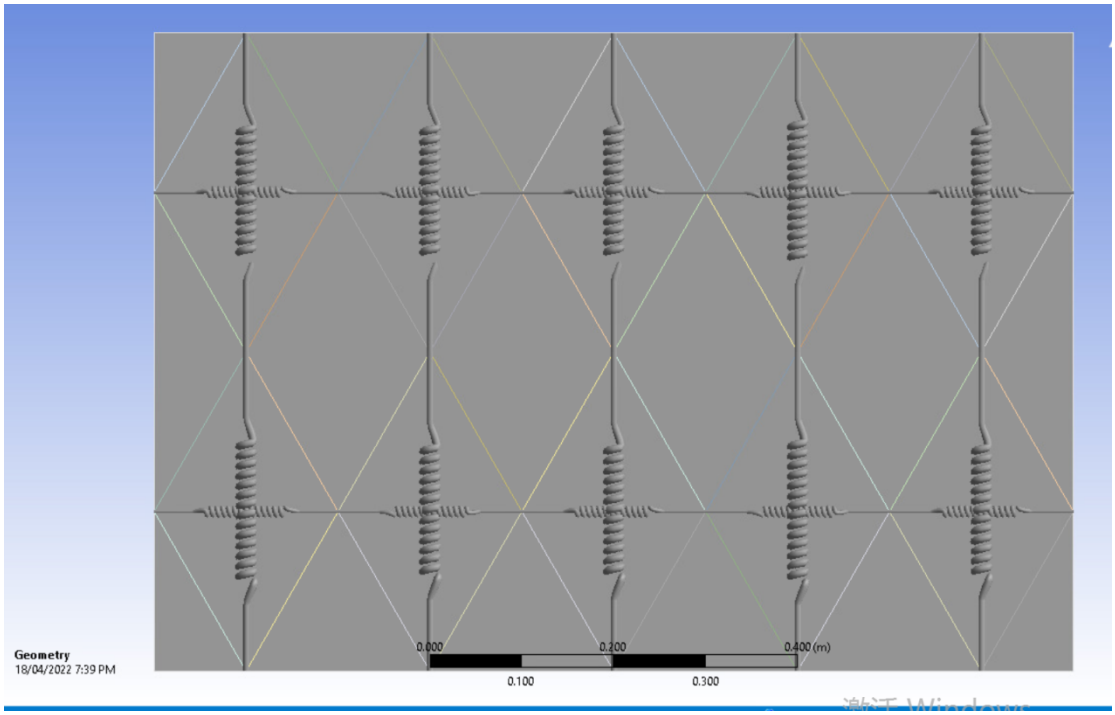

Figure 53: 10 cells with matrix at 60degree

Figure 53-56 shows the 10-cell model in which cells are directly connected

The boundary conditions are as follows: the bottom surface is a fixed surface; the force is applied to the top surface.

Figure 53 shows the ANSYS model of 10-cell with matrix, and Figure 54 shows the force-displacement curves of 10-cell with matrix

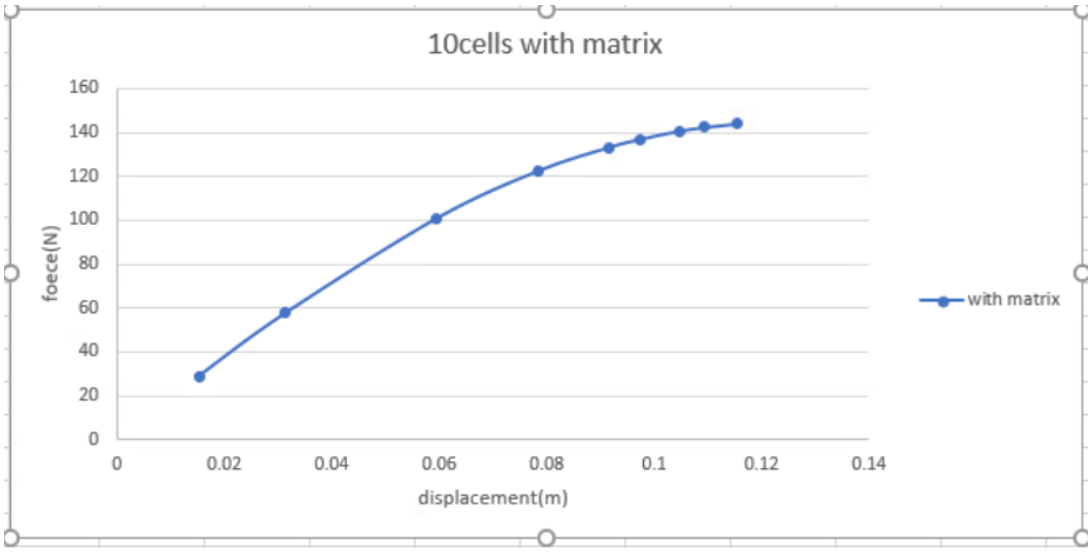

Figure 54: The force-displacement curve

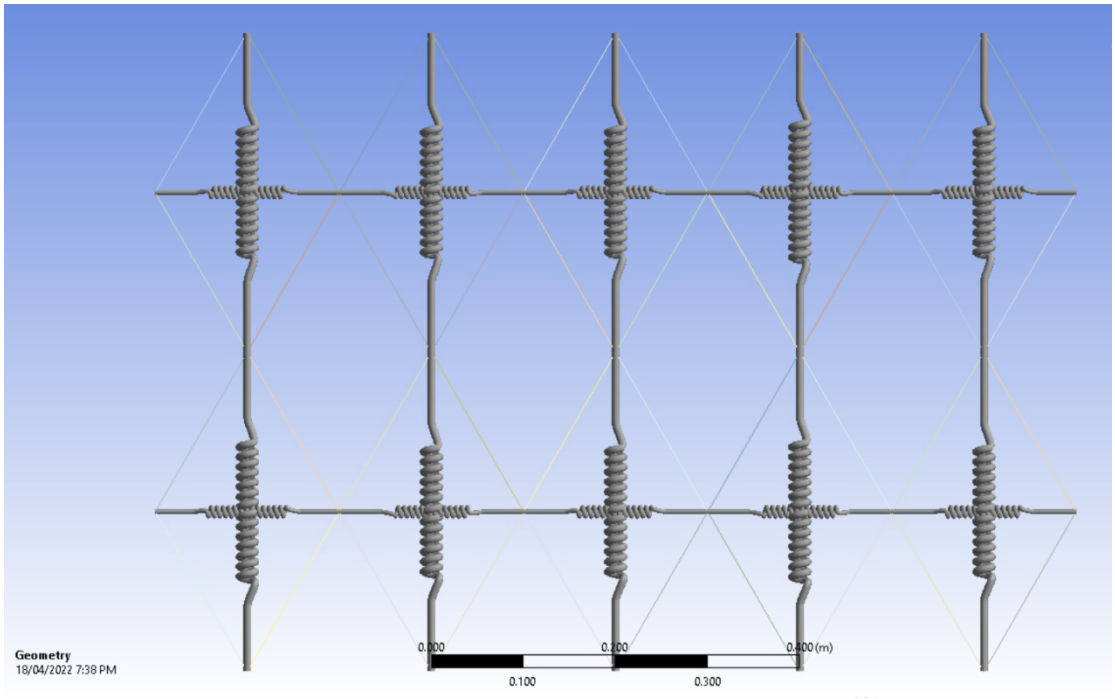

Figure 55: 10 cells without matrix at 60degree

Figure 55 shows the ANSYS model of 10-cell without matrix, and Figure 56 shows the force-displacement curves of 10-cell without matrix

The boundary conditions are: the point in the middle of the bottom is the fixed point; The force is applied at all points on the top; The points on the left and right of the bottom can only move horizontally; And the middle vertex can only move vertically with its middle connection point.

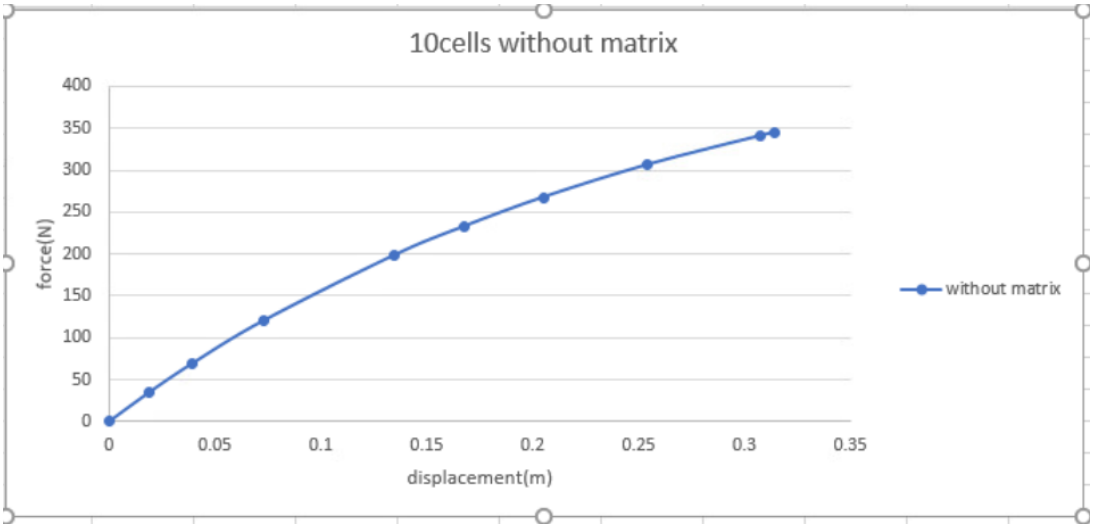

Figure 56: The force-displacement curve

The comparison between Figure 54 and Figure 56 shows that the stiffness of the overall structure changes more obviously after a matrix is added. After the addition of matrix, the confining effect of the matrix makes the structure more complicated but increases the rigidity of the structure to a certain extent and allows horizontal compression forces in the springs to develop sufficiently to cause non-linearity in force-deflection curve.

4.4 The analysis of a honeycomb-like structure:

A better model can be used to avoid the problem of too little spring space caused by large angles.

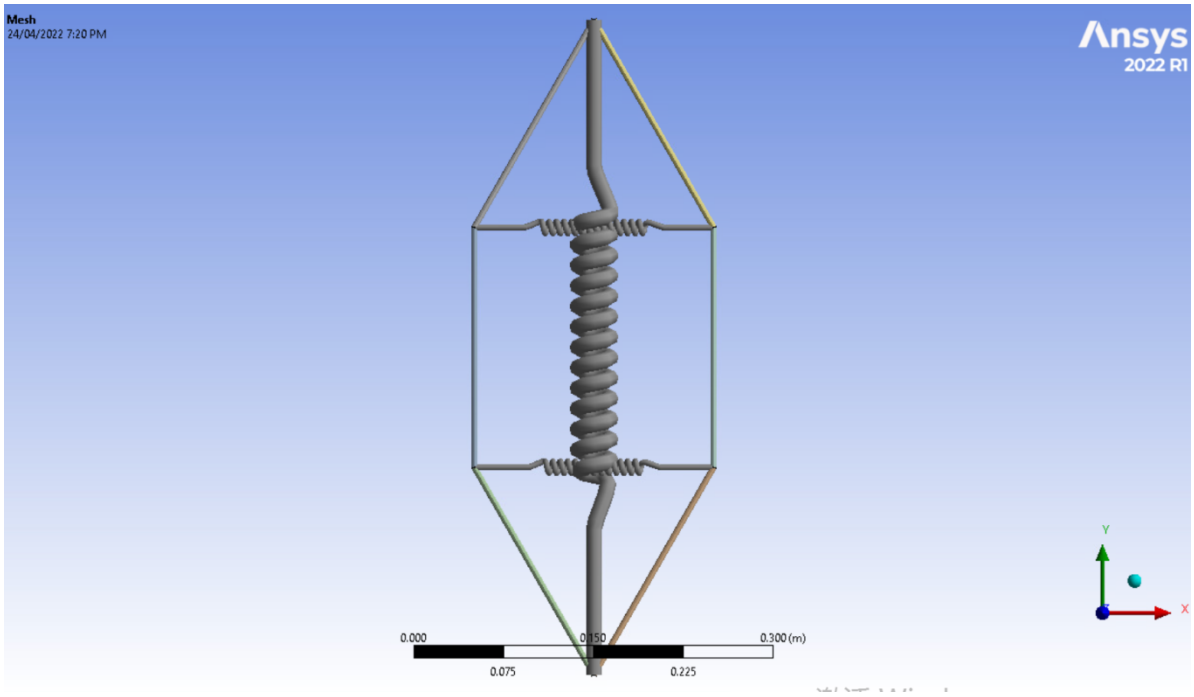

Figure 57: Honeycomb structure

Figure 57 shows a structure resembling a honeycomb. The initial Angle is still 60 degrees.

The boundary conditions are: the bottom point is the fixed point, the force is applied to the vertex, and the top point can only move up and down.

Figure 58 shows the final compressed state of a Honeycomb structure without matrix.

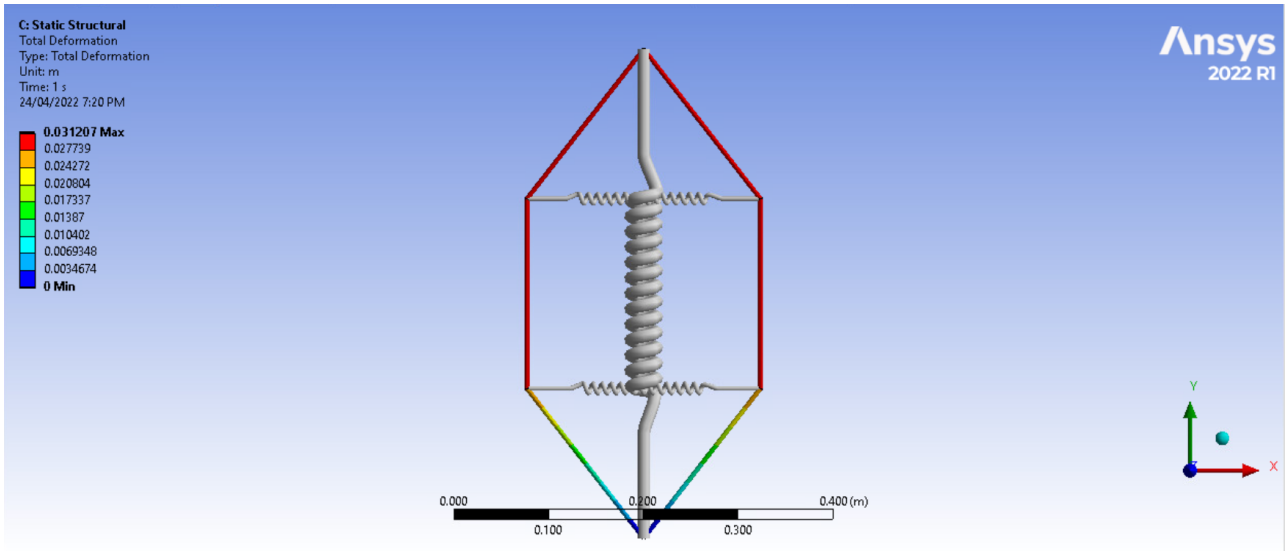

Figure 58: Deformation diagram of the structure of 1 honeycomb structure spring on the inside without matrix under 67N force

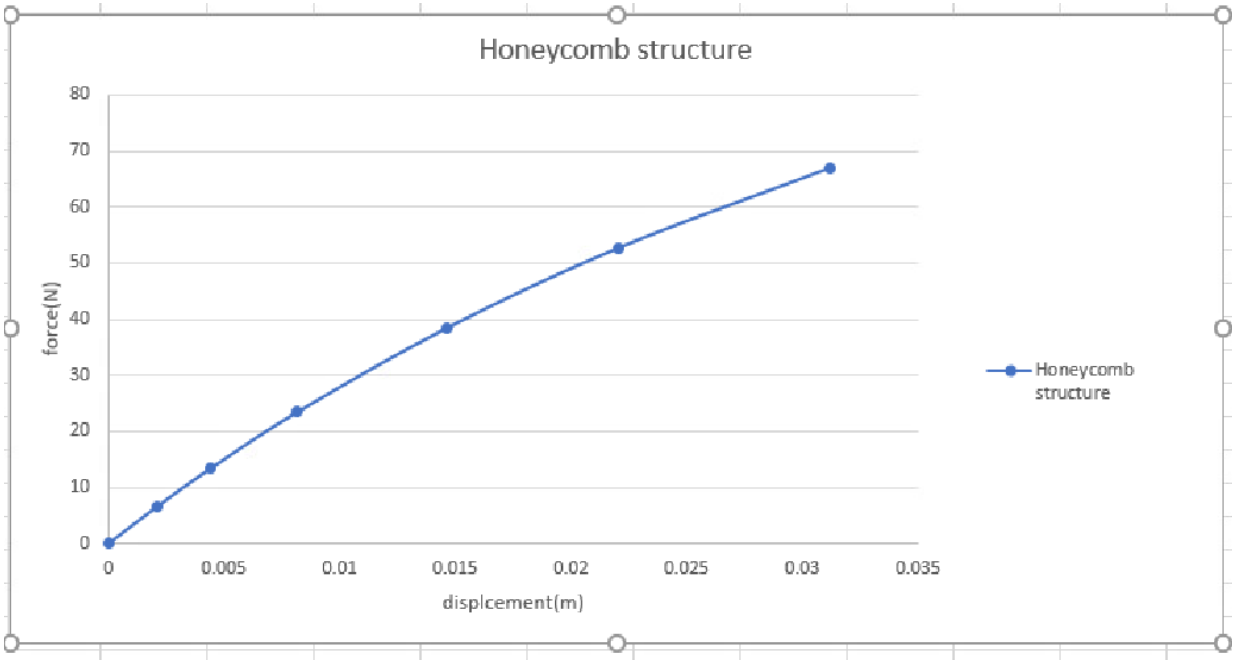

Figure 59: The force-displacement curve with 67N applied

Figure 59 shows the force-displacement curves of a Honeycomb structure without matrix

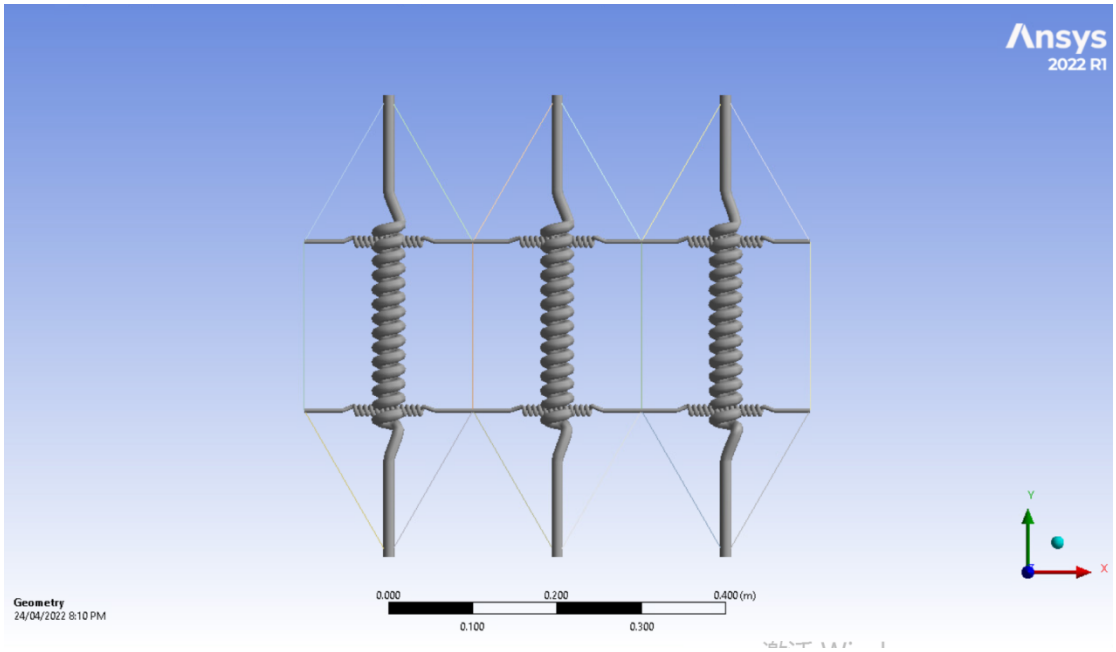

Figure 60: Three Honeycomb structure without matrix

Figure 60 is the ANSYS structure diagram of three honeycomb structures without matrix.

The boundary conditions are: the point in the middle of the bottom is the fixed point; The force is applied at all points on the top; The points on the left and right of the bottom can only move horizontally; And the middle vertex can only move vertically with its middle connection points.

Figure 61 is the ANSYS structure diagram of three honeycomb structures with matrix.

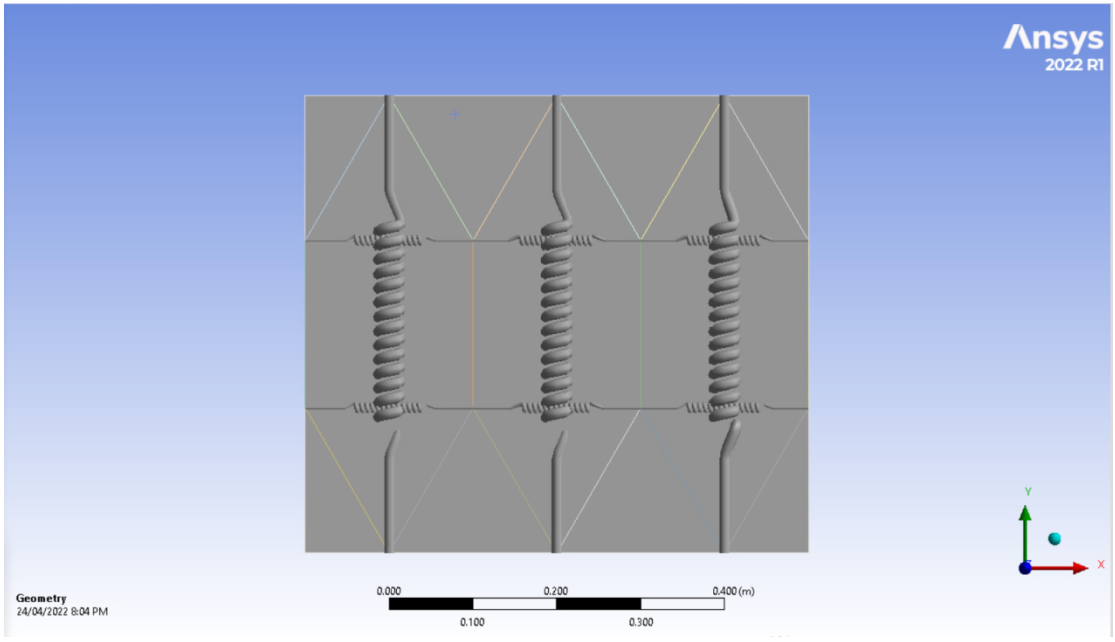

Figure 61: Three Honeycomb structure with matrix

The boundary conditions are as follows: the bottom surface is a fixed surface; the force is applied to the top surface.

Figure 62 and 63 show the force and displacement curves of three honeycomb structures without and with matrix, respectively.

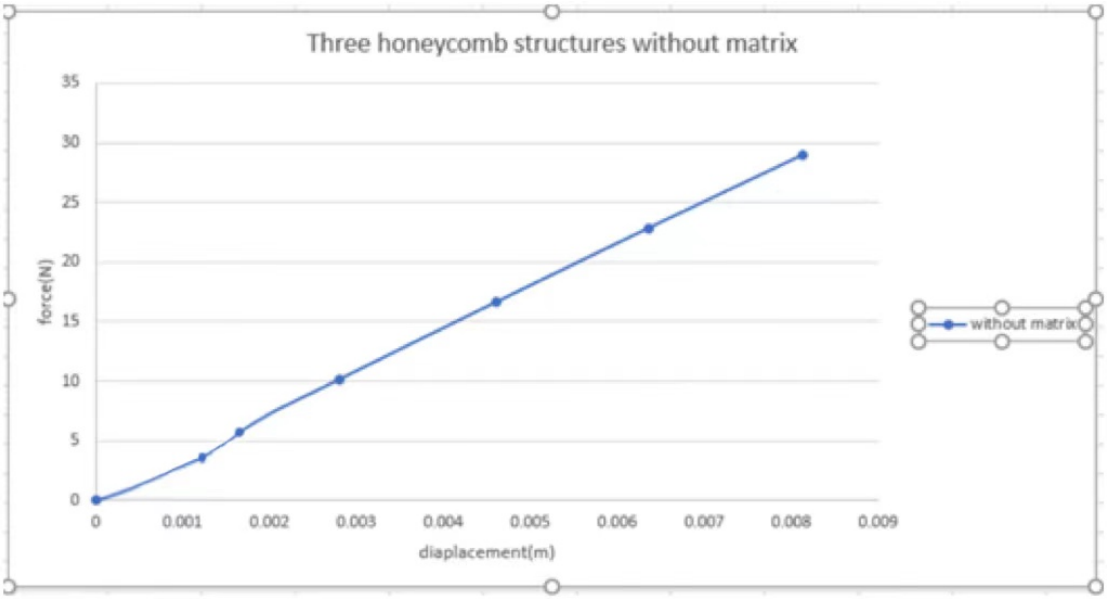

Figure 62: The force-displacement curve with 29N applied

It was found that when the structure was without matrix, if the bottom center point was taken as the fixed point, the whole structure would become very unstable and could bear very little force.

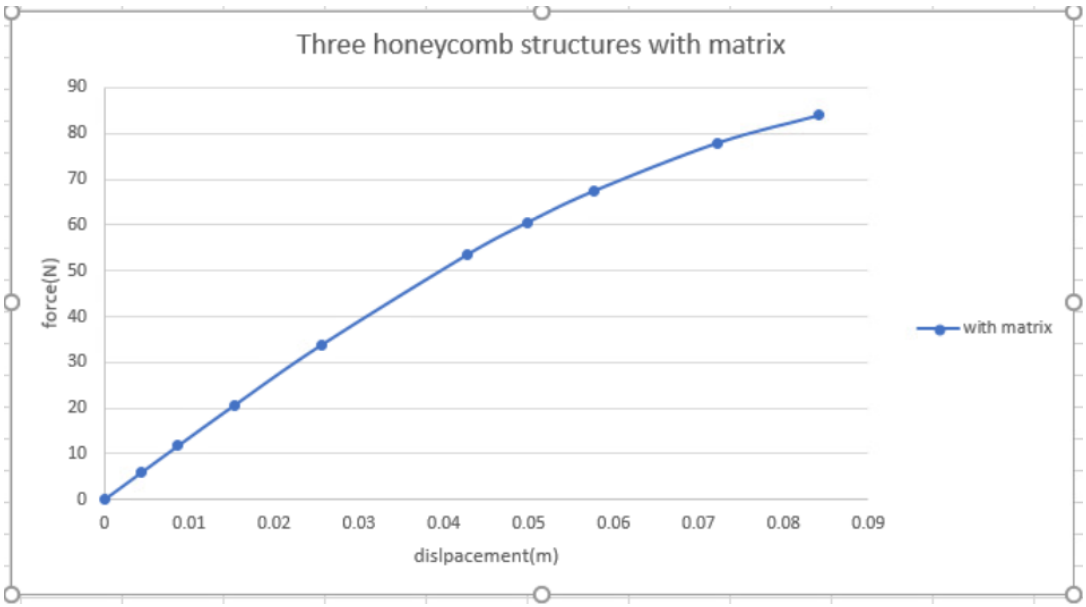

Figure 63: The force-displacement curve with 84N applied

Figure 62 and Figure 63 maintain the same boundary conditions.

Figure 64 and 65 show the force and displacement curves of three honeycomb structures without and with matrix, respectively

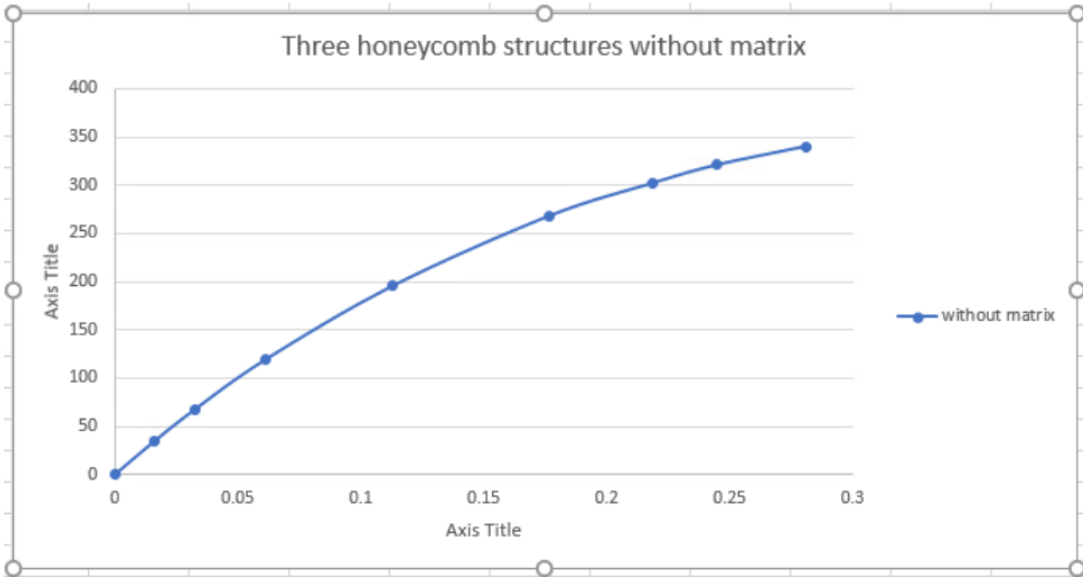

Figure 64: The force-displacement curve with 340N applied

When the boundary condition of without matrix is adjusted from the bottom center point as a fixed point to the bottom side as a fixed point, the structure becomes very stable.

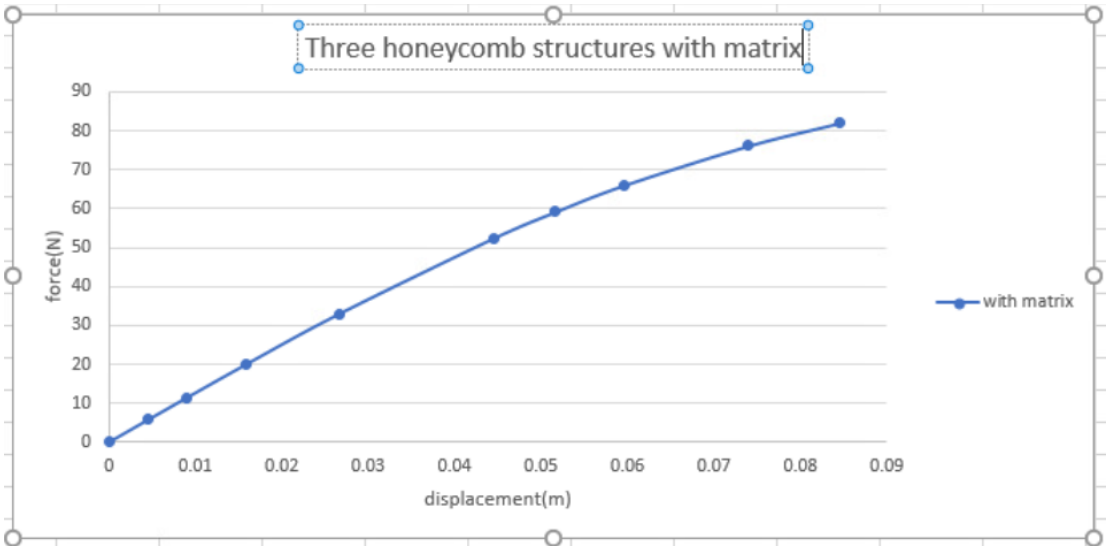

Figure 65 The force-displacement curve with 82N applied

Figure 64 and Figure 65 maintain the same boundary conditions.

4.5 The effect of tangential loading

While in some cases it may be possible to know the most likely force direction, it is often difficult to predict this. Therefore, it is important to understand how metamaterials behave under vertically oriented forces in order to test the performance of the device in the horizontal direction, two kinds of simulation are carried out because the force in the earthquake will never exist purely in the vertical direction, but will also have components in the horizontal directions.

The only difference between the two simulations is the position of force application. Figure 66 shows the application of a tangential force on the top surface of the structure, while Figure 69 shows the application a horizontal force on the side of the structure. Other parameters, such as boundary conditions, are fixed on the bottom, and spring Settings, such as the horizontal stiffness and vertical stiffness of both are consistent.

Figure 66-68 shows a set of figures of force applied on the top plane, which are ANSYS model diagram, final state diagram after force application, and force-displacement curve diagram respectively.

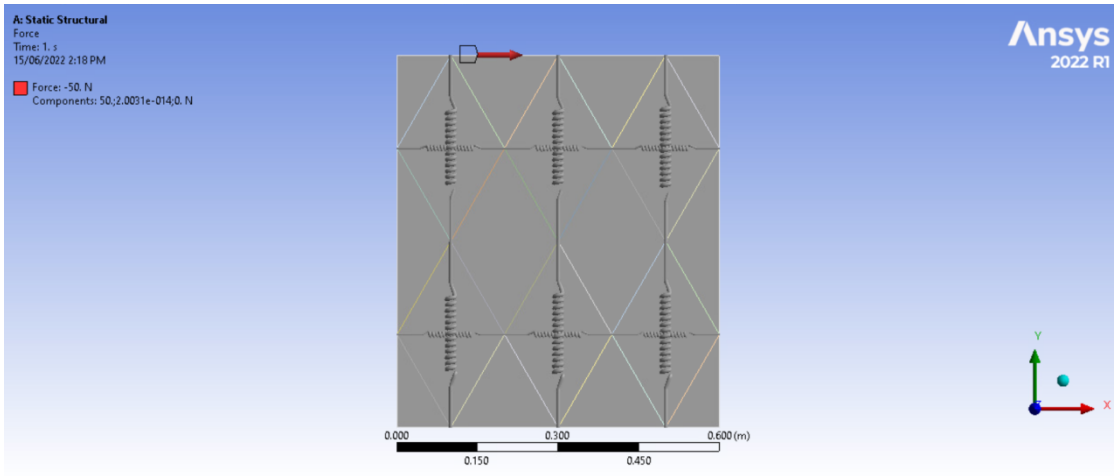

Figure 66: Horizontal force is applied at top surface

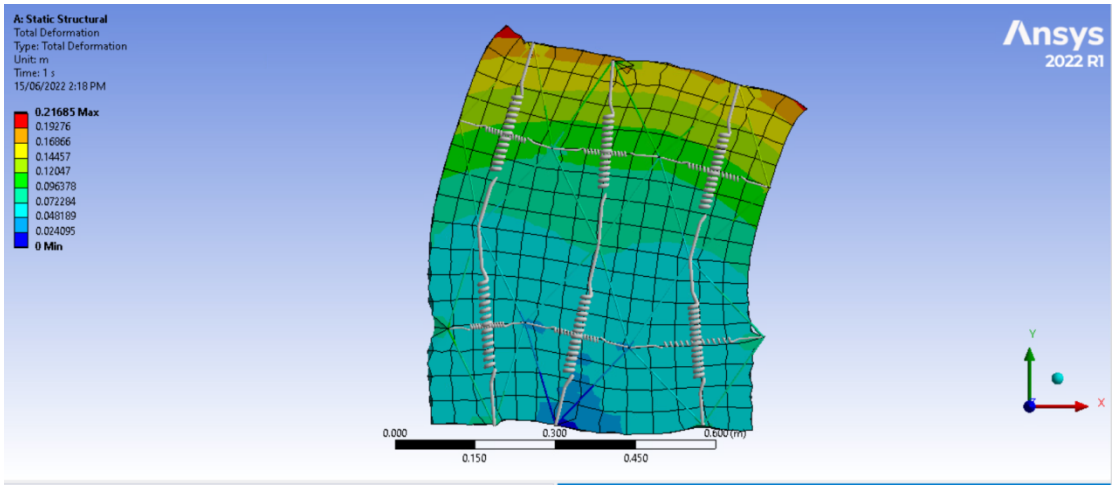

Figure 67: The final shape of the horizontal force at top surface

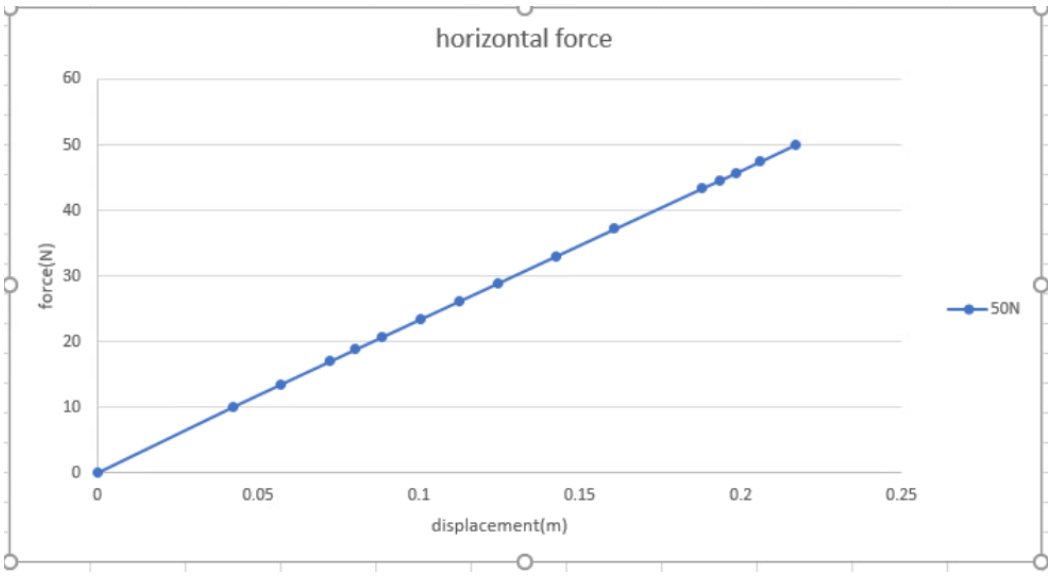

Figure 68: The force-displacement curve with 50N applied

Figure 69-71 shows a set of figures of force applied on the side plane, which are ANSYS model diagram, final state diagram after force application, and force-displacement curve diagram respectively.

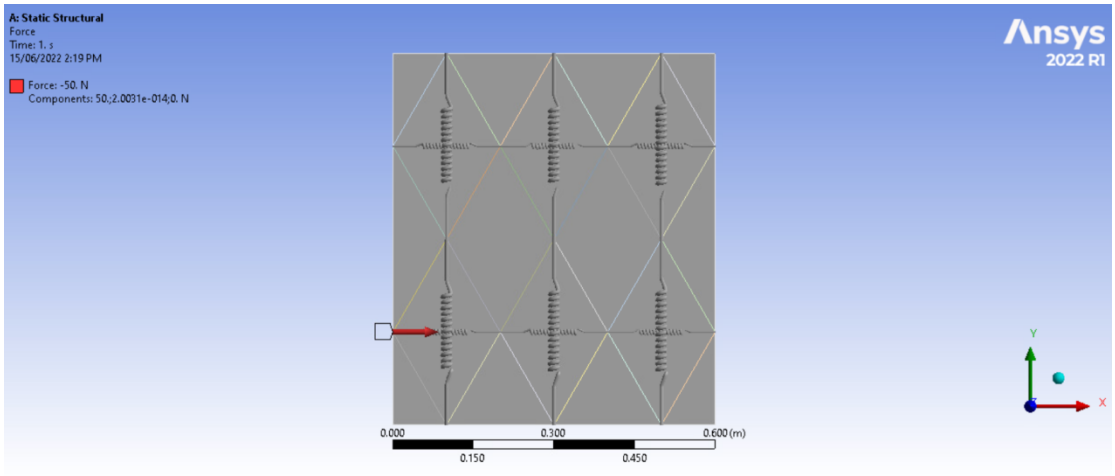

Figure 69: Horizontal force is applied at side surface

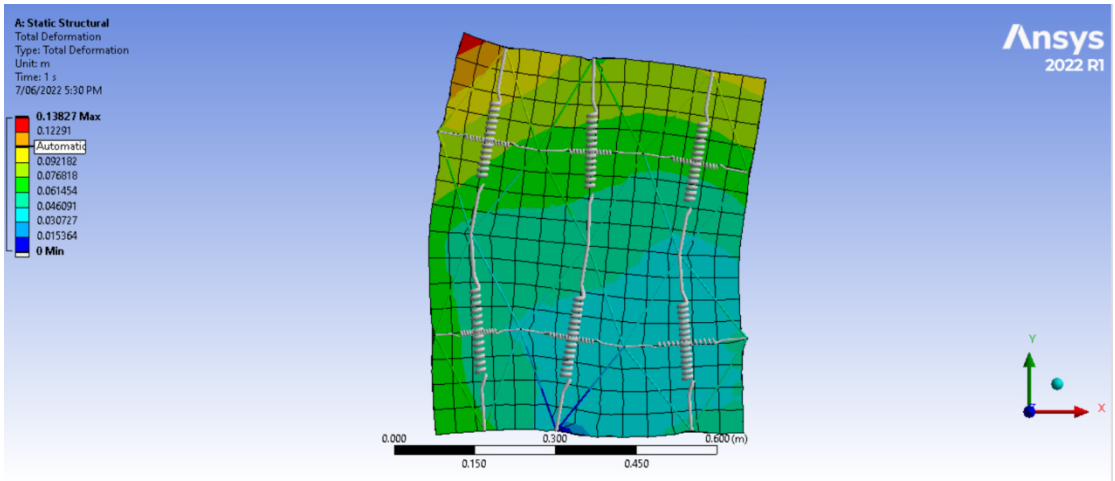

Figure 70: The final shape of the horizontal force at top surface

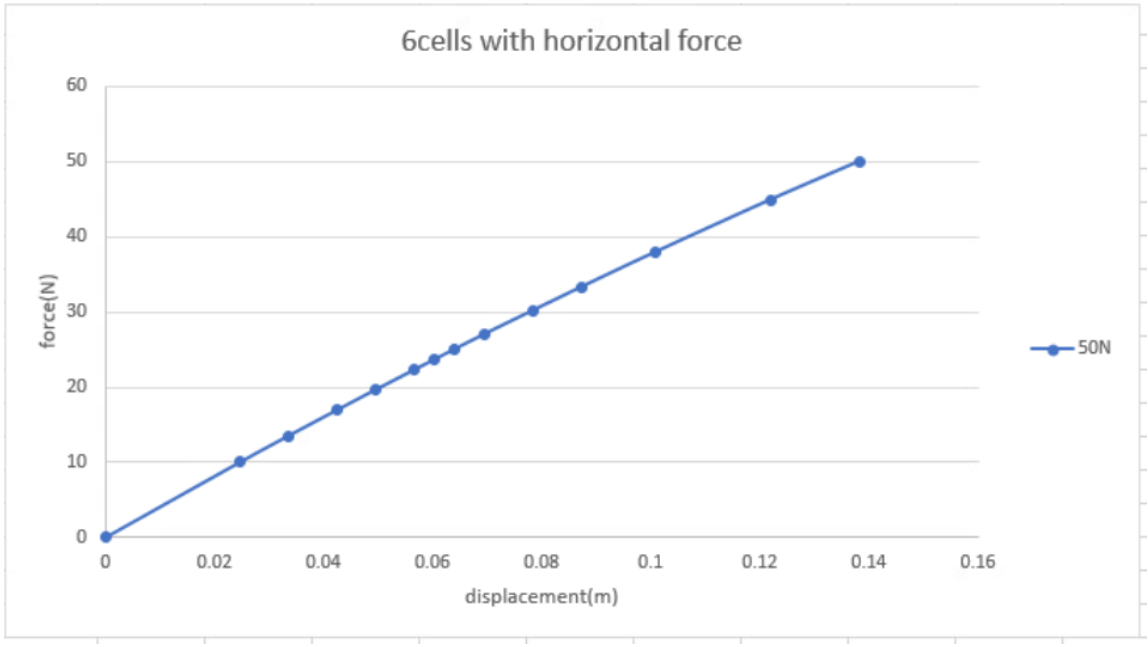

Figure 71: The force-displacement curve with 50N applied

It can be seen from Figure 68 and Figure 71 that although the force directions are different, 50N force is applied in both simulations, and the obtained force and displacement images tend to be straight lines.

It was also found that the stiffness in the horizontal direction is greater compared to the model where the force in the vertical direction is applied. It may due to the different boundary conditions with respect to the different loading directions.

4.6 Discussion

Model Verification

Comparison of MATLAB and ANSYS Results for a Single Cell Structure.

At first, MATLAB was chosen because it could analyze and study the behavior of a single cell, but when trying to use MATLAB for more complex analysis, it was found that MATLAB is not the appropriate software without a mathematical model to use, when a matrix and more cells were added. The author was unfamiliar with ANSYS, so the ANSYS model was checked by comparing it with the model analysis results of MATLAB for the case without any matrix.

The results show that the force-displacement plots obtained by ANSYS and MATLAB were in good agreement. Consequently, ANSYS was used to complete the more complex parts of the study.

Multiple celled structure without matrix

From the behavior of a single cell, it was found that a single cell can indeed bring nonlinear results of variable stiffness. Therefore, the superposition of cells in two different directions, horizontal and vertical, was introduced in the following simulation. In the subsequent process, various simulations were carried out, including the analysis of one cell, analysis of two cells arranged vertically one below the other, and analysis of four celled structure cells arranged as two rows and two columns of cells. From a comparison of the results, it can be seen that even one cell can show good variable stiffness results. When cells are added vertically, the flexibility increases but when cells are added horizontally the stiffness increases. However, when the cells are added horizontally, the load at which the structural stiffness becomes zero also increases.

By comparing the curves of force and displacement shown in Figure28 and Figure 31, it can be seen that when cells are added in the horizontal direction, the curve as a whole tends to be smoother, and also tends to be horizontal at the end of the graph line. This means that stiffness changes from large to small are more pronounced. However, there was a loss of non-linearity in some cases when the horizontal springs

were placed externally to the cell, possibly due to insufficient horizontal forces because of the lack of any side support to give the necessary compression in the springs.

The Effect of the Matrix

Once multi-celled structures were analyzed, another material was added as a matrix. Overall, the structures with an initial angle of 30 degrees and 60 degrees were compared. In this part of the simulation, in order to make the experiment as close as possible to reality, some details were adjusted (the spring is removed from the inside of the structure and placed at both ends). The reason for this operation is that in frame construction, the internal space is small, and placing two springs close to each other can cause friction and placement difficulties. Another important reason is that spring deformations (stroke) are usually possible only up to about 50% of the initial length of the spring. This means the change in geometry needed for non-linear behavior may not be possible. Placing it outside the structure solved this problem.

However, when more cells were added later, it was found that because the number of horizontal directions of the internal frame was even, the bottom fixed point could not be in the middle of the structure and thus could not be symmetrical. (If the number is even, there is no easy way to set the fixed point in the middle, which will lead to uneven and asymmetric forces in the whole structure). In order to better observe the influence of a matrix, there was always an odd number of cells. in the subsequent process.

From the experimental results of placing the spring at both ends (e.g. Figure 42 and Figure 43) it is indeed seen that the structure exhibits more nonlinear states as the spring is moved outward. As the number of cells increases (for example, Figure 46 and Figure 47), it is found that the nonlinear state of the structure increases with the addition of matrix. This may be because the vertical boundaries at both ends of the matrix can move freely, resulting in no effect of the horizontal spring. When more cells are added, there are more connecting springs in the middle, and the influence of ability of the springs at both ends to move freely can be gradually ignored.

Therefore, in order to solve this problem, a more appropriate structural shape was proposed, which could ensure there is sufficient space inside the frame for the horizontal and vertical springs to be telescoped (in real life, the springs in a cell structure cannot be compressed or stretched by more than 50% because the stroke of a spring is limited to about 50% of its length). In this shape, there is enough space for the springs not to interact with each other, but also enough tension for the springs to move. As described in Section 4.4, a pattern similar to a honeycomb structure was used for analysis.

Limitations and Recommendations for Further Research:

The results presented and the above findings are all based on numerical analysis and need to be verified experimentally.

Further work is needed to understand whether this idea can be used to make metamaterials for the purpose of reducing force transmission. The challenges include whether it is easy to produce metamaterials with springs. One possible way to do this would be to 3D print the metamaterial. Ideally, the fibers are evenly distributed in the frame and then soaked in the matrix. However, it may be challenging in practical experiments, because the accuracy of 3D printing will not be high enough if the structure is too small. In the later stage of this study, 3D printing experiments were indeed carried out. However, due to the spread of COVID-19, the author was unable to return to the University or use a laboratory to conduct complete tests.

To maximize sustainability, ideally the springs need to be replaced by elements such as natural fiber which would give same flexibility. For example, the spring part could be made of the same material as the frame. The difference is that in order to ensure the characteristics of the spring, the shape of the material should be consistent with a spring.

In subsequent experiments, there can be more numerical modeling of the spring shape of the fibers, such as the following figures. For example, Figures 72 and 73 below show two types of fibers that can be tried in real experiments. Figure 72 is the spring structure a similar two-dimensional plane, and Figure 73 is the natural growth form of some plants, such as bitter gourd plants and some ferns.

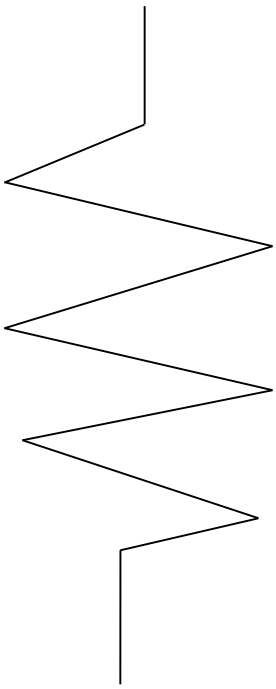

Figure 72 ： Common spring type construction

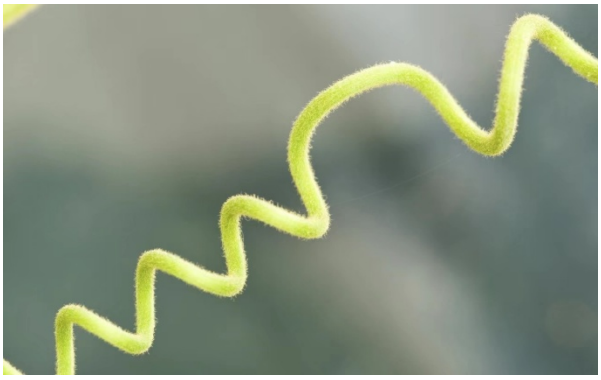

Figure 73 ： The spiral structure of natural plant fibers[52]

The above provides some ideas about the shape of the spring for the follow-up work. For future work, dynamic modeling to study the transmission of force also needs to be done. This should include random forces such as earthquake forces and impulse to represent forces during accidents.

The method of vibration mitigation tested throughout this article is isolation, but this is not the only solution because the springs only convert the energy into potential energy, so testing the effect of damping should be considered in future studies as it allows the energy that could cause damage to be absorbed. Metamaterials could be designed not only to isolate a structure from forces due to vibration but also to absorb vibrational energy. This work is currently in the static analysis stage, and better

products will be designed by adding damping design into dynamic analysis in the future.

The damping shock absorber has the advantages of compound vibration isolation and noise reduction, low natural frequency and good vibration isolation effect. In seismic instruments, dampers are used to absorb the natural vibration energy of the vibrating system [53].

A new frame-damping frame-tube structure system composed of outer frame, inner frame and damping wall is proposed. Twin two-story single-span 1:2 scaled sub-structure models were designed and fabricated, and the seismic performance of the frame-damping frame-tube structure system was studied through low-cycle reciprocating loading tests. The results show that the frame-damping frame-tube structural system has excellent seismic performance and can be applied to super high-rise buildings [54].

In conclusion, although it is difficult to say whether variable stiffness metamaterials are feasible in practice from the work completed, the theoretical analysis and numerical results are encouraging and therefore further research including experimental study is recommended.

5 Conclusions

From the thesis, the following conclusions can be drawn:

The use of cells containing springs and rigid elements embedded in a matrix can result in a non-linear force-displacement relationship, with stiffness decreasing with displacement. This can ensure that in the event of an earthquake or a collision or accident, transfer of damaging forces can be reduced, thus protecting people from injury or ensuring human safety.

This method of relying on the overall deformation of the metamaterial has great advantages as it provides isolation of the structure from the forces that could potentially cause damage. For example, the material and structure will not be damaged, and all the deformation is in non-permanent elastic deformation, which ensures repeated utilization and thus is environmentally friendly.

MATLAB or ANSYS simulations, metamaterial can be designed to find the best stiffness variation, whether it is applied to a building foundations or anti-collision items. The metamaterial can rely on the deformation in the elastic phase to isolate the forces created during an accident or earthquake.

It was found that the most critical factor that determines the degree of non-linearity of force-displacement curve is the ratio of $\frac{K_v}{K_h}$. Theoretically, when the initial angle is 60 degrees, the closer the ratio of $\frac{K_v}{K_h}$ is to 0.5, the more non-linear the result is. If the ratio is above 0.5, The system becomes unstable, while a lower ratio means less nonlinearity, so 0.5 is the best value for variable stiffness. When the ratio of K_v and K_h remains the same, 60° is the best initial angle for achieving a non-linear state. If the angle is less than 60 degrees, a satisfactory range of nonlinear state cannot be reached, and if the angle is more than 60 degrees, the system will eventually become unstable for the above stiffness ratio, and the inner space of the cell will be too small for the spring to move. So, 60 degrees is the best angle.

After verifying that the results of MATLAB and ANSYS were consistent for a single cell mechanism without a matrix, ANSYS was used to simulate multiple cells and the full metamaterial structure incorporating a matrix. By just adding a cell without

matrix, it was found when cells are added vertically, the flexibility increases but when cells were added horizontally the stiffness increases. When matrix was added it is found that the nonlinear state of the structure increases

The position of the spring was initially located inside the frame structure, but due to the limited space inside, and because the springs can only be extended by about 50% of their length at most, the range of non-linearity was limited. This means the change in geometry needed for non-linear behavior may not be possible. Placing the springs outside the structure solved this problem. However, there was still a drawback after the spring was removed from the inside: the springs at either end of the structure had no anchoring points to exert the compressive force, which meant that the horizontal spring did not work very well. So, another structure similar to a honeycomb was used. This honeycomb-like structure provides enough internal space to ensure that the spring can be stretched or compressed internally, and also ensures that the nonlinearity of the structure is well maintained. This is different from the traditional honeycomb structure. The special honeycomb structure used in this paper is like a mechanism; the components include springs which allow large displacements. The commonly used honeycomb structure does not allow large elastic displacements.

6 Reference

[1] X. Lu Metamaterials are the ultimate weapon against earthquakes *http://news.mydrivers.com/1/287/287924/htm%20taiget%3D*, P1, 2013

[2] L. Zhipeng, Analysis and Prediction of Earthquake Casualties, Based on Yushu Earthquake Casualty Modeling, Classification number: *R129*, 2014

[3] L. Shengcai, X. lei Statistical analysis of domestic production safety accidents from November to December 20221, Journal of Safety and Environment. 2021(06), DOI : 10.13637/j.issn.1009-6094.2022.0208, 2022

[4] D. Chuan. https://image.baidu.com/search/detail.

[5] M. Qiang Discussion on seismic structure design of high-rise concrete buildings. Classification number: TU973.31, P1-3, 2021

[6] F. Basone et al, Finite locally resonant Metafoundations for the seismic protection of fuel storage tanks[J]. Earthquake Engineering & Structural Dynamics. DOI: 10.1002/eqe.3134,P1, 2019

[7] A. Palermo et al, Metabarriers with multi-mass locally resonating units for broad band Rayleigh waves attenuation[J]. Soil Dynamics and Earthquake Engineering. DOI: 10.1016/j.soildyn.2018.05.035, Volume 113, 2017. PP 265-277, 2018

[8] J. Hwan Zero-frequency Bragg gap by spin-harnessed metamaterial[J]. New Journal of Physics. Volume 20, Issue 8 DOI: 10.1088/1367-2630/aada38, 2018

[9] X.chang et al, Application of a dynamic vibration absorber with negative stiffness for control of a marine shafting system[J] . Ocean Engineering. Volume 155, 2018. DOI: 10.1016/j.oceaneng.2018.02.047, PP 131-143, 2018

[10] Z.B. Cheng, Z.F. Shi. Composite periodic foundation and its application for seismic isolation[J]. Earthquake Engineering & Structural Dynamics, Volume 47, Issue 4. 2018. DOI: 10.1002/eqe.2999, PP 925-944, 2018

[11] L. Siqi, Investigation on seismic metamaterial with negative- stiffness dynamic vibration absorbers, Album: Engineering Technology II, DOI：10.27040/d.cnki.ggzdu.2020.000687, 2021

[12] Y. Lan and Z. Zhixia Earthquake disasters-disaster mitigation strategies directly under the city, Urban and Disaster Reduction, Classification number: P315.9, 2021

[13] G. Binbin et al, Analysis of seismic design and application of building steel structure. South China Branch of China Construction Second Engineering Bureau Co., Ltd. DOI: *10.13616/j.cnki.gcjsysj.2021.11.006*, P1-3, 2021

[14] L. Yuan et al, Loss analysis of building components based on New Zealand detailed earthquake damage data. DOI: *10.13197/j.eeev.2021.05.186.liuy.018, P1-4, 2021*

[15] Y. Meng. Seismic analysis of super high-rise buildings using hybrid technology of shock absorption and isolation. DOI: *10.26991/d.cnki.gdllu.2021.001347,* P1-5,89-95, 2021

[16] Y. Qing. Optimal Design of Lightweight Bumper Installation Structure for Automobiles in Low-speed Collision. DOI: *10.19475/j.cnki.issn1674-957x.2021.21.001*, P1-2, 2021

[17 L. Jinwei et al, Research on the status quo and control strategies of waste plastic pollution Classification number: X705, P1-2, 2021

[18] The New Zealand Injury Prevention Outcomes Report – June 2012, Wellington, N.Z.: ACC, 2011

[19] R. Ji et al, why is the death rate of motorcycles so high? Retrieved 30 March 2019 form http://www.sohu.com/a/285426720_616781,2018

[20] W. Xin et al, Research on Weather ability of Polypropylene Automobile Bumper. Classification number: *U463.326*, P1-2, 2021

[21] Z. Haiyang et al, Research on lightweight of fiber reinforced composite car bumper anti-collision beam. Classification number: *U463.326; U465.6*, P1-10, 2017

[22] C.E. Crede, Vibration and Shock Isolation, Wiley, New York,

[23] J.C. Snowdon, Vibration and Shock in Damped Mechanical Systems, Wiley, New York,

[24] J.C. Snowdon, Vibration isolation use and characterization, Journal of the Acoustical Society of America

[25] E.I. Rivin, Passive Vibration Isolation, ASME Press, New York, 2001

[26] A.J.H. Goodwin, Vibration isolators, U.S. Patent No. 3,202,388,

[27] D.R. Halwes, Vibration suppression system, U.S. Patent No. 4,236,607.

[28] W.G. Flannelly, Dynamic anti-resonant vibration isolator, U.S. Patent No. 3,322,379,

[29] A.D. Rita, J.H. McGravey, R. Jones, Helicopter rotor isolation evaluation utilizing the dynamic anti-resonant vibration isolator, Journal of the American Helicopter Society 23

[30] D. Braun, Development of anti-resonance force isolators for helicopter vibration reduction, Journal of the American Helicopter Society 27

[31] D. Braun, Vibration isolator particularly of the anti-resonance force type, U.S. Patent No. 4,781,363, 1988

[32] R.A. Desjardins, Vibration isolation system, U.S. Patent No. 4,140,028.

[33] R.A. Desjardins, W.E. Hooper, Anti-resonant rotor isolation for vibration reduction, Journal of the American Helicopter Society 25

[34] V.A. Ivovich, M.K. Savovich, Isolation of floor machines by lever-type inertia vibration corrector, Proceedings of the Institution of, Civil Engineers: Structures and Buildings 146, 2001

[35] R.A. Ibrahim. Recent advances in nonlinear passive vibration isolators. Journal of Sound and Vibration 314 (2008) 371–452, 2008

[36] S, Liu, et al, Design and characteristics of a novel QZS vibration isolation system with origami-inspired corrector. Nonlinear Dynamics 106:255–277, *https://doi.org/10.1007/s11071-021-06821-5*, 2021

[37] C. Xuchao et al, Adaptive Control of Quasi-Zero Stiffness Vibration Isolation System. Classification number: *U661.44; TB535.1; TP273.2* ,2021

[38] Z. Xinghua et al, The Design and Analysis of a Novel Passive Quasi-Zero Stiffness Vibration Isolator https://doi.org/10.1007/s42417-020-00221-6 ,2020

[39] G. Wen et al, Design, analysis and semi-active control of a quasi-zero stiffness vibration isolation system with six oblique springs. *https://doi.org/10.1007/s11071-021-06835-z,* 2021

[40] P. Alabuzhev, et al, Vibration Protecting and Measuring Systems with Quasi-Zero Stiffness, Hemisphere Publishing Co., Taylor & Francis Group, New, York, 1989
[41] V.P. Roslyakov, N.G. Nakhtigal, Choice of parameters of vibration protecting system with nonlinear characteristics, Mechanization and Electrification of Agriculture 10
[42] A.K. Zuyev, A.A. Nikitin, Vibration protecting mechanism for a riveting hammer, Proceedings of Dynamics of Vibro-Impact Mechanical Systems, NETI, Novosibirsk,
[43] P. Alabuzhev, et al, Studies of vibro-protecting systems with stiffness correction, Physico-Technical Problems of Exploitation of Mineral Resources.
[44] P.T. Stepanov, Investigation of Vibro-impact Mechanical Systems, NETI, Novosibirsk
[45] I.I. Gerner, et al, Calculation of nonlinear corrector for vibration isolated suspension, Proceedings of the Research
for Railway Transportation, Nauchnii Institut Zheleznodoro-zhnogo Transporta (NIZhT), Novosibirsk
[46] A.F. Yashin, et al, Nonlinear vibrations of systems with an arbitrary polynomial restoring force, Proceedings of Mechanics of Deformed Bodies and Structural Calculations, Novosibirsk, NIIZhT,
[47] M. Shahraeeni, et al, Effect of damping nonlinearity on the dynamics and performance of a quasi-zero-stiffness vibration isolator
https://doi.org/10.1016/j.jsv.2022.116822
[48] Mochida, Y, et al, Base isolator of vertical seismic vibration using a negative stiffness mechanism. In Vibration Engineering and Technology of Machinery, P1113-1119, 2015
[49] Asai, T. A., et al, Adjustable vertical vibration isolator with a variable ellipse curve mechanism, Earthquake Engineering & Structural Dynamics, 2017
[50] Eskandary-Malayery, F., et al, F, Experimental and numerical investigation of a vertical vibration isolator for seismic applications. Nonlinear Dynamics, doi:10.1007/s11071-022-07613-1, 2022

[51] J.H., Dunne, P.C. A simple theory of geometrical stiffness with applications to beam and shell problems. *https://doi.org/10.1007/BFb0120586*, 1976

[52] Wustrow-K https://www.veer.com/photo/128313957?utm_source=360&utm_medium=imagesearch ID：128313957

[53] https://baijiahao.baidu.com/s?id=1597288064642470836 Electric state service Dianbang Technology (Beijing) Co., Ltd, 2018

[54] C. Jiachun et al, Research on the technology of frame-damping frame-tube structure system, DOI: 10.19701/j.jzjg.HDY2244

Appendices

Appendices A and B present the procedures and results of some preliminary work, which could not be continued, due to Covid lockdowns.

Appendix A. Experimental Methods and Results

The properties of the resin were tested first, and two types were selected, namely epoxy and vinyl ester resins.

Health & Safety Precautions

During the entire experiment, it is necessary to wear gloves and masks to avoid skin contact with liquids and avoid exhaling chemical gases.

A.1 Experimental steps：

1: A male mold was designed with Solidworks sotware, and made using a 3D printer (See Figure. 74).

2: Using the male mold prepared, a female mold was made of silicone rubber, after pouring into silicone, it was left in the oven at a controlled temperature of 70℃

3: A layer of mold release agent was sprayed in the silicone mold for easy removal after the resin is fully formed.

4: To prepare epoxy resin samples, first mix epoxy and hardener in a ratio of 5: 1, and stir well with a stirring rod for one minute and pour the mixed liquid into a silicone mold. (Figure 75).

5: Gently shake the silicone mold by hand to help eliminate bubbles faster.

6: Move the sample into oven, the temperature should be controlled at 50 ℃, and the storage time should be more than 12 hours.

Figure 74: male mold

Figure 75: Mold after pouring resin

A.2 Experimental results

After following the above steps, the sample was obtained as shown in figure 76. Some strip-shaped gaps only existed in the required samples, and at the same time, the ordinary strip-shaped resin samples under the same environmental conditions did not show cracks.

Because the difference between the two samples is only in the shape, it may be because the thickness of the required sample is 7mm larger than the ordinary sample (5mm), and the curing speed of the surface layer and the bottom layer is not the same when curing。The gap that appears is like bubbles at the edges trying to gather toward the center, but because the surface layer has cured, the bubbles cannot reach the surface, leaving a trail of traces.

Figure 76: Comparison of required samples and ordinary samples

Figure 77: Crack of desired sample

In the second experiment, the curing temperature was adjusted, and the sample was left in the fume hood for curing.

This time the result was different. The previously observed cracks did not appear in the required sample. Although there are some small bubbles on the surface, it could be eliminated by grinding. (Figure 77).

Figure 78: Second sample

Due to the COVID-19 outbreak, the author could not return to the original laboratory, and the subsequent experimental materials and equipment have been partially adjusted.

In the initial preparation stage, as the availability of materials changed due to the relocation of the work, and the difficulty of experimental operation in the new lab, made it difficult to source the same materials to continue with the planned experiments. It was decided to test the characteristics of long straight fiber first as it was easily available.

In this stage, due to some limitations, easily available epoxy resins and amine curing agents, as well as sisal fibers, were initially selected.

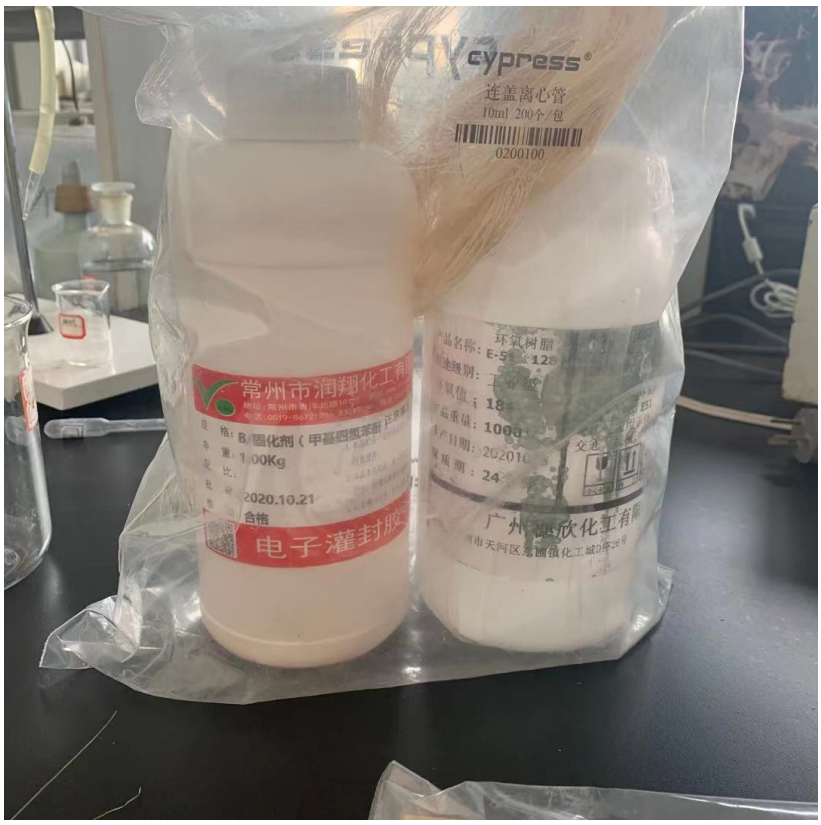

Figure 79: The second type of epoxy resin and curing agent

Because of the desired target shape and the nature of the fiber, it was not straight and it was a little wet.

Therefore, for the pretreatment of the fiber, it was chosen to first soak the fiber in water (30 minutes) and then hold the fiber in the oven with a heavy weight (4 hours) in order to achieve the purpose of straightening. In this way, the processed fibers become dry and straight.

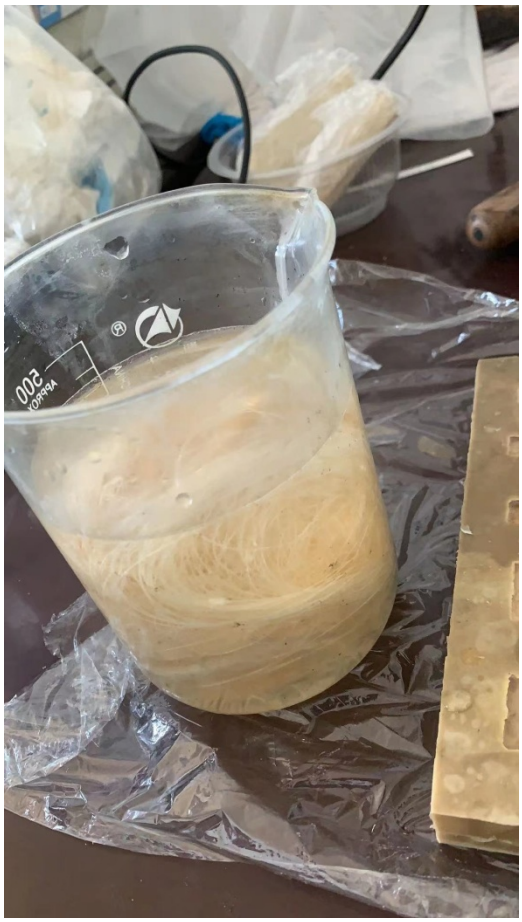

Figure 80: Sisal fiber preimpregnated

Figure 81: The fiber has been straightened and shaped by the oven

Then at the assembly stage, the fibers were prepared to minimize the formation of bubbles.

Figure 82: The mass fraction is about 5% of the sample

Then a sample with a mass fraction of about 5% was obtained.

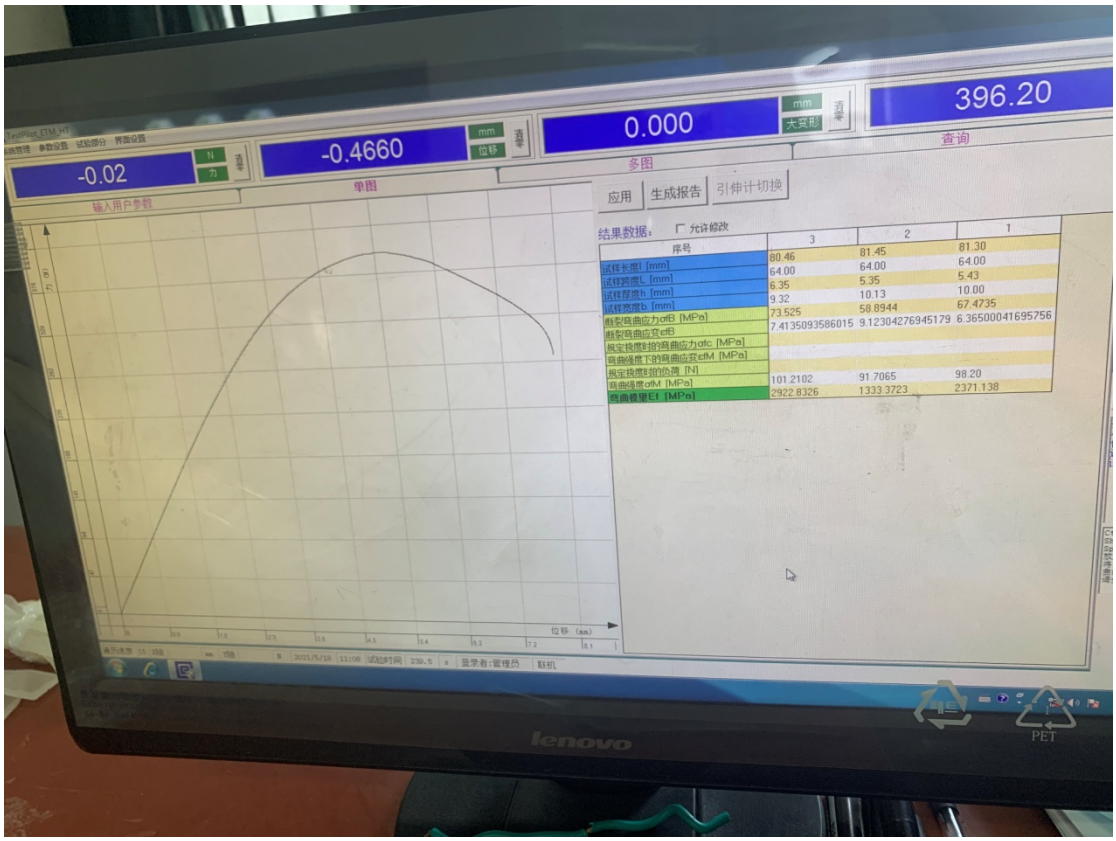

Figure 83: Tensile test results

The curves in the figure are stress-strain curves. Due to the inability to access the lab

again, it was not possible to obtain the digital data to present better graphs.

Simplified experimental procedure

Because the ideal fiber arrangement was too difficult to operate in the actual experiment, the operation part was then planned to be simplified as in Fig. 84.

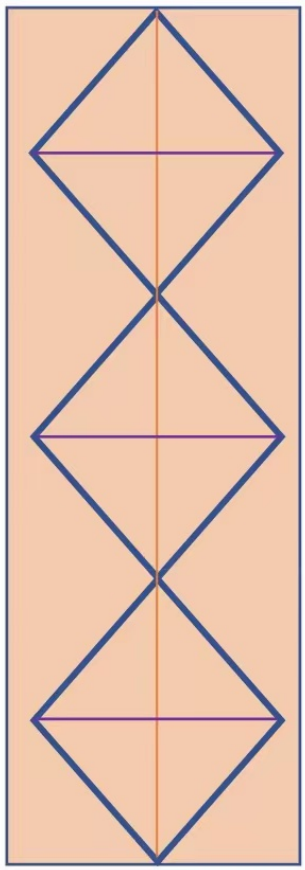

Figure 84: A simplified model

The blue part of the picture is made of fiber, filled with resin.

The inclined reinforcements are thick and broad.

The vertical and horizontal ones are much thinner behave like springs.

The stress analysis of the structure was carried out.

Appendix B

Stiffness of Bars Used in ANSYS Modelling

In this section, the initial modelling process for the planned experiments is described. In order to analyze the system in ANSYS and MATLAB, initially the vertical and horizontal stiffnesses were found using the force-displacement relationship.

Since bars were replaced by springs in the subsequent process, no detailed calculation will not be carried out here. Only one concept is explained here.

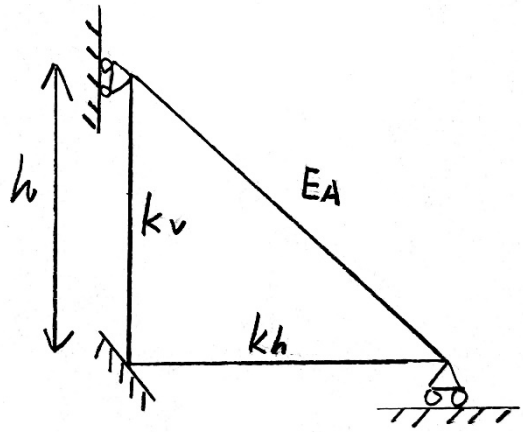

Figure 85 Simplified model

The point of this process is that instead of springs, bars were placed inside the structure. In this way, it can also be calculated. Firstly, the appropriate length and diameter of bars are given, and the stiffness value of bar in horizontal and vertical directions is obtained through the following equations:

$$k_v = \frac{EA}{h} \qquad \text{(B.1)}$$

$$k_h = \frac{EA}{l} \qquad \text{(B.2)}$$

Then the process is the same as the spring, put into MATLAB to get the result of the force, and then put the force into ANSYS to get the curve of the force-displacement.